

This is to certify that the dissertation entitled

The Use of Exciton-Coupled Circular Dichroism for the Absolute Stereochemical Determination of _-Chiral Carboxylic Acids and Erythro Diols and Aminoalcohols

presented by

Courtney C. Olmsted

has been accepted towards fulfillment of the requirements for the

Ph.D. degree in Chemistry

Major Professor's Signature

12/14/2006

Date

MSU is an Affirmative Action/Equal Opportunity Institution

LIBRARY Michigan State University

PLACE IN RETURN BOX to remove this checkout from your record.

TO AVOID FINES return on or before date due.

MAY BE RECALLED with earlier due date if requested.

DATE DUE	DATE DUE	DATE DUE
MAY 2 2 208		
10V 2 0 2009	· · · · · · · · · · · · · · · · · · ·	
		
		6/07 av/CIDC/DataDus india a

6/07 p:/CIRC/DateDue.indd-p.1

THE USE OF EXCITON-COUPLED CIRCULAR DICHROISM FOR THE ABSOLUTE STEREOCHEMICAL DETERMINATION OF α -CHIRAL CARBOXYLIC ACIDS AND *ERYTHRO* DIOLS AND AMINOALCOHOLS

Ву

Courtney C. Olmsted

A DISSERTATION

Submitted to
Michigan State University
in partial fulfillment of the requirements
for the degree of

DOCTOR OF PHILOSOPHY

Department of Chemistry

2006

ABSTRACT

THE USE OF EXCITON-COUPLED CIRCULAR DICHROISM FOR THE ABSOLUTE STEREOCHEMICAL DETERMINATION OF α -CHIRAL CARBOXYLIC ACIDS AND *ERYTHRO* DIOLS AND AMINOALCOHOLS

By

Courtney C. Olmsted

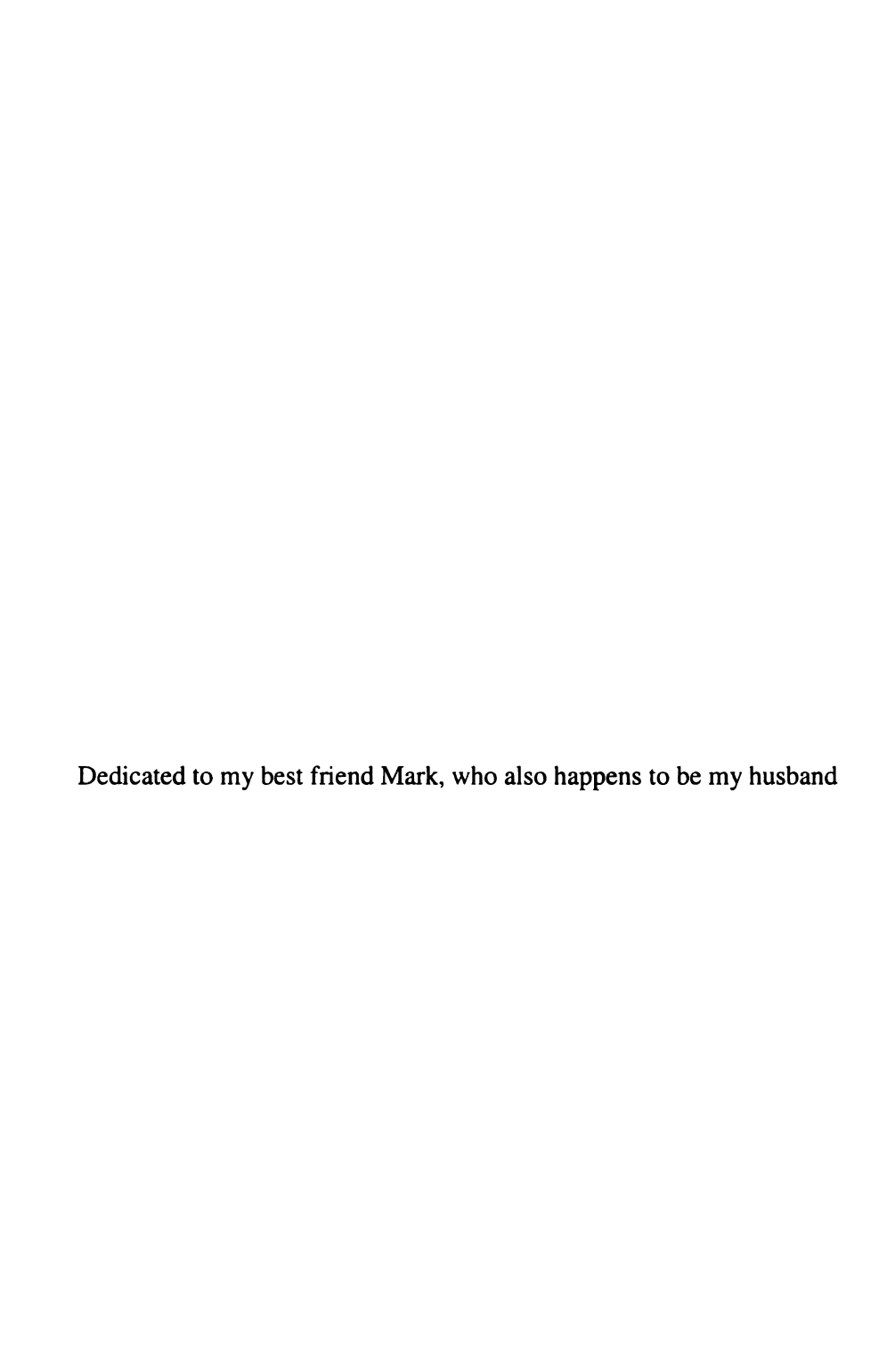
Chirality affects all of life, from the very simplest amino acids to pharmaceuticals used to treat diseases, but there is still much we have to learn about chirality. We are interested in the use of Exciton-Coupled Circular Dichroism (ECCD) to probe chirality in small molecules. ECCD is a non-empirical method which allows for the determination of the absolute stereochemistry of chiral compounds using the through-space coupling between two or more chirally oriented non-conjugated chromophores. ECCD has been used on compounds without chromophores through interaction of a chiral molecule with a host chromophoric molecule, causing induced chirality in the host-guest complex which is observable by ECCD.

Porphyrins are ideally suited for use in ECCD due to their strong extinction coefficient, low-energy absorption band, and a central metal core for binding to guest molecules. As a bisporphyrin tweezer with a 1,5-pentanediol linker, these molecules can bind with many small chiral molecules and the resultant ECCD can be observed. However, we noticed in our research that α -chiral carboxylic acids derivatized as amides did not always show the expected ECCD sign. Therefore we set out to explore the

rotation of the $C_{C=O}$ - C_{α} bond in our carboxylic acids derivatized as amides. Computational modeling of the derivatized carboxylic acids and as zinc tetraphenylporphyrin complexes have given us insight into the nature of the complexes formed. We have also explored binding modes beyond our initial models for α -halocarboxylic acids, including the possibility of cooperative binding occurring between the carbonyl oxygen, the halogen, and the metal core of the porphyrin.

To improve the reliability of our ECCD predictions, we have also developed alternate porphyrin tweezer systems, including tweezers with a diacetylene linkage, a ferrocene linkage, and a urea linkage. Synthesis of the porphyrin tweezer with the urea linkage actually generated porphyrin polymers which may have use outside the field of ECCD.

We wished also to extend the ECCD method to *erythro* diols and aminoalcohols, which traditionally have posed difficulties in standard stereochemical determination methods. We initially pursued the possibility of converting *erythro* diols into dioxanes with chromophores. However, we discovered a novel method through the use of *cis*-Ru(bpy)₂Cl₂. Addition of *erythro* diols and aminoalcohols to *cis*-Ru(bpy)₂Cl₂ provides ECCD spectra which are equal and opposite for enantiomers.



ACKNOWLEDGMENTS

First of all, I would like to express my heartfelt thanks to Babak. He has always been a willing listener to my often outrageous ideas and has encouraged my pursuit of answers. Due to him, I have become a better researcher and chemist. Beyond that, he has always been a friend and a mentor, encouraging me to try new opportunities and giving me freedom to express my opinions. I have learned much from him outside of organic chemistry, and I will always cherish the years I have spent in his labs.

Many thanks are due to the Borhan lab members. Qifei started the circular dichroism project in our labs and was the source of many wonderful discussions. I especially cherish the discussions of life in China and the many differences and similarities in US and Chinese culture. Marina has taken over the CD project and is doing a phenomenal job of extending the scope of this project. Спасибо for your help with Russian and especially the MacCoffee. Thanks also to Chrysoula, Ben, and Montserrat who started graduate school with me. It was amazing to find people so different who could get along so well. Additional thanks are also due to past and present members of the Borhan lab, including Rachael, Radha, Tao, Jennifer, Jun, Stewart, and Dan and many others who worked as high school and undergraduate researchers. The laughter and tears I have shared with all of you are a treasured part of graduate school. Keep up the great work and never let Babak rest.

I would also like to thank my committee members, in particular Prof. Rob Maleczka and Prof. Ned Jackson. Ned, your insight into the computational aspects of my research was invaluable and you were always willing to help. Rob, thank you for the

many challenges you have presented during graduate school. You are an amazing researcher but an even more phenomenal teacher. Thanks for pushing me to become a better chemist.

A special thanks goes to the many other friends I have made while at MSU. To name them all would be impossible; yet, I will always remember the wonderful discussions and time spent discussing life as well as research. You have all broadened my horizons and my understanding and acceptance of the global world we live in.

Thanks to my family for their continual support through this long process, especially my mom who introduced me to science at a young age and encouraged my experimentation as long as I cleaned up the kitchen. Most importantly, thanks to Mark for never allowing me to give up. I could not ask for a better friend to go through life with.

TABLE OF CONTENTS

List of	f Figuresix
List of	f Schemesxv
List of	f Tablesxvii
List of	f Abbreviationsxviii
Chapt	ter 1. Introduction
1.1.	The Exciton Coupled Circular Dichroism Method (ECCD)1
1.1.1.	Chirality1
1.1.2	Optical Rotary Dispersion (ORD) and Circular Dichroism (CD) Spectroscopy4
1.1.3.	Exciton Coupled Circular Dichroism (ECCD)12
1.1.4	ECCD Based on Quantum Mechanics16
1.2.1	The Use of ECCD to Determine the Absolute Stereochemistry of Chiral Molecules
1.2.1	Use of Chromophoric Hosts for ECCD of Non-chromophoric Chiral Molecules
1.2.2	Porphyrins as Chromophoric Receptors22
Refere	ences
Chapt	ter 2. Use of ECCD for Absolute Stereochemical Determination of α -Chiral Carboxylic Acids
2.1.	Use of Computational Modeling to Understand the Rotation About the $C_{C=O}$ - C_{α} Bond
2.1.1.	Modeling of Derivatized Carboxylic Acids Complexed to Zinc Tetraphenylporphyrin
2.1.2.	Modeling of Derivatized Carboxylic Acids with a Second-Generation Carrier
2.1.3.	Modeling of Chiral Carboxylic Acids Derivatized as Amides45

2.2.	Exploration of Possible Binding Modes for Derivatized Carboxylic Acids with Zinc Tetraphenylporphyrin 1,5-Pentanediol Tweezer53
2.3.	Exploration of a Novel Binding Model Involving Coordination of an α-Halogen and an Amide Carbonyl Oxygen to Zinc
Refere	ences
Chap	ter 3. Development of Alternate Tweezers for Use with ECCD in the Absolute Stereochemical Determination of Small Molecules
3.1.	Porphyrin Tweezer with a Diacetylene Linkage73
3.2.	Porphyrin Tweezer with a Ferrocene Linkage83
3.3.	Porphyrin Tweezer with a Urea Linkage91
Exper	imental materials and general procedures103
Refere	ences
Chapt	ter 4. Use of Ru(bpy) ₂ Cl ₂ for Determination of Absolute Stereochemistry of Erythro 1,2-Diols and Aminoalcohols
4.1.	Conversion of Erythro 1,2-Diols Into Dioxanes
4.2.	Consideration of cis-Ru(bpy) ₂ Cl ₂ as a Chromophoric Host
4.3	Studies of cis-Ru(biq) ₂ Cl ₂ and cis-Ru(bpy) ₂ Cl ₂
4.3.1.	Complexation and Studies of cis-Ru(bpy) ₂ Cl ₂ with Erythro 1,2-Diols and -Aminoalcohols
Experi	mental materials and general procedures
Defer	nces 152

LIST OF FIGURES

Note: Images	in this dissertation are presented in color.
Figure 1-1.	Examples of chiral molecules, (S)-2-bromobutane (left) and gingkolide B (right)
Figure 1-2.	Examples of some chiral molecules and their enantiomers
Figure 1-3.	Structures of (R)- and (S)-Thalidomide
Figure 1-4.	The magnetic (blue) and electric (green) components of light, where the direction of light propagation is to the right
Figure 1-5.	The circular and linear components of polarized light5
Figure 1-6.	Representation of linearly polarized light passing through a chiral medium, where the left circular component is absorbed to a greater extent than the right
Figure 1-7.	(a) Positive and (b) negative CD Cotton effects8
Figure 1-8.	Use of the "right hand rule" to determine magnetic transition dipole moment direction
Figure 1-9.	(P)-Hexahelicene and (M)-hexahelicene, showing the direction of current and the parallel [(P)-hexahelicene] and antiparallel [(M)-hexahelicene] transition moments
Figure 1-10.	The observed ECCD spectrum of a steroidal 2,3-bisbenzoate12
Figure 1-11.	Qualitative explanation of ECCD using a dibenzoate ester. (a) Orientation of the electric transition dipole moment in dibenzoate esters; (b) Preferred conformation of a 1,2-dibenzoate with a positive dihedral angle, ω ; (c) Inphase combination of the electric transition dipole moments; (d) Out-of-phase combination of the electric transition dipole moments
Figure 1-12.	Bisignate ECCD curve expected from the example given in Figure 1-1115
Figure 1-13.	Possible orientations of chromophores (clockwise and counterclockwise) and their corresponding ECCD signs16

Figure 1-14.	Splitting of the two excited states of non-conjugated chromophores i and j by exciton interaction. The energy gap V_{ij} is known as Davydov splitting
Figure 1-15.	A chiral (denoted by an asterisk) guest molecule can complex with an achiral host chromophore to produce a chiral complex capable of generating ECCD
Figure 1-16.	Complexation between racemic biphenol 1 and chiral diamine 2 leading to a chiral complex
Figure 1-17.	Examples of an achiral porphyrin and an inherently chiral porphyrin23
Figure 1-18.	UV-vis spectra of tetraphenylporphyrin methyl ester and zinc tetraphenylporphyrin methyl ester showing changes in the Q band upon metallation
Figure 1-19.	Bismetallated porphyrin tweezer 4 and shorthand representations25
Figure 1-20.	Example of stereochemical determination for chiral diamines complexed to zinc porphyrin tweezer 4 using ECCD
Figure 1-21.	Carrier 5 reacts with (S)-1-cyclohexylethylamine to form conjugate 6, which has a preferred conformation where the carbonyl is <i>anti</i> to the pyridine nitrogen and the small group (hydrogen) of the chiral center is syn to the carbonyl
Figure 1-22.	Complexation of conjugate 6 with tweezer 4 leading to the most favored conformation for the complex and the observed ECCD spectrum30
Figure 2-1.	Bis(tetraphenylporphyrin) tweezer 1 and its simplified representation36
Figure 2-2.	Complexation of a chiral acid conjugate with zinc bisporphyrin tweezer 1 leading to the most favored conformation for the complex and the observed ECCD spectrum
Figure 2-3.	Carriers A and B used to derivatize chiral molecules with one site of attachment for use with ECCD (site of derivatization shown in blue)40
Figure 2-4.	Binding of zinc porphyrin to the derivatized carboxylic acid forces rotation of the C(aryl)-N(amide) bond, causing the near coplanar amide to become staggered with respect to the aromatic ring
Figure 2-5.	Mnemonic developed for determining the absolute stereochemistry of derivatized carboxylic acids using ECCD

Figure 2-6.	Rotation around the C(C=O)-C(chiral) bond leading to opposite ECCD predictions
Figure 2-7.	Possible conformational changes due to dipole interactions (shown in blue) between the carbonyl and the pyridine ring upon binding to the porphyrin tweezer
Figure 2-8.	Relative energies of the lowest energy conformers generated from a conformational search of (S)-phenylpropionic acid derivatized with carrier A
Figure 2-9.	The plane of the carbonyl and the plane of one group on the chiral center used for coordinate driving47
Figure 2-10.	Graph of the energy values obtained for the coordinate driving of (2R)-2-bromopropionic acid derivatized with carrier B 48
Figure 2-11.	Graph of the energy values obtained from the coordinate driving of (2S)-2-acetoxypropionic acid derivatized with carrier B 48
Figure 2-12.	Graph of the energy values obtained from a molecular mechanics geometry optimization of each molecule from the coordinate driving of $(2S)$ -2-acetoxypropionic acid derivatized with carrier $\bf B$ (Newman projections represent the view from α -carbon to carbonyl carbon)50
Figure 2-13.	Graph of the energy values obtained from a PM3 geometry optimization of each molecule from the coordinate driving of $(2S)$ -2-acetoxypropionic acid derivatized with carrier $\bf B$ (Newman projections represent the view from α -carbon to carbonyl carbon)
Figure 2-14.	Examples of 1,2- and 1,3-carriers, from chiral amines and carboxylic acids, respectively
Figure 2-15.	Possible binding modes for carboxylic acids derivatized with carrier A53
Figure 2-16.	Pseudo-A-1,2- and A-1,3-interactions of the amide nitrogen and carbonyl with the substituents on the chiral center55
Figure 2-17.	Possible conformation changes due to hydrogen bonding leading to a switch in the expected ECCD sign
Figure 2-18.	Possible cooperative binding between the carbonyl oxygen and the α -halogen with the metal core of the porphyrin60
Figure 2-19.	(2R)-2-bromopropionic acid as both diastereomers of a Mosher amide60

Figure 2-20.	CCD data depicting dihedral angles of α -halocarbonyls
Figure 2-21.	Lowest energy conformation for bromoacetamide based on DFT calculations
Figure 2-22.	DFT geometry optimization of N-methyl-(2R)-2-bromoacetamide using implicit solvation leading to a conformation with the bromine <i>anti</i> to the carbonyl
Figure 2-23.	Geometry optimization of water molecules hydrogen bonded to N-phenyl-2-bromopropionamide
Figure 2-24.	Rotation around the C(C=O)-C(chiral) bond due to coordination of the carbonyl oxygen with zinc
Figure 3-1.	Representation of possible differences in binding between porphyrin tweezers and guest molecules, leading to opposite ECCD signs72
Figure 3-2.	Indication of bite angle in proposed <i>meta</i> -substituted bisphenylacetylene linker
Figure 3-3.	Proposed rigid porphyrin tweezer 1 utilizing a bisacetylene linker75
Figure 3-4.	Red shift in UV-vis absorption of tweezer 1 with 1,5-diaminopentane77
Figure 3-5.	Alternative bisacetylene porphyrin tweezer 779
Figure 3-6.	Structure of the proposed bisporphyrin ferrocene tweezer 1184
Figure 3-7.	Representation of possible binding outside of tweezer core for bis(zince porphyrin) ferrocene 11
Figure 3-8.	Representation of Takagishi's dimer showing steric interaction between the urea carbonyl and the methyl substituents on the phenyl rings92
Figure 3-9.	Schematic showing control of helix direction upon addition of a chiral guest to a porphyrin trimer connected by urea linkages, leading to ECCD
Figure 3-10.	Spartan molecular model of helix formed from urea-linked porphyrins (phenyl rings not shown for clarity)93
Figure 4-1.	Newman projections of low energy conformers of $(2R, 3R)$ -2,3-dihydroxypentane. When derivatized with chromophores (X) , the expected lowest energy conformer would lead to a negative ECCD bisignate curve

Figure 4-2.	Newman projections of low energy conformers of (2S, 3S)-2,3-dihydroxypentane. When derivatized with chromophores (X), the expected lowest energy conformer would lead to a positive ECCI bisignate curve
Figure 4-3.	Newman projections of low energy conformers of (2R, 3S)-2,3-dihydroxypentane. When derivatized with chromophores, no ECCD is expected to be observed
Figure 4-4.	Newman projections of low energy conformers of (2S, 3R)-2,3-dihydroxypentane. When derivatized with chromophores, no ECCD is expected to be observed
Figure 4-5.	Transformation of erythro diols into six-membered rings functionalized with chromophores (X)
Figure 4-6.	Newman projections of the product formed from $(2R, 3S)$ -2,3-pentanedio or $(2S, 3R)$ -2,3-pentanediol and an (R, R) bis-chromophore127
Figure 4-7.	Newman projections of the product formed from $(2R, 3S)$ -2,3-pentanedio and an (R, S) meso bis-chromophore (X) indicating an expected negative ECCD bisignate curve
Figure 4-8.	Newman projections of the product formed from (2S, 3R)-2,3-pentanedic and an (R, S) bis-chromophore (X) indicating an expected positive ECCD bisignate curve
Figure 4-9.	Λ and Δ forms of cis -Ru(bpy) ₂ Cl ₂
Figure 4-10.	Possible method of stereodifferentiation where the chiral erythro dio binds preferentially to Λ -cis-Ru(bpy) ₂ Cl ₂
Figure 4-11.	Transfer of chirality from the <i>erythro</i> diol to the ruthenium complex changing the initial stereochemistry of the ruthenium to match the diol
Figure 4-12.	Spartan models of $Ru(bpy)_2Y$ where Y is $(2R,3S)$ -pentanediol. Note the curve of the bipyridine in the structure on the right (emphasized with a blue curved line)
Figure 4-13.	UV-Vis studies on RuCl ₃ in acetonitrile (solid line), benzene (large dashes), CH ₂ Cl ₂ (small dashes), MeOH (dash-dot-dash), and methylcyclohexane (dash-dot-dot-dash)

Figure 4-14.	UV-Vis studies on <i>cis</i> -Ru(bpy) ₂ Cl ₂ in acetonitrile (solid line), benzene (large dashes), CH ₂ Cl ₂ (small dashes), MeOH (dash-dot-dash), and methylcyclohexane (dash-dot-dot-dash)
Figure 4-15.	ECCD spectra of <i>cis</i> -Ru(bpy) ₂ Cl ₂ refluxed with (1 <i>S</i>)-1-phenylethane-1,2-diol (solid blue line) and (1 <i>R</i>)-1-phenylethane-1,2-diol (dashed pink line) in spectroscopy grade MeOH
Figure 4-16.	ECCD spectra of <i>cis</i> -Ru(bpy) ₂ Cl ₂ refluxed with (-)-norephedrine (solid blue line) and (+)-norephedrine (dashed pink line) in spectroscopy grade MeOH
Figure 4-17.	ECCD spectra of <i>cis</i> -Ru(bpy) ₂ Cl ₂ refluxed with L- <i>allo</i> -threonine methyl ester (solid blue line) and D- <i>allo</i> -threonine methyl ester (dashed pink line) in spectroscopy grade MeOH
Figure 4-18.	Representation of pseudo-axial and -equatorial positions for the possible complex forming between cis-Ru(bpy) ₂ Cl ₂ and erythro compounds (bipyridine rings not shown for clarity)

LIST OF SCHEMES

Scheme 1-1.	Esterification of binaphthalene 3 with a chiral secondary alcohol21
Scheme 1-2.	Conversion of amino acids and amino alcohols for use as diamine guests for the host porphyrin tweezer 427
Scheme 3-1.	Synthesis of (trimethylsilyl)acetylene derivatized porphyrin 475
Scheme 3-2.	Synthesis of bisacetylene tweezer 176
Scheme 3-3.	Proposed synthesis of alternate tweezer 880
Scheme 3-4.	Proposed synthesis of tweezer 8 using a functionalized aldehyde82
Scheme 3-5.	Attempted synthetic routes for p-(1-trimethylsilylpropargyl)benzaldehyde83
Scheme 3-6.	Reported synthesis of porphyrin monosubstituted ferrocenes84
Scheme 3-7.	Synthesis of 5-(p-bromophenyl)-10,15,20-triphenylporphyrin85
Scheme 3-8.	Reported synthesis of bis(tributyltin)ferrocene 1287
Scheme 3-9.	Attempted coupling of 5-(p-bromophenyl)-10,15,20-triphenylporphyrin 9 with bis(tributyltin)ferrocene 12 using PdCl ₂ (PPh ₃) ₂ 87
Scheme 3-10.	Attempted coupling of 5-(p-bromophenyl)-10,15,20-triphenylporphyrin 9 with bis(tributyltin)ferrocene 12 using Pd ₂ (dba) ₃
Scheme 3-11.	Synthesis of bis(boronic acid)ferrocene 1389
Scheme 3-12.	Coupling of zinc 5-(p-bromophenyl)-10,15,20-triphenylporphyrin with bis(boronic acid)ferrocene90
	Synthesis of alcohol 15 and benzaldehyde 16 from 4-methyl-3,5-dinitrobenzoic acid
Scheme 3-14.	Synthesis of 5-(4-methyl-3,5-dinitrophenyl)-10,15,20-triphenylporphyrin 1795
Scheme 3-15.	Attempted synthesis of 5-(4-methyl-3,5-dinitrophenyl)-10,15,20-triphenylporphyrin using propionic acid95

Scheme 3-16.	Synthesis of (4-methyl-3,5-dinitrophenyl)dipyrrole 18 and phenyldipyrrole 19
Scheme 3-17.	Synthesis of 5-(4-methyl-3,5-dinitrophenyl)-10,15,20-triphenylporphyrin 17 from (4-methyl-3,5-dinitrophenyl)dipyrrole 18
Scheme 3-18.	Synthesis of 5-(4-methyl-3,5-dinitrophenyl)-10,15,20-triphenylporphyrin 17 using a pseudo "one pot" procedure
Scheme 3-19.	Reduction of the nitro groups of 17 to give 5-(3,5-diamino-4-methylphenyl)-10,15,20-triphenylporphyrin 20 99
Scheme 3-20.	Formation of porphyrin polymer 21 from 5-(3,5-diamino-4-methylphenyl)-10,15,20-triphenylporphyrin 20 and triphosgene100
Scheme 3-21.	Synthesis of zinc porphyrin polymer 22 from porphyrin polymer 21102
Scheme 4-1.	Synthesis of meso-1,2-dibromo-1,2-(4,4'-dinitrophenyl)ethane 2 from 4-nitrobenzyl chloride
Scheme 4-2.	Synthesis of the unexpected product bis-(4-nitrophenyl)acetylene 3130
Scheme 4-3.	Attempted derivatizations of <i>trans</i> -1,2-cyclohexanediol in various solvents
Scheme 4-4.	Attempted derivatization of <i>trans</i> -1,2-cyclohexanediol using HMPA in ACN
Scheme 4-5.	Attempted synthesis of cis-Ru(biq) ₂ Cl ₂ 137
Scheme 4-6.	Synthesis of chirally enhanced cis-Ru(bpy) ₂ Cl ₂ 137
Scheme 4-7.	Synthesis of racemic cis-Ru(bpy) ₂ Cl ₂
Scheme 4-8.	Attempted complexation of (S,S)-(-)-hydrobenzoin with cis- Ru(bpy) ₂ Cl ₂ 140
Scheme 4-9.	Attempted complexation of (S,S) -(-)-hydrobenzoin with cis -Ru(bpy) ₂ Cl ₂ using n -BuLi
Scheme 4-10.	Control reaction of (S,S) -(-)-hydrobenzoin with n -BuLi

LIST OF TABLES

Table 1-1.	Definition of positive and negative exciton chirality for a binary system
Table 2-1.	Predicted and observed ECCD signs for chiral acids derivatized as amides and complexed with tweezer 1
Table 2-2.	Conformational search results of various chiral carboxylic acids complexed to carrier A
Table 2-3.	Conformational search results of various chiral carboxylic acids complexed to carrier B
Table 2-4.	Representative α-halocarboxylic acids derivatized with carrier B showing unexpected ECCD signs

LIST OF ABBREVIATIONS

 α angle of rotation

[a] specific rotation

A CD amplitude

Ac acetate

ACN acetonitrile

a.u. atomic units

biq 2,2'-biquinoline

bpy 2,2'-bipyridine

Boc *tert*-butoxycarbonyl

bu butyl

CCD Cambridge Crystallographic Database

CD circular dichroism

CE Cotton effect

p-chloranil tetrachloro-1,4-benzoquinone

cm centimeter

d doublet

dba dibenzylidene acetone

DFT density functional theory

DIEA diisopropylethyl amine

DMF N,N-dimethylformamide

DMSO dimethyl sulfoxide

ε molar absorption coefficient

ECCD exciton-coupled circular dichroism

equiv equivalents

Et ethyl

g gram

GUI graphical user interface

h hour

HF Hartree-Fock

HMPA hexamethylphosphoramide

IR infrared

J NMR coupling constant

kcal kilocalorie

m magnetic transition dipole moment

M molar (moles/liter)

MALDI matrix-assisted laser desorption ionization

MCH methylcyclohexane

MeOH methanol

min minute

mg milligram

MHz megahertz

mL milliliter

MLCT metal-ligand charge transfer

mmol millimole

MM4 molecular mechanics force field

mol mole

MS mass spectrometry

n refractive index

nm nanometer

NMP N-methyl-2-pyrrolidone

NMR nuclear magnetic resonance

NOE nuclear Overhauser effect

ORD optical rotatory dispersion

PC personal computer

PCC pyridinium chlorochromate

Ph phenyl

PM3 Parametric Method Number 3

PPh₃ triphenylphosphine

ppm parts per million

q. v. quod vide

R rotational strength

rt room temperature

Ru(bpy)₂Cl₂ ruthenium (II) bis(2,2'-bipyridine) dichloride

s singlet

S_N1 nucleophilic substitution, first order

S_N2 nucleophilic substitution, second order

t triplet

TBAF tetrabutyl ammonium fluoride

TEA triethylamine

TFA trifluoroacetic acid

THF tetrahydrofuran

TLC thin layer chromatography

TMEDA tetramethylethylenediamine

TMS trimethylsilyl

TPP tetraphenylporphyrin

p-TSA *p*-toluenesulfonic acid

μL microliter

UV-vis ultraviolet-visible spectroscopy

Chapter 1

Introduction

1-1. The Exciton Coupled Circular Dichroism Method

1-1.1. Chirality

Mystical and enigmatic, chirality affects all of life, from the very simplest amino acids to pharmaceuticals used to treat diseases, yet the origin of chirality is still a mystery. In the past few centuries we have begun to understand the impact of chirality in our universe. Chirality refers to non-superimposable mirror images, and was named after the non-superimposable mirror images always with us—our hands—coming from the Greek word *cheir*, meaning "hand". In chemistry, chirality refers to the asymmetric position of atoms in a molecule, such that the mirror images of that molecule are non-superimposable. Examples of chiral molecules can range from the simplest—a single atom with four different substituents such as 2-bromobutane—to large natural molecules with multiple chiral centers, such as ginkgolide B (Figure 1-1). The simplest example of

Figure 1-1. Examples of chiral molecules, (S)-2-bromobutane (left) and ginkgolide B (right).

a chiral compound is a molecule containing one chiral center; such as a tetrahedral carbon with four different substituents. Chemists use the letters R (from the Latin "rectus") and S (from the Latin "sinister") to indicate the configuration (arrangement of groups) of the chiral center, based on priorities set in place by Cahn, Ingold, and Prelog.²

1

Molecules do not have to have a chiral center to be chiral. Some of the most fascinating chiral molecules include substituted allenes,³ helicenes,⁴ and atropisomers,⁵ which all have no plane of symmetry and therefore do not have superimposable mirror images. This type of chirality is referred to as axial chirality. Figure 1-2 shows examples of chiral molecules and their non-superimposable mirror images (enantiomers).

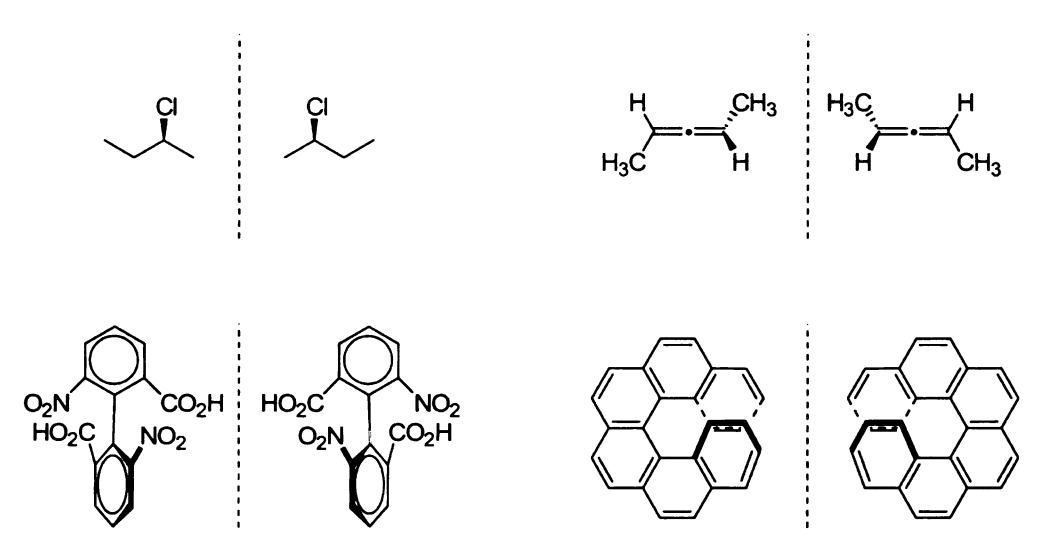


Figure 1-2. Examples of some chiral molecules and their enantiomers.

While stereochemistry is interesting from a visual standpoint, the stereochemistry of molecules also affects their chemical and biological properties. Much work has been done to understand chirality and how it relates to our lives, as it has become apparent that molecules of different chirality have different properties. Many enantiomeric natural products used as drugs have different actions within the body. One particular molecule of historical note is thalidomide. Thalidomide was introduced as a commercially available sedative and anti-nausea drug in Europe and Canada in the mid-1950's. As shown in Figure 1-3, thalidomide has a single stereogenic center and can thus exist in two stereoisomeric forms.² One of the enantiomers, (R)-thalidomide, has strong sedative properties, while the other enantiomer, (S)-thalidomide, is highly teratogenic.

Unfortunately, the drug was produced and distributed in racemic form, and women who were given thalidomide during the first few months of pregnancy had babies with a wide variety of birth defects.

$$(R)$$
-Thalidomide (S) -Thalidomide

Figure 1-3. Structures of (R)- and (S)-thalidomide.

It is, therefore, of great importance to know the absolute stereochemistry of chiral compounds for natural product chemistry, pharmaceutics, and biochemistry. However, determination of the absolute stereochemistry of molecules is not simple since enantiomers have the same physical properties such as boiling point. Separation of isomers originally focused on crystallization of a racemic mixture and separation of the enantiomeric crystals by hand—a very tedious and time-consuming task. However, this did allow compounds to be labeled with a stereochemistry based on their crystal formation. Other molecules that formed crystals of the same handedness were then assigned the same stereochemistry. Scientists now use methods such as X-ray crystallography, chiroptical methods such as optical rotatory dispersion (ORD) and circular dichroism (CD),⁶ nuclear magnetic resonance (NMR) spectroscopy of Mosher esters and related derivatives,⁷ and chemical correlation with known chiral compounds for determination of absolute stereochemistry.¹

While X-ray crystallography is the most unambiguous method for absolute stereochemical determination, suitable crystals can be hard to obtain. Crystallization often requires large amounts of compound that may not be available for recently

discovered natural products or complicated synthetic endeavors. If the compound of interest is not particularly amenable to crystallization, searching for the correct crystallization conditions can take months or even years. Thus, other methods have been developed to help offset the difficulties associated with crystallography.

One of the most common methods for stereochemical determination is the use of Mosher-ester type derivatives of the chiral molecule in question. Analysis using Mosher's technique involves derivatization of the compound of interest into two diastereomers containing an aryl ring. The NMR spectrum of each is obtained and a comparison is made between the diastereomers and the chemical shift observed for protons within the molecule. This method requires enough sample to do two derivatizations and to prepare NMR solutions. To circumvent some of the abovementioned problems, a new technique has been developed which uses chromophores to explore the chiroptical properties of molecules. This technique is known as circular dichroism.

The goal of our research is to develop general and sensitive exciton-coupled circular dichroic (ECCD) methods for the absolute stereochemical determination of chiral compounds.

1-1.2. Optical Rotatory Dispersion (ORD) and Circular Dichroism (CD) Spectroscopy

Optical Rotatory Dispersion (ORD) and Circular Dichroism (CD) are both methods that take advantage of the different chiroptical properties of enantiomers. In these methods, light is used to distinguish between enantiomers. Light consists of both an electric and a magnetic field, which oscillate perpendicular to one another and to the

direction of the propagation of light (Figure 1-4). The direction of the electric field



Figure 1-4. The magnetic (blue) and electric (green) components of light, where the direction of light propagation is to the right.

vector defines the polarization of light. Light from ordinary light sources, such as the sun or a light bulb, is unpolarized, since it consists of light waves propagating in all directions. However, if unpolarized light passes through a polarizing filter, only the light waves with oscillation parallel to the direction of the filter pass through. The light passing through the filter is now aligned in one plane of oscillation, and is defined as linearly polarized light. Linearly polarized light is composed of two circularly polarized

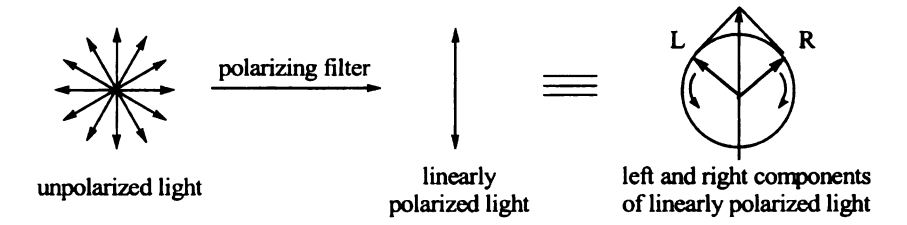


Figure 1-5. The circular and linear components of polarized light.

light beams: one left circular component and one right circular component. Figure 1-5 shows the composition of linearly polarized and circularly polarized light.⁹

The magnitude the electric field of circularly polarized light is constant, but traces out a helix as a function of time. When linearly polarized light passes through an achiral compound or a racemic mixture, the velocity and absorbance of the circular components are affected in the same way, so there is no change in the polarization of the light.

However, if linearly polarized light passes through an optically active medium, the velocity and absorbance of one circularly polarized component (either the left or the right) is altered to a greater extent as compared to the opposite circularly polarized component. ¹⁰ In Figure 1-6, the representation of linearly polarized light passing through a chiral medium leads to greater absorption of the left circular component than the right,

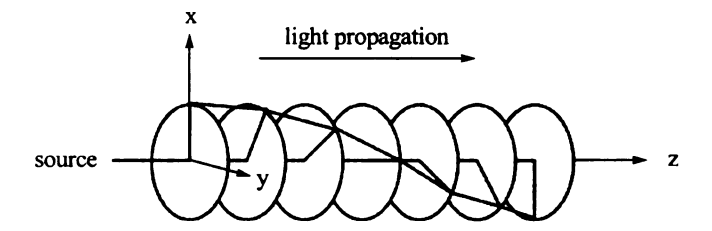


Figure 1-6. Representation of linearly polarized light passing through a chiral medium, where the left circular component is absorbed to a greater extent than the right.

generating right circularly polarized light. This is referred to as a Cotton effect (CE), in honor of French physicist Aimé Cotton, who observed both optical rotatory dispersion (ORD) and circular dichroism (CD) phenomena.

The difference in the velocity of the left and right components of circularly polarized light is known as optical rotatory dispersion (ORD). A different velocity for left and right circularly polarized light correlates to differences in the respective refractive indices. In equation (1-1), 8 n_L and n_R are the refractive indices for left and right circularly polarized light, respectively, when passing through an optically active medium.

$$\Delta n = n_L - n_R \neq 0 \tag{1-1}$$

If the left and right circularly polarized light components travel in an optically active medium at different velocities, the two components become out of phase. The resultant addition vector of the two light components is rotated by an angle α relative to the original plane of polarization. The direction of the addition vector is determined by the

direction of the component less affected by the optically active medium. ORD spectroscopy is the measurement of the specific rotation, $[\alpha]$, of an optically active medium as a function of wavelength.

The angle of rotation, α , is related to the difference in the refractive indices for left and right circularly polarized light through equation 1-2:⁸

$$\alpha = \frac{(n_L - n_R)1800l}{\lambda_0} \tag{1-2}$$

where α is the angle of rotation in degrees, n_L and n_R are the refractive indices for left and right circularly polarized light respectively, l is the path length in decimeters, and λ_0 is the wavelength in a vacuum of the light beam in centimeters.

The observed angle of rotation, α , can then be used to calculate the specific rotation, $[\alpha]$, using the standard equation 1-3:⁸

$$[\alpha] = \frac{\alpha}{cl} \tag{1-3}$$

where α is the angle of rotation, with the unit in degrees, c is the concentration of the sample in g mL⁻¹, and l is the path length in decimeters.

All chiral substances exhibit a molecular refraction at almost any wavelength of irradiation. So in theory, ORD may be detected over all wavelengths, since it is based on the unequal refractive indices for left and right circularly polarized light. Most often, optical activity is detected and quantified at a single wavelength, such as 589 nm (sodium D-line). However, as with refractive index, ORD in and of itself does not allow for absolute stereochemical determination, since it is not possible to know based on the molecular structure of a compound which circularly polarized light component (right or left) will be affected more.

Another development related to ORD is circular dichroism (CD), which uses the absorption of the circular components as opposed to the refraction. When circularly polarized light passes through an optically active medium, the velocity of the left and right circularly polarized components are different, as well as the absorbance (equation 1-4). Circular dichroism is a measure of the difference in the molar absorptivity, $\Delta \varepsilon$, where ε_L and ε_R are the molar absorption coefficients for left and right circularly polarized light, respectively. Circular dichroism is observed when ε_L and ε_R are not equal.

$$\Delta \varepsilon = \varepsilon \iota - \varepsilon_R \neq 0 \tag{1-4}$$

Since circular dichroism describes the difference in absorption of the left and right circularly polarized light, it is to be expected that CD should occur near an absorption band. Thus, in order to observe a CD spectrum the chiral substance being studied needs to contain a chromophore. Since CD is related to absorbance, the shape and appearance

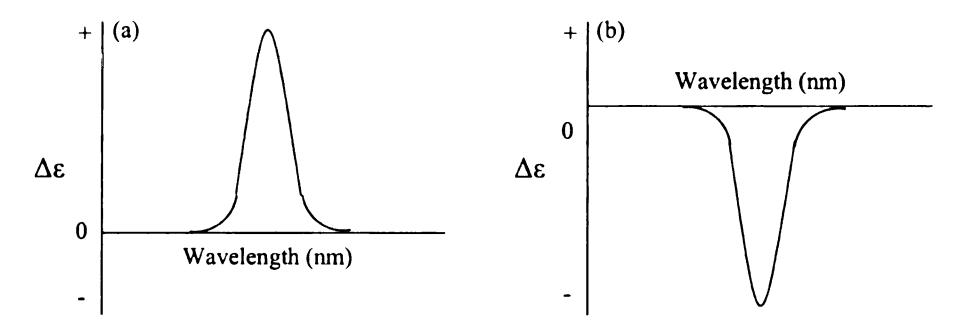


Figure 1-7. (a) Positive and (b) negative CD Cotton effects.

of a CD curve closely resembles that of a UV-Vis absorption curve. However, unlike ordinary UV-Vis absorption curves, CD curves may be positive or negative as they reflect the difference in absorbance (Figure 1-7). CD curves plot $\Delta \varepsilon$ vs. wavelength.⁸

Circular Dichroism (CD) and Optical Rotatory Dispersion (ORD) are two different observations of the same phenomenon. Since they are related, the molar amplitude a of ORD can be approximated by the intensity of a CD curve, $\Delta \varepsilon$, for the same molecule (Equation 1-5):¹¹

$$a \approx 40.28\Delta\varepsilon$$
 (1-5)

Physically, the phenomenon of CD can be explained through the interaction of the electric and magnetic transition dipole moments. When light is absorbed by a molecule, electrons are promoted from the ground state to an excited state, creating a momentary dipole. This dipole is known as the electric transition dipole moment and is denoted by the vector μ . In an achiral molecule, the overall net redistribution of electrons is planar, however, in a chiral molecule the electrons are redistributed in a helical fashion. For chiral molecules, this rotation of electric charge creates a magnetic field whose strength and direction may be described by the magnetic transition dipole moment, denoted by the vector m. The direction of the magnetic transition dipole moment m can be determined by the application of the "right hand rule" to the rotation of the electric charge: If the right hand fingers are curled in the direction of the charge, then the outstretched thumb points the direction of m (Figure 1-8). m

$$m \rightarrow m$$

Figure 1-8. Use of the "right hand rule" to determine magnetic transition dipole moment direction.

The sign and strength of a Cotton effect (CE), is given by the theoretical parameter R, designated the rotational strength. Rotational strength is determined from the scalar product of the electric and magnetic transition moments (equation 1-6):¹

$$R = \mu \bullet m = |\mu| m |\cos \beta \tag{1-6}$$

where μ and m are the electric and magnetic transition dipole moments, respectively, and β is the angle between the two transition moments. The sign of the CE is positive when the angle is acute $(0 < \beta < 90^{\circ})$ or parallel and it is negative when the angle is obtuse $(90^{\circ} < \beta < 180^{\circ})$ or antiparallel. So, if R > 0, a positive CD curve is observed, and if R < 0, a negative CD curve is observed. No Cotton effect is observed when the electric and magnetic transition dipole moments are perpendicular.

The interaction of the electric and magnetic dipole transition moments is seen clearly with hexahelicene (Figure 1-9). Upon excitation, the electrons flow in a helical manner as described above, following the path of the helix. The electric transition dipole moment μ is identical for each enantiomer, but the magnetic transition dipole moment

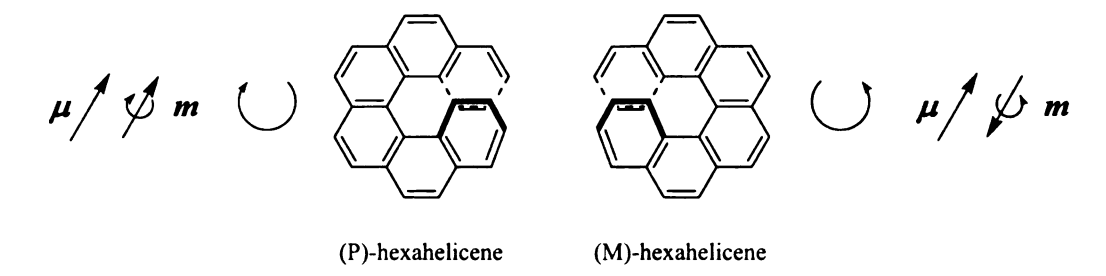


Figure 1-9. (P)-Hexahelicene and (M)-hexahelicene, showing the direction of current and the parallel [(P)-hexahelicene] and antiparallel [(M)-hexahelicene] transition moments.

direction m is reversed based on the "right hand rule". (P)-Hexahelicene has its electric and magnetic dipole transition moments parallel and (M)-hexahelicene antiparallel. Thus (P)-hexahelicene has a positive CE according to equation 1-6, and (M)-hexahelicene has a negative CE, leading to positive and negative CD spectra, respectively.

Both ORD and CD spectroscopy can be recorded by spectropolarimeters known as circular dichrometers. Circular dichrometers use a double monochromator to polarize the light beam linearly. This linearly polarized light is then passed through a modulator

to generate left and right circularly polarized light. The circularly polarized light is then passed through the sample, into a photomultiplier tube, and into an amplifier before being recorded as a CD spectrum. Most CD spectropolarimeters measure differential absorbance, ΔA , which is converted to $\Delta \varepsilon$ based on Lambert-Beer's Law (equation 1-7):

$$\Delta A = A_L - A_R = \Delta x c l \tag{1-7}$$

Although ORD and CD are phenomena only observed in chiral compounds, they still cannot be used for absolute stereochemical determination. Since the discovery of ORD and CD, much work has been undertaken to determine empirical rules. 14 semiempirical rules, such as sector or quadrant rules, ¹⁵ or quantum chemical calculations ^{16, 17} which permit a priori calculation of the ORD or CD of a given structure. However, to date no empirical or semi-empirical rules have been found to be valid for all molecules. Although many of the rules developed can be useful for stereochemical analysis, care must be taken not to apply the rules too liberally, and it must be understood that none of these rules allow for the determination of absolute stereochemistry. Quantum chemical calculations allow for the rotation angle of chiral molecules to be determined, and thus the absolute stereochemistry can be assigned for a given molecule by comparing the calculations with the experimental result. In one method, the contributions of all of the atoms of a molecule are calculated and used to determine the specific rotation angle for a given chiral molecule. 18, 19 This method has been of great use in assigning the absolute stereochemistry of large molecules with multiple chiral centers, including natural products, 20-22 as the structure of the compound is related to the sign and magnitude of the calculated optical rotation angle.²³ However, these methods are still being developed and it is yet to be shown if they are truly applicable for all situations.

1-1.3. Exciton-Coupled Circular Dichroism (ECCD)

Exciton-Coupled Circular Dichroism (ECCD)²⁴ is a method developed out of the principles of CD. Based on the coupled oscillator theory²⁵ and group polarizability theory,²⁶ ECCD is a non-empirical method which allows for the determination of the absolute stereochemistry of chiral compounds using the through-space exciton coupling between two or more chirally oriented non-conjugated chromophores. As shown in Figure 1-10, which presents the observed ECCD spectrum of a steroidal 2,3-bisbenzoate,²⁴ a typical ECCD spectrum is a bisignate curve. The peak (positive or negative) at longer wavelength is called the first Cotton effect, and subsequently, the peak (positive or negative) at shorter wavelength is called the second Cotton effect. If the sign of the first Cotton effect is positive, the ECCD spectrum is defined as positive, and if

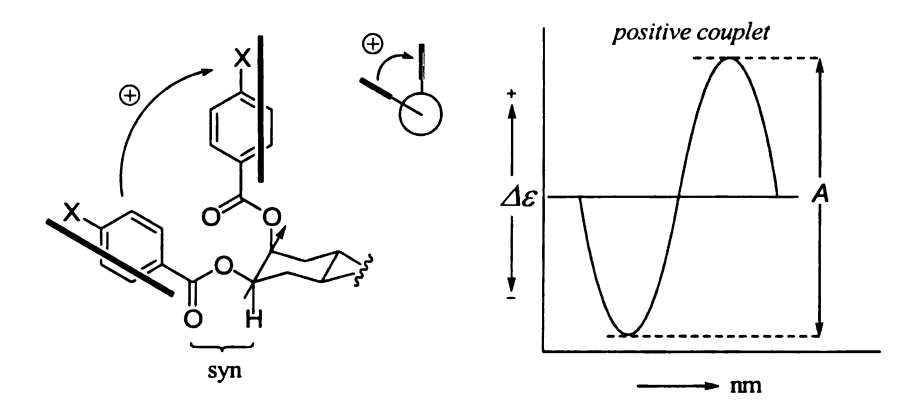


Figure 1-10. The observed ECCD spectrum of a steroidal 2,3-bisbenzoate.

the sign of the first Cotton effect is negative, then the sign of the ECCD spectrum is designated negative. The amplitude (A) of the ECCD spectrum is defined as $A = \Delta \varepsilon_l$ - $\Delta \varepsilon_2$ where $\Delta \varepsilon_l$ and $\Delta \varepsilon_2$ are the amplitudes of the first and second Cotton effect, respectively. The observed sign of the ECCD spectrum is dictated by the relative orientation of the chromophores in the chiral molecule. As seen in Figure 1-10, a

clockwise orientation of the two chromophores (looking from front to back) results in a positive ECCD curve, and a counterclockwise orientation will show a negative ECCD curve.²⁴

ECCD results from the interactions of two non-conjugated chromophores, as mentioned above. When the chromophores are identical, the most significant interaction occurs at the transitions which occur at the same energy. The through-space coupling of the electric transition dipole moments of these two chromophores generates one of two helices, depending upon whether they are in-phase (symmetric) or out-of-phase (antisymmetric), so a CD spectrum with two peaks is generated. This can be explained by examining the results of a 1,2-dibenzoate ester (Figure 1-11).¹²

Benzoate esters have a strong UV absorption band at about 230 nm resulting from

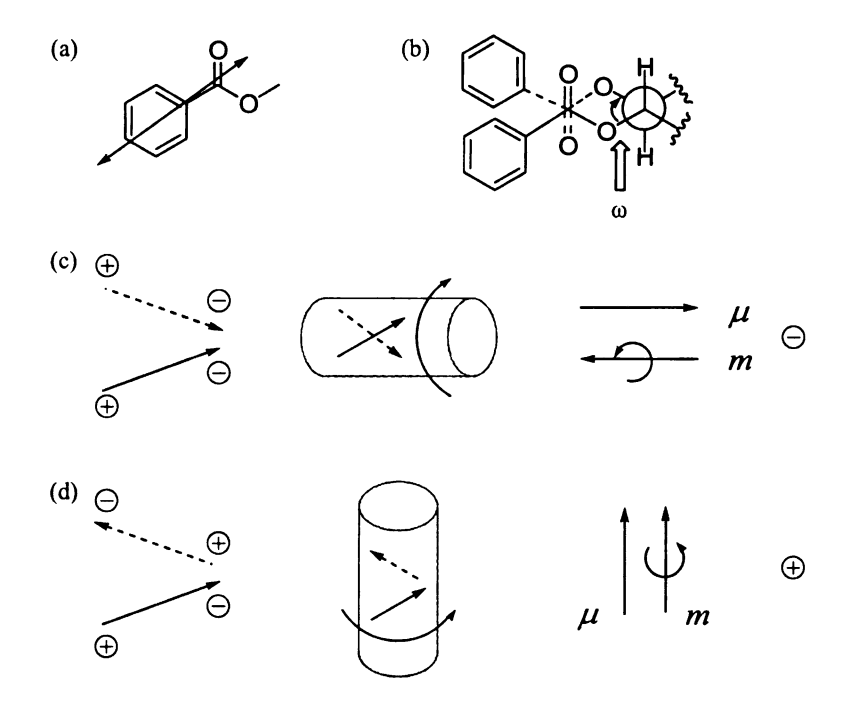


Figure 1-11. Qualitative explanation of ECCD using a dibenzoate ester. (a) Orientation of the electric transition dipole moment in dibenzoate esters; (b) Preferred conformation of a 1,2-dibenzoate with a positive dihedral angle, ω ; (c) In-phase combination of the electric transition dipole moments; (d) Out-of-phase combination of the electric transition dipole moments.

the $\pi \rightarrow \pi^*$ transition involving the benzene ring and the carbonyl of the ester group.²⁷ The electric transition dipole moment u of each benzoate group is approximately oriented along the long axis of the benzoate group and nearly parallel to the direction of the C-O ester bond (Figure 1-11a). The conformations of 1,2-dibenzoates are well known and orient either clockwise or counterclockwise depending on the chirality of the substrate. Figure 1-11b shows a 1,2-dibenzoate with the two benzoate groups oriented clockwise, leading to a dihedral angle ω which is positive and which correlates roughly to the angle between the two electric transition dipole moments of the two benzoates. The individual electric transition dipole moments μ couple both in-phase (symmetric) and out-of-phase (anti-symmetric) with the other chromophore's electric transition dipole moment (Figure 1-11c and d, respectively). When the two chromophores couple in-phase (Figure 1-11c) the overall electric transition dipole moment is oriented along the C2 axis of the two chromophores, and when the two chromophores couple out-of-phase (Figure 1-11d) the overall electric transition dipole moment is oriented perpendicular to the C2 axis. The helix associated with the charge rotation generated from the transition can be determined by visualizing each chromophores' electric dipole transition moment placed on the outside of a cylinder with the cylinder aligned along the axis of the overall electric transition dipole moment. Using the right hand rule, m can be determined by following the helix described around the cylinder by the individual electric transition dipole moments. For Figure 1-11c, the electric transition dipole moment μ and the resultant magnetic transition dipole moment m are oriented antiparallel to each other, and according to equation 1-6, $R = \mu \bullet m = |\mu| |m| \cos \beta$, this leads to a negative Cotton effect and thus a negative CD band. For Figure 1-11d, the electric transition dipole moment

 μ and the resultant magnetic transition dipole moment m are oriented parallel to each other, leading to a positive Cotton effect and a positive CD band. Thus, the two CD bands generated from the through-space coupling of the electric transition dipole moments of the dibenzoate have equal magnitude but opposite sign. The observed bisignate ECCD curve thus results from the overlapping of the positive and negative CD bands occurring very close in energy.

Which CD band, positive or negative, occurs at lower energy is determined by the phasing of the coupling. Repulsion between poles of the same sign (Figure 1-11c) creates in-phase coupling that is higher in energy than the out-of-phase coupling (Figure 1-11d), where the poles of opposite sign are closest together. Consequently, the CD band associated with the out-of-phase mode (in this example, positive) is at longer wavelengths than the CD band resulting from the in-phase mode (in this example, negative). Since the positive CD band is at the longer wavelength than the negative CD band, for the absolute configuration shown in Figure 1-11b, the bisignate couplet is designated positive (Figure 1-12).

The above demonstration can be performed for chromophores in a

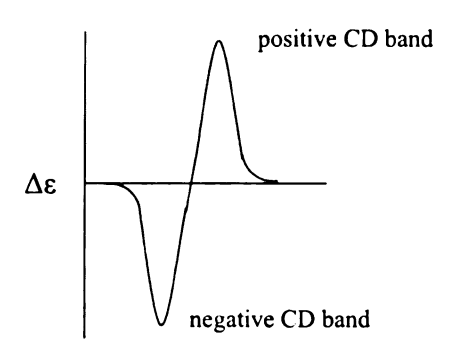


Figure 1-12. Bisignate ECCD curve expected from the example given in Figure 1-11.

counterclockwise conformation as well. Thus, the sign of an ECCD spectrum can be correlated to the orientation of the interacting chromophores. For chromophores oriented clockwise, the observed ECCD bisignate will always be positive, and for chromophores oriented counterclockwise, the observed ECCD bisignate will always be negative (Figure 1-13).²⁸ Thus when the orientation of the chromophores is known the ECCD bisignate curve can be predicted and *vice versa*.



Figure 1-13. Possible orientations of chromophores (clockwise and counterclockwise) and their corresponding ECCD signs.

1-1.4. ECCD Based on Quantum Mechanics

ECCD can also be explained by quantum mechanical theories. When a molecule contains two identical non-conjugated chromophores, because of the through-space interactions, excitation is delocalized between the two chromophores and the excited state

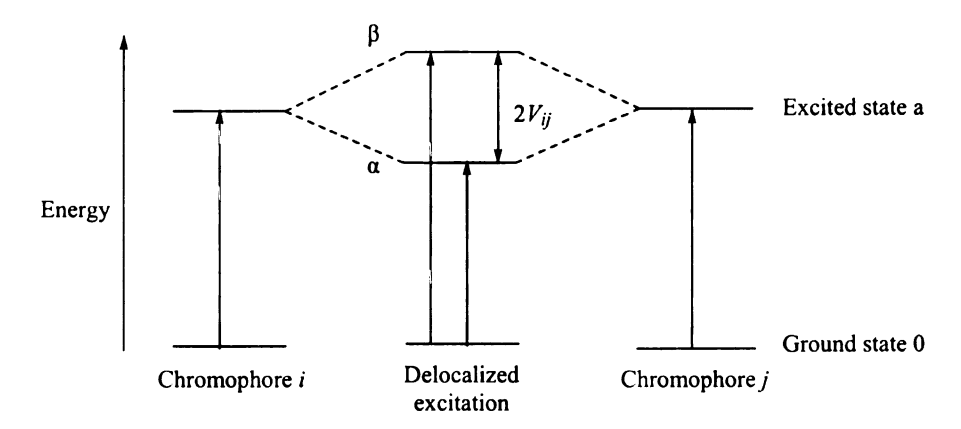


Figure 1-14. Splitting of the two excited states of non-conjugated chromophores i and j by exciton interaction. The energy gap V_{ij} is known as Davydov splitting.

(exciton)²⁹ is split into two states, α and β , by resonance interaction of the local excitations (Figure 1-14). The energy gap between the two excited states is designated $2V_{ij}$, and is known as Davydov splitting.²⁴

For a binary system, the rotational strength, R, which is a theoretical parameter representing the sign and strength of a CD Cotton effect, can be approximated as equation 1-8:²⁴

$$R_{\alpha}, \beta = \pm (\frac{1}{2})\pi\sigma_{o}\vec{R}_{ij} \bullet (\vec{\mu}_{ioa} \times \vec{\mu}_{joa})$$
 (1-8)

where the positive and negative signs correspond to the α - and β - state, respectively, \vec{R}_{ij} is the distance vector from chromophore i to j, $\vec{\mu}_{ioa}$ and $\vec{\mu}_{joa}$ are the electric transition dipole moments for excitation from the ground state to excited state a of chromophores i and j, respectively, and σ_0 is the excitation number of transition from the ground state to excited state a, which can be expressed as: $\sigma_0 = v_0 / c = (E_a - E_0)/(hc)$, where h is Planck's constant and c is the speed of light in vacuum. As is evident from equation 1-8, the Cotton effect of the α - and β - state have identical rotational strength of opposite sign, leading to a bisignate CD spectrum with two Cotton effect peaks of opposite signs, which are separated by the energy gap (Davydov splitting) (Figure 1-12).

The sign and amplitude of the bisignate ECCD spectrum is theoretically defined in equation 1-9 as:²⁴

$$\vec{R}_{ij} \bullet (\vec{\mu}_{ioa} \times \vec{\mu}_{joa}) V_{ij} \tag{1-9}$$

where \vec{R}_{ij} is the distance vector from chromophore i to j, $\vec{\mu}_{ioa}$ and $\vec{\mu}_{joa}$ are the electric transition dipole moments for excitation from the ground state to excited state a of chromophores i and j, respectively, and V_{ij} is the interaction energy between the two

chromophores i and j. If equation 1-9 is positive, the observed ECCD spectrum is defined as positive, and if it is negative, then the observed ECCD spectrum is defined as negative. Thus it is clear that the sign of the bisignate curve depends entirely on the spatial orientation of the two chromophores (Table 1-1).^{28,30}

Qualitative Definition	Quantitative Definition	Cotton effects	
	$ec{R}_{ij}ullet (ec{\mu}_{loa}\! imes\!ec{\mu}_{joa})V_{ij}>0$	positive first and negative second Cotton effects	
\$	$ec{R}_{ij}ullet (ec{\mu}_{ioa}\! imes\!ec{\mu}_{joa})V_{ij}< 0$	negative first and positive second Cotton effects	

Table 1-1. Definition of positive and negative exciton chirality for a binary system.

The amplitude (A) of the ECCD couplet, defined as the difference in $\Delta\varepsilon$ between the first and second Cotton effects of the couplet, is affected by the number of interacting chromophores, the molar absorptivity coefficient of the chromophores, the distance between the chromophores, and the projection angle between the chromophores.³¹ The number of interacting chromophores (x, y, z) affects A in an additive effect, such that A for the whole molecule is determined by the sum of A of each interacting pair, i.e., $A_{molecule} = A_{xy} + A_{yz} + A_{xz}$. This has proven to be true through experimental and theoretical testing of systems with multiple chromophores.³²⁻³⁴ Since A is proportional to the square of the molar absorptivity coefficient (ε) of the chromophores, chromophores with strong absorption lead to greater sensitivity for ECCD. A is also inversely proportional to R^2 , where R is the distance between chromophores. Consequently it is beneficial to have the chromophores oriented close to each other in space. A is at a maximum when the

projection angles between chromophores is close to 70°, as a result it is beneficial to use systems which allow for the orientation of the chromophores close to this angle.

1-2. Use of ECCD to Determine the Absolute Stereochemistry of Chiral Molecules

Since ECCD is a based on quantum mechanical principles as shown in the previous section, the absolute stereochemistry of chiral molecules which display ECCD can be determined non-empirically. Due to the sensitivity of the method, ECCD can be utilized with samples as small as micrograms, making it ideal for stereochemical determination of rare natural products and newly synthesized compounds. ECCD has been used for the absolute stereochemical determination of many types of compounds, including polyols, 35 carbohydrates, 36 quinuclidines, 37 hydroxy acids, 38 and others. 39

1-2.1. Use of Chromophoric Hosts for ECCD of Non-chromophoric Chiral Molecules

ECCD is an effective method for assigning the absolute stereochemistry of chiral compounds in a non-empirical fashion, yet molecules must contain two interacting, non-conjugated chromophores in order to display ECCD. This limits the use of ECCD to only a very small subset of chiral compounds. To circumvent this problem and make ECCD amenable to more chiral molecules, chromophoric molecules have been designed to act as hosts for chiral molecules without chromophores. The chiral molecule is introduced as a guest to the host chromophoric molecule. Through covalent or non-covalent binding,

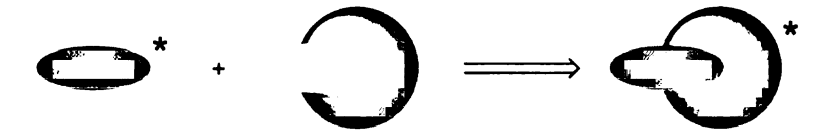


Figure 1-15. A chiral (denoted by an asterisk) guest molecule can complex with an achiral host chromophore to produce a chiral complex capable of generating ECCD.

the host is designed to adopt a chiral conformation based on the chirality of the guest molecule (Figure 1-15). The chiral conformation of the host chromophoric molecule is then observed as an ECCD bisignate curve.

Chiral induction is not a new phenomenon, and in fact was used with polypeptides bound to dyes to probe changes in the helical conformations.⁴⁰ Induction of chirality through intermolecular forces between two molecules has also been used for probing the conformations of macromolecules.⁴¹ Chiral induction requires two processes to occur between the molecules: (1) complex formation and (2) some dynamic process or processes associated with the formation of the complex, such as conformational changes of the interacting molecules.⁴²⁻⁴⁴ If the steric or electronic interactions between two molecules are strong enough, chiral information will be transferred from one to the other.

In order to simplify the observed ECCD, most chromophoric hosts used for ECCD studies are achiral. However, upon binding to a chiral substrate, the chromophoric host will adopt an induced chirality dictated by the chirality of the substrate. This induced chirality of the complex can then be monitored by ECCD and used to determine the absolute stereochemistry of the chiral guest molecule. As mentioned previously, binding between the host and guest molecules can be either covalent or non-covalent,

Br HO OH Br H H H H H
$$O_{2}N \qquad NO_{2} \qquad H \qquad Br \qquad O_{2}N \qquad NO_{2}$$

$$R = -CH_{2}CH_{2}t\text{-Bu}$$

$$O_{2}N \qquad NO_{2}$$

Figure 1-16. Complexation between racemic biphenol 1 and chiral diamine 2 leading to a chiral complex.

depending on the nature of the complex being formed. One example of non-covalent complex formation can be seen in Figure 1-16.⁴⁵ In this example, the racemic biphenol 1 hydrogen bonds to the chiral diamine 2,⁴⁶⁻⁴⁸ forming a new chiral complex. In the absence of chiral induction, biphenol 1 has two chiral conformations which rapidly interconvert. Formation of the complex causes rotation about the C-C biphenyl bond, locking it into a single conformation. Although it would appear that the phenyl rings are conjugated and would not show ECCD, steric interactions between the substituents on the phenyl rings cause the rings to be nonplanar, and therefore non-conjugated and able to undergo exciton coupling. Thus the ECCD spectrum that is observed reflects the absolute stereochemistry of chiral diamine 2.

Covalent bonding has been used to form chiral complexes of binaphthalenes to determine the absolute stereochemistry of chiral secondary alcohols (Scheme 1-1).⁴⁹ The chromophoric reagent, 3-cyanocarbonyl-3'-methoxycarbonyl-2,2'-binaphthalene 3 is used to esterify the chiral secondary alcohol and the resultant complex exhibits induced ECCD as a result of favoring one atropisomer due to restricted rotation about the C-C phenyl bonds. The chirality of the secondary alcohol favors one atropisomer due to steric interactions between the methyl ester and the new chiral ester leading to induction of chirality to the binaphthalene system.⁴⁹

Scheme 1-1. Esterification of binaphthalene 3 with a chiral secondary alcohol.

1-2.2. Porphyrins as Chromophoric Receptors

Some of the most widely used chromophoric receptors are porphyrins or porphyrin derivatives, due to several properties which make them highly suitable for chiral recognition.⁵⁰ Porphyrins have an ideally situated absorption band near 418 nm for their main absorption band (known as the Soret band). This absorption band can vary depending on the substituents on the porphyrin. Since this absorption band is much lower in energy than most other chromophores, the chance of unwanted interactions between the porphyrin and any chromophores in the guest molecule is unlikely. Not only do they absorb at low energy, porphyrins are also strong chromophores with a molar absorptivity coefficient (ε) of 400,000 or higher. Since the amplitude of the observed ECCD bisignate is proportional to ε^2 , a larger molar absorptivity coefficient for the host chromophore leads to enhanced sensitivity in ECCD, allowing for the use of smaller sample amounts. This enhanced sensitivity also makes the porphyrins able to detect subtle changes in their environment, including the binding of chiral ligands, which can be followed by UV-Vis, fluorescence, NMR, and resonance Raman spectroscopy. 50 Porphyrins have a central core consisting of four nitrogens which may incorporate a variety of metals with different properties and sizes. This metal core can then also be used for binding chiral guest molecules. Porphyrins with no metal or small metal cores are generally planar structures with a well-defined binding pocket in the center, which can be enhanced by substituents on the outside of the porphyrin ring. There are many sites that can be derivatized such as the *meso* and β -positions, the central metal and the inner nitrogen atoms. Adjusting the substituents on the porphyrin can also control solubility for use in both polar and non-polar solvents.

As with other molecules, porphyrins can be both achiral and chiral due to the steric effects of outer substituents on the conformation of the porphyrin ring (Figure 1-17).⁵¹ Achiral porphyrins tend to be planar molecules, while the chiral porphyrins are usually "saddle" shaped where two sides point up and two sides point down. Achiral porphyrins have found wide use in stereochemical studies with circular dichroism for absolute configurational assignments, ⁵²⁻⁵⁴ stereochemical differentiations of sugars and amino acids, ^{55, 56} and interactions with bio-macromolecules. ^{57, 58}

Figure 1-17. Examples of an achiral porphyrin and an inherently chiral porphyrin.

Porphyrins are used extensively in UV-Vis and CD spectroscopy due to their redshifted absorption band and their strong molar extinction coefficient (ε). The most intense band around 415 nm in the near ultraviolet is the B band, usually called the Soret band. Additional bands (N, L, M bands) in the ultraviolet region may be observed but these bands are usually much weaker. Substituents on the outside ring of the porphyrin usually have a small effect on the energy of the absorbance of the Soret band, depending on the type and position of the substituents. If the molar absorption coefficient is known for a given porphyrin, the concentration of the solution can be calculated using the observed absorbance and Beer-Lambert's law, $A = \varepsilon cl$.

Porphyrin free base generally has four absorption bands (Q bands) in the visible region due to π - π * transitions. Upon metallation of the porphyrin core, the four Q bands

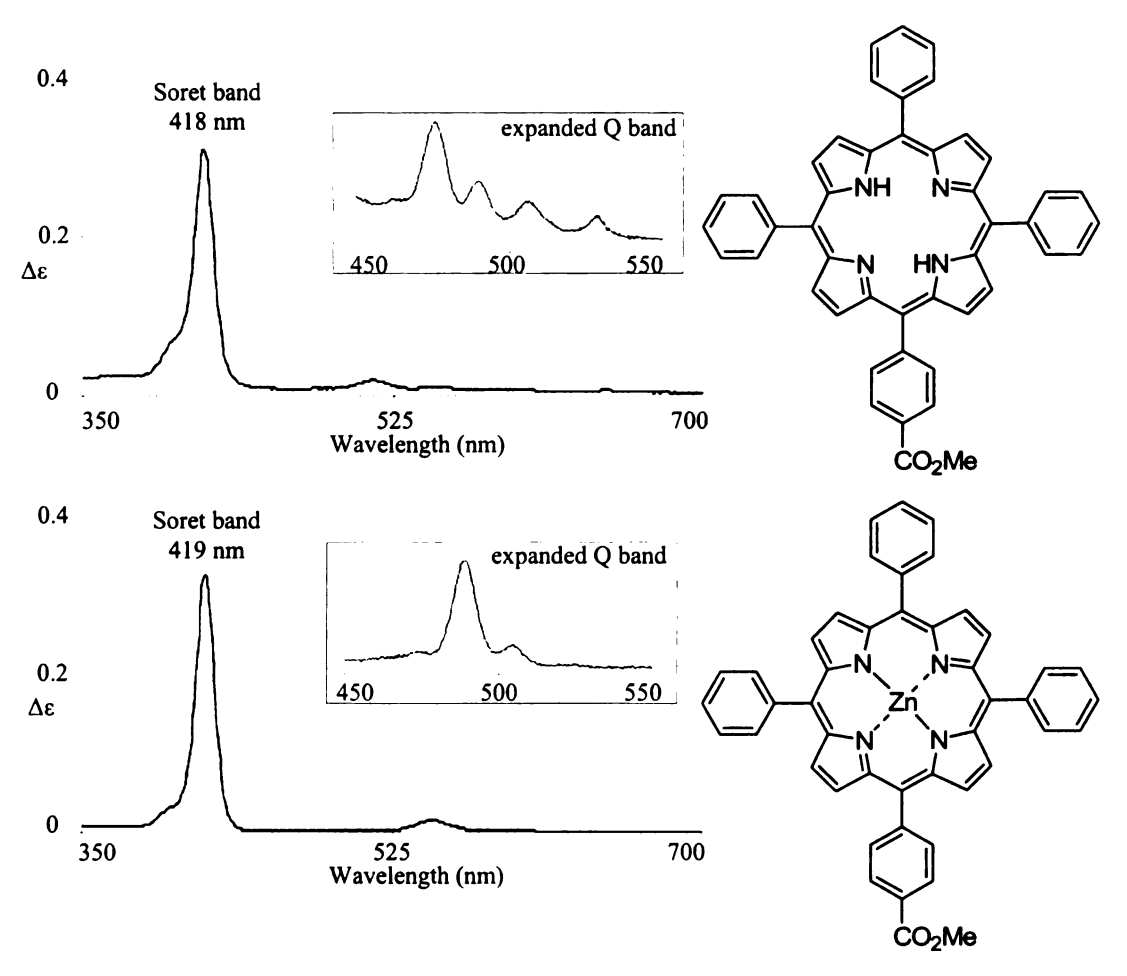


Figure 1-18. UV-vis spectra of tetraphenylporphyrin methyl ester and zinc tetraphenylporphyrin methyl ester showing changes in the O band upon metallation.

in the visible region collapse into essentially two bands due to higher symmetry, while the Soret band may remain in the usual range or shift to higher or lower energy (Figure 1-18). The molar absorption coefficient (ε) of the Soret band also changes with the insertion of metals into the porphyrin core. For example, zinc porphyrin methyl ester (ε =550,000)⁵⁹ has a higher molar absorption coefficient than the corresponding porphyrin free base (ε =440,000)⁶⁰ and the position of this band is also slightly red shifted (Figure 1-18).

Although useful for UV-Vis and CD studies, single porphyrins are not useful as host chromophores for ECCD due to the lack of a second chromophore that will absorb at

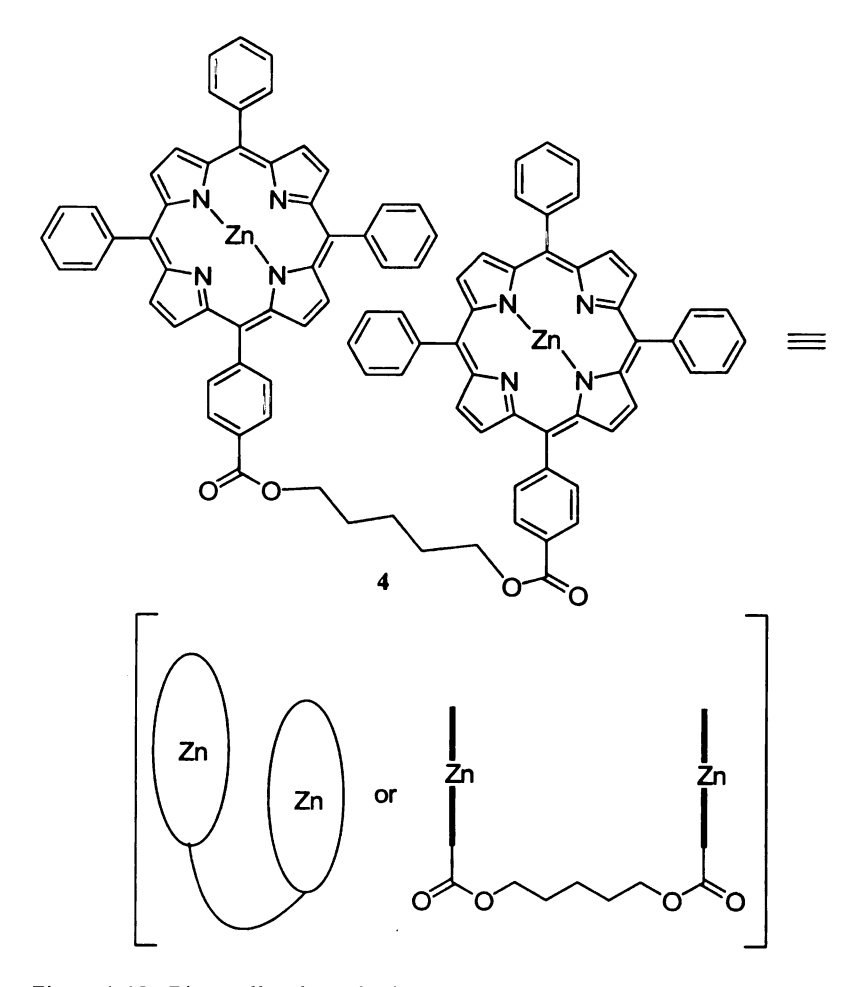


Figure 1-19. Bismetallated porphyrin tweezer 4 and shorthand representations.

a similar energy. However, recently bismetalloporphyrin systems have been developed specifically for use with ECCD (Figure 1-19). These compounds are achiral and present an ideal environment for chiral guest molecules to bind, creating a chiral complex that can then be monitored by ECCD and used to determine the absolute stereochemistry of the guest molecules.⁶¹⁻⁶⁶

Zinc porphyrin tweezer 4 (Figure 1-19) was originally designed for use in the absolute stereochemical determination of chiral diamines. This host molecule can undergo host-guest complexation through the zinc centers of the porphyrins. The porphyrin tweezer then adopts a chirally oriented conformation leading to a bisignate ECCD spectrum revealing the helical nature of the chromophores. This helicity can then be related back to the structure of the guest chiral diamine. As shown in Figure 1-20,

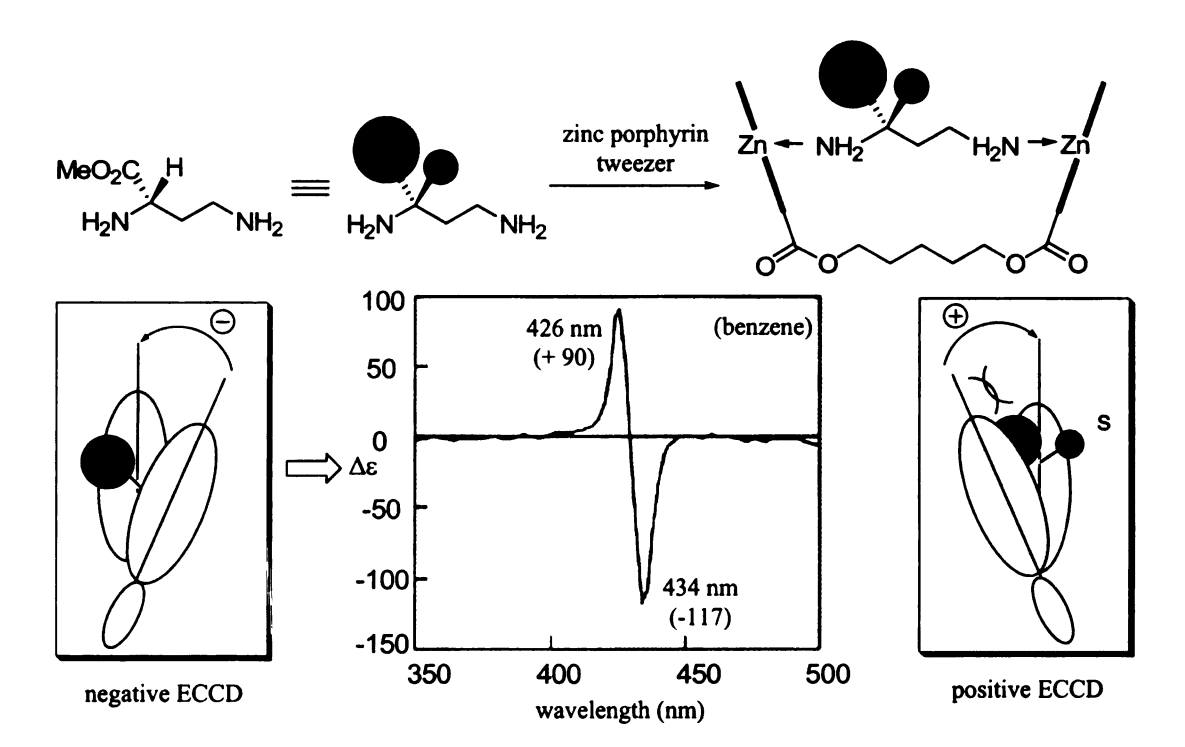


Figure 1-20. Example of stereochemical determination for chiral diamines complexed to zinc porphyrin tweezer 4 using ECCD.

when zinc porphyrin tweezer 4 is added to a solution of chiral diamine (S)-methyl-2,4-diaminobutyrate, the chiral diamine binds to the zinc centers of the porphyrin tweezer through Zn-N coordination to form a complex where the chiral guest is held in between the two porphyrin chromophores. The porphyrin which is farther away from the chiral center does not interact with the chiral center and merely coordinates to the primary amine. However, the porphyrin coordinated to the amine closest to the chiral center interacts with the groups on the chiral center. Due to steric interactions, the porphyrin closest to the chiral center prefers to slide away from the large group and cover the small group (Figure 1-20a). This conformation is more stable than the alternate (Figure 1-20b), in which the porphyrin has strong steric interactions with the large group. The more stable conformation (a), leads to the two porphyrin planes adopting a counterclockwise orientation and a negative ECCD couplet is predicted, which matches the observed ECCD (Figure 1-20, center).

The diamine approach has been extended to determine the absolute stereochemistry of chiral amino acids and amino alcohols, which have a primary amino group directly attached to the stereogenic center.⁶¹ Although not able to act as guest molecules since they only contain one amine group, simple chemical modifications

Scheme 1-2. Conversion of amino acids and amino alcohols for use as diamine guests for the host porphyrin tweezer 4.

convert these compounds into diamines (Scheme 1-2), making them suitable for use with the method described above.

As was evident with the above examples, molecules with only one site of attachment are not suitable for use with zinc porphyrin tweezer 4 since the porphyrins need to be aligned such that they can interact through space for exciton coupling to occur. To overcome this problem, molecules have been designed to convert compounds with only one site of attachment to molecules possessing two sites of attachment. These molecules are known as carriers, and are achiral molecules which can be used to create derivatives of the chiral substrates which have two sites of attachment. In order to be effective, carriers need to have a functional group that can react with the chiral compounds to form a derivative, *i.e.*, a carboxylic acid can be coupled with a chiral amine or alcohol. The carrier molecules should also be rigid, since flexible structures will lead to a molecule with multiple possible conformations which could create difficulties in the interpretation of the ECCD data. The carriers should be achiral to avoid the formation of diastereomers which will also interfere with interpretation of the ECCD data. Finally, the derivatized molecules should be able to bind to zinc porphyrin tweezer 4 or another desired host in a 1:1 ratio.⁶²

Ideally, each guest molecule will bind with the host porphyrin tweezer in only one conformation. However, this is most often not the case, and the lowest energy conformation for the complex must be determined in order to accurately determine the stereochemistry of the guest molecule. The conformation of the complex is dependent on the conformation of the guest molecule, thus an ideal carrier generates a rigid and predictable conformation with any derivative chiral molecules. Too many degrees of

Figure 1-21. Carrier 5 reacts with (S)-1-cyclohexylethylamine to form conjugate 6, which has a preferred conformation where the carbonyl is *anti* to the pyridine nitrogen and the small group (hydrogen) of the chiral center is *syn* to the carbonyl.

freedom in the derivatized compounds will lead to multiple ECCD signals due to varying interactions of the porphyrins with the groups on the chiral center. Because of this necessity for rigidity, carrier 5 was designed and synthesized in order to determine the absolute stereochemistry of chiral monoamines complexed with zinc porphyrin tweezer 4 (Figure 1-21).⁶² This carrier can be derivatized with chiral monoamines through coupling of the carboxylic acid functionality to form an amide bond. After removal of the Boc protecting group, the derivatized monoamine has two nitrogens available for binding to zinc porphyrin tweezer 4. Based on the knowledge of amide bond rotation, the conformation of the derivatized monoamine can be predicted with relative confidence. This conjugate can bind to the zinc porphyrin tweezer to form a complex, the stereochemistry of which can be assigned based on the observed ECCD spectrum. Derivatization of (S)-1-cyclohexylethylamine with carrier 5, followed by deprotection, leads to conjugate 6 with two nitrogen atoms, the pyridine nitrogen and the free amino nitrogen, able to bind to both zinc centers of porphyrin tweezer 4. Molecular modeling of conjugate 6 suggests that it is a rigid molecule which has a predictable low energy conformation. 62 In the most favorable conformation, the free rotations around the single

bonds C_{Aryl} - $C_{C=0}$, $C_{C=0}$ -NH, and NH- C_{chiral} are restricted. Molecular modeling has also shown that conjugate 6 favors a coplanar orientation of the carbonyl group to the pyridine ring, yet due to electrostatic repulsion, the conformation with the carbonyl oxygen *anti* to the pyridine nitrogen is preferred by ~30 kJ/mol. It is also well known that in most amides, the small group prefers to be *syn* to the carbonyl oxygen due to pseudo A-1,3 interactions between the carbonyl oxygen and the groups on the carbon attached to the nitrogen.

Since the conformation of conjugate 6 is known with relative certainty, the orientation of the porphyrins in the host-guest complex can be similarly determined. The

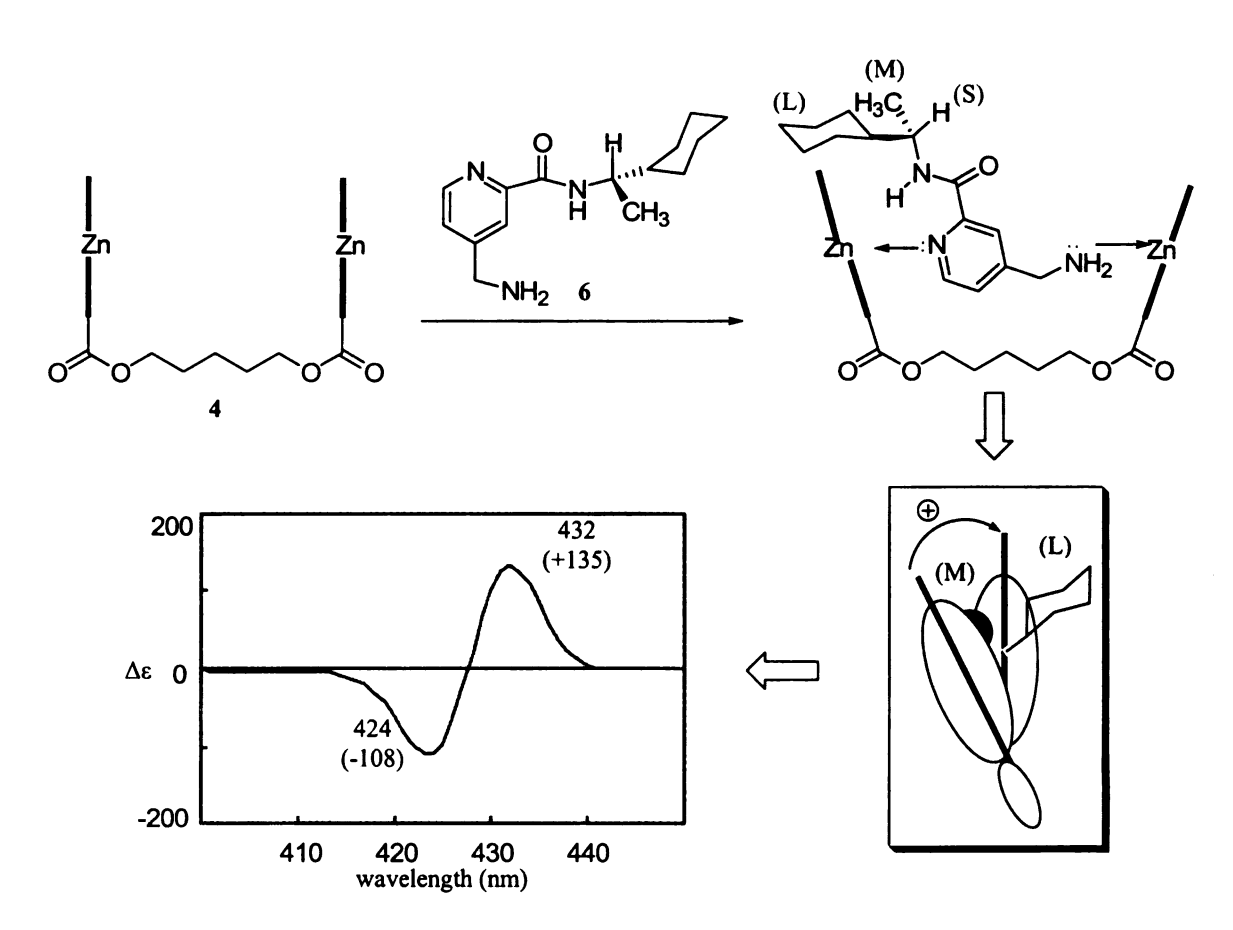


Figure 1-22. Complexation of conjugate 6 with tweezer 4 leading to the most favored conformation for the complex and the observed ECCD spectrum.

three substituent groups at the chiral center are assigned S (small), M (medium), and L (large) according to their size, with hydrogen being the S group, methyl being the M group and cyclohexyl being the L group (Figure 1-22). Upon binding to zinc porphyrin tweezer 4, the zinc porphyrin's approach to the pyridine nitrogen will favor approaching the side of the M group in order to avoid unfavorable steric interactions with L. Thus, the two porphyrin planes of the tweezer orient in a clockwise way, and dictate a positive ECCD spectrum. This prediction matches the experimental observation (Figure 1-22).

The previous work that has been done has introduced the concept of using porphyrin tweezers for absolute stereochemical determination with ECCD. However, the compounds that this method has been extended to are not diverse. Ideally, we would like to develop a system that will allow for the absolute stereochemical determination of any molecule using ECCD. Our work presented in this dissertation has focused on extending the previous work done with porphyrin tweezer 4 to include other porphyrin tweezers as well as determining the conformations of the complexes formed between porphyrin tweezers and their guest molecules. We have focused on using molecular modeling to probe the dynamics of these complexes and explore the effects of different carriers for molecules with one site of attachment. We have also explored the synthesis and ECCD of novel porphyrin tweezers with various linkers. Finally, we have probed the possibility of using metal complexes, specifically Ru(bpy)₂Cl₂, for complexation with *erythro* diols to facilitate the use of ECCD with these molecules.

References:

- 1. Eliel, E. L.; Wilen, S. W.; Mander, L. N., Stereochemistry of Organic Compounds. Wiley: New York, 1994.
- 2. Bruice, P. Y., Organic Chemistry. 3rd ed.; Prentice-Hall, Inc.: Upper Saddle River, New Jersey, 2001.
- 3. Rossi, R.; Diversi, L. Synthesis 1973, 25.
- 4. Laarhoven, W. H.; Prinsen, W. J. C. Top. Curr. Chem. 1984, 125, 63.
- 5. Eliel, E. L., Stereochemistry of Carbon Compounds. McGraw-Hill: New York, 1962.
- 6. Humpf, H.-U.; Berova, N.; Nakanishi, K.; Jarstfer, M. B.; Poulter, C. D. J. Org. Chem. 1995, 60, 3539.
- 7. Dale, J. A.; Mosher, H. S. J. Am. Chem. Soc. 1973, 95, 512-519.
- 8. Lambert, J. B.; Shurvell, J. F.; Lightner, D. A.; Cooks, R. G., Organic Structural Spectroscopy. Prentice Hall: Upper Saddle River, 1998.
- 9. Solomon, T. W. G., Organic Chemistry. John Wiley & Sons. Inc.: New York, 1978.
- 10. Velluz, L.; LeGrand, M.; Grosjean, M., Optical Circular Dichroism. Academic Press Inc.: New York, 1965.
- 11. Mislow, K.; Glass, M. A. W.; O'Brien, R. E.; Rutkin, P.; Steinberg, D. H.; Weiss, J.; Djerassi, C. J. Am. Chem. Soc. 1962, 84, 1455.
- 12. Snatzke, G. Angew. Chem. Int. Ed. Engl. 1979, 18, 363.
- 13. Nogrady, M., Stereochemistry. Pergamon Press Ltd.: Oxford, 1981.
- 14. Moffitt, W.; Woodward, R. B.; Moscowitz, A.; Klyne, W.; Djerassi, C. J. Am. Chem. Soc. 1961, 83, 4013.
- 15. Snatzke, G., Optical Activity and Chiral Discrimination. Reidel, Dordrecht, and Neatherlands: 1979.
- 16. Polavarapu, P. L. Molec. Phys. 1997, 91, 551.
- 17. Polavarapu, P. L.; Chakraborty, D. K. J. Am. Chem. Soc. 1998, 120, 6160.
- 18. Kondru, R. K.; Wipf, P.; Beratan, D. N. Science 1998, 282, 2247.
- 19. Kondru, R. K.; Lim, S.; Wipf, P.; Beratan, D. N. Chirality 1997, 1997, 469.

- 20. Kondru, R. K.; Chen, C. H.; Curran, D. P.; Beratan, D. N.; Wipf, P. *Tetrahedron: Asymmetry* **1999**, *10*, 4143.
- 21. Kondru, R. K.; Beratan, D. N.; Friestad, G. K.; Smith, A. B.; Wipf, P. Org. Lett. **2000**, *2*, 1509.
- 22. Ribe, S.; Kondru, R. K.; Beratan, D. N.; Wipf, P. J. Am. Chem. Soc. 2000, 122, 4608.
- 23. Kondru, R. K.; Wipf, P.; Beratan, D. N. J. Phys. Chem. A 1999, 103, 6603.
- 24. Harada, N.; Nakanishi, K., Circular Dichroic Spectroscopy: Exciton Coupling in Organic Stereochemistry. University Science Books: Mill Valley, 1983.
- 25. Kuhn, W. Transactions of the Faraday Society 1930, 26, 293.
- 26. Kirkwood, J. G. J. Chem. Soc. 1937, 5, 479.
- 27. Wiesler, W. T.; Vazquez, J. T.; Nakanishi, K. J. Am. Chem. Soc. 1987, 109, 5586.
- 28. Harada, N.; Chen, S.-M. L.; Nakanishi, K. J. Am. Chem. Soc. 1975, 97, 5345.
- 29. Chen, S.-M. L.; Harada, N.; Nakanishi, K. J. Am. Chem. Soc. 1974, 96, 7352.
- 30. Harada, N.; Nakanishi, K. Acc. Chem. Res. 1972, 5, 257.
- 31. Weckerle, B.; Schreiber, P.; Humpf, H.-U. J. Org. Chem. 2001, 68, 8160.
- 32. Dong, J.-G.; Akritopoulou-Aanae, I.; Guo, J.; Berova, N.; Nakanishi, K.; Harada, N. Enantiomer 1997, 2, 397.
- 33. Liu, H. W.; Nakanishi, K. J. Am. Chem. Soc. 1981, 103, 7005.
- 34. Lichtenthaler, F. W.; Sakakibara, T. Carbohydr. Res. 1977, 59, 47.
- 35. Rele, D.; Zhao, N.; Nakanishi, K.; Berova, N. Tetrahedron 1996, 52, 2795.
- 36. Wiesler, W. T.; Nakanishi, K. J. Am. Chem. Soc. 1989, 111, 9205.
- 37. Zhao, N.; Berova, N.; Nakanishi, K.; Rohmer, M.; Mougenot, P.; Jurgnes, U. J. *Tetrahedron* **1996**, *52*, 2777.
- 38. Gimple, O.; Schreiber, P.; Humpf, H.-U. Tetrahedron: Asymmetry 1997, 8, 11.
- 39. Nakanishi, K.; Berova, N., Circular Dichroism. Principles and Applications. VCH Publishers: New York City, 1994.
- 40. Blout, E. R.; Stryer, L. *Proc. Natl. Acad. USA* **1959**, *45*, 1591.

- 41. Stryer, L.; Blout, E. R. J. Am. Chem. Soc. 1961, 83, 1411.
- 42. Beer, P. D.; Rothin, A. S. J. Chem. Soc., Chem. Commun 1988, 52.
- 43. Hayashi, T.; Asai, T.; HoKazono, H.; Ogoshi, H. J. Am. Chem. Soc. 1993, 115, 12210.
- 44. Mizutani, T.; Yagi, S.; Honmaru, A.; Ogoshi, H. J. Am. Chem. Soc. 1996, 118, 5318.
- 45. Mizutani, T.; Takagi, H.; Hara, O.; Horiguchi, T.; Ogoshi, H. *Tetrahedron Lett.* **1997,** *38*, 1991.
- 46. Hanessian, S.; Gomtsyan, A.; Simard, M.; Roelens, S. J. Am. Chem. Soc. 1995, 117, 7630.
- 47. Kramer, R.; Zundel, G. J. Chem. Soc., Faraday Trans. 1990, 86, 301.
- 48. Bell, C. L.; Barrow, G. M. J. Chem. Phys. 1959, 36, 5.
- 49. Hosoi, S.; Kamiya, M.; Ohta, T. Org. Lett. 2001, 3, 3659.
- 50. Ogoshi, H.; Mizutani, T. Acc. Chem. Res. 1998, 31, 81.
- 51. Mizutani, T.; Ema, T. J. Am. Chem. Soc. 1994, 116, 4240.
- 52. Matile, S.; Berova, N.; Nakanishi, K. Enantiomer 1996, 1, 1.
- 53. Matile, S.; Berova, N.; Nakanishi, K. J. Am. Chem. Soc. 1995, 117, 7021.
- 54. Arimori, S.; Takeuchi, M.; Ahinkai, S. J. Am. Chem. Soc. 1996, 118, 245.
- 55. Crossley, M. J.; Hambley, T. W.; Mackay, L. G.; Try, A. C.; Walton, R. J. Chem. Soc., Chem. Commun. 1995, 1077.
- 56. Crossley, M. J.; Mackay, L. G.; Try, A. C. J, Chem. Soc., Chem. Commun. 1995, 1925.
- 57. Suenaga, H.; Arimori, S.; Shinkai, S. J, Chem. Soc., Perkin Trans. 2 1996, 607.
- 58. Foster, N.; Singhal, A. K.; Smith, M. W.; Marcos, N. G.; Schra, K. J. *Biochim. Biophys. Acta.* **1988**, *950*, 118.
- 59. Matile, S.; Berova, N.; Nakanishi, K.; Fleischhauer, J.; Woody, R. W. J. Am. Chem. Soc. 1996, 118, 5198.

- 60. Rickman, B. H.; Matile, S.; Nakanishi, K.; Berova, N. Tetrahedron 1998, 54, 5041.
- 61. Huang, X. F.; Rickman, B. H.; Borhan, B.; Berova, N.; Nakanishi, K. J. Am. Chem. Soc. 1998, 120, 6185.
- 62. Huang, X. F.; Borhan, B.; Rickman, B. H.; Nakanishi, K.; Berova, N. Chem.-Eur. J. **2000**, *6*, 216.
- 63. Huang, X. F.; Fujioka, N.; Pescitelli, G.; Koehn, F. E.; Williamson, R. T.; Nakanishi, K.; Berova, N. J. Am. Chem. Soc. 2002, 124, 10320.
- 64. Huang, X. F.; Nakanishi, K.; Berova, N. Chirality 2000, 12, 237.
- 65. Kurtan, T.; Nesnas, N.; Li, Y. Q.; Huang, X. F.; Nakanishi, K.; Berova, N. J. Am. Chem. Soc. 2001, 123, 5962.
- 66. Proni, G.; Pescitelli, G.; Huang, X. F.; Quraishi, N. Q.; Nakanishi, K.; Berova, N. Chem. Commun. 2002, 1590.

Chapter 2

Use of ECCD for Absolute Stereochemical Determination of α -Chiral Carboxylic Acids

2-1. Use of Computational Modeling to Understand the Rotation About the $C_{C=0}\text{-}C_{\alpha}$ Bond

The idea of being able to "see" a molecule and know what its structure looks like is not a new one—various kinds of modeling have been used for centuries. Beginning

$$\begin{array}{c|c} & & & & \\ & & \\ & & & \\ & & & \\ & & & \\ & & & \\ & & & \\ & & \\ & & & \\ & & & \\ & & & \\ & & & \\$$

Figure 2-1. Bis(tetraphenylporphyrin) tweezer 1 and its simplified representation.

with simple stick-and-ball type models, we have progressed to the point of being able to visualize molecules *in silico* through the use of supercomputers and even our own PCs. Now, with the advent of faster, even more powerful computers, it has become practical to model molecules in such a way as to be able to predict stable conformations both in solution and gas phase. Small molecules can be modeled with good accuracy at a small cost (referring to computing time and resources), but macromolecules pose special problems in that there are usually a large number of degrees of freedom, leading to many possible low-energy conformers. Although a molecule may exist in several forms in solution, it is often useful to know if one conformer is preferred, particularly for chiral compounds.

Initial work in the field of absolute stereochemical determination of derivatized carboxylic acids using porphyrin tweezer 1 (Figure 2-1) and ECCD provided a mnemonic that allowed for the prediction of an ECCD sign for a given chiral monoamine derivatized as an amide (Figure 2-2). However, in expanding this method to chiral molecules with other functional groups, we determined that the usual method of predicting the sign of the CD couplet does not always work for chiral carboxylic acids derivatized as amides. It was noticed that several chiral carboxylic acids produced the opposite ECCD sign as expected (Table 2-1). It was not immediately obvious why some chiral acids produced the opposite ECCD sign as expected. To probe the possible conformational issues that might be affecting the observed ECCD sign, we decided to use molecular modeling, as crystals of derivatized porphyrins can be difficult to grow and obtaining a crystal structure of a host-guest complex poses even more problems.

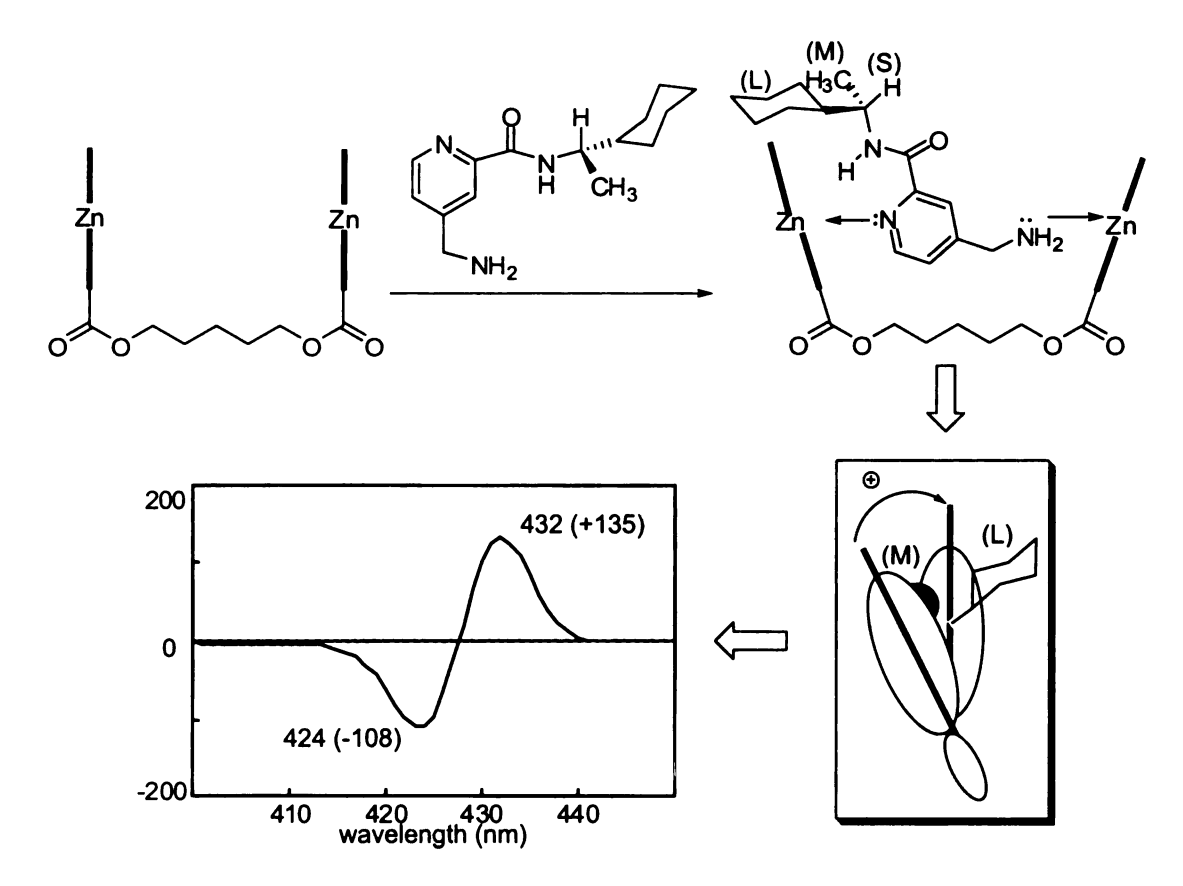


Figure 2-2. Complexation of a chiral acid conjugate with zinc bisporphyrin tweezer leading to the most favored conformation for the complex and the observed ECCD spectrum.

To perform molecular modeling on our systems, we chose to initially use Macromodel, a suite of visualization and computational tools for building, manipulating, and calculating various properties of molecules.² Monte Carlo, a conformational search program applicable to macromolecules with multiple degrees of freedom, is contained within Macromodel. Monte Carlo methods work through molecular mechanics, a low-level minimization technique.³ Although higher level calculations such as semi-empirical and *ab initio* generate more accurate results, these types of calculations are prohibitively

TI

٦.

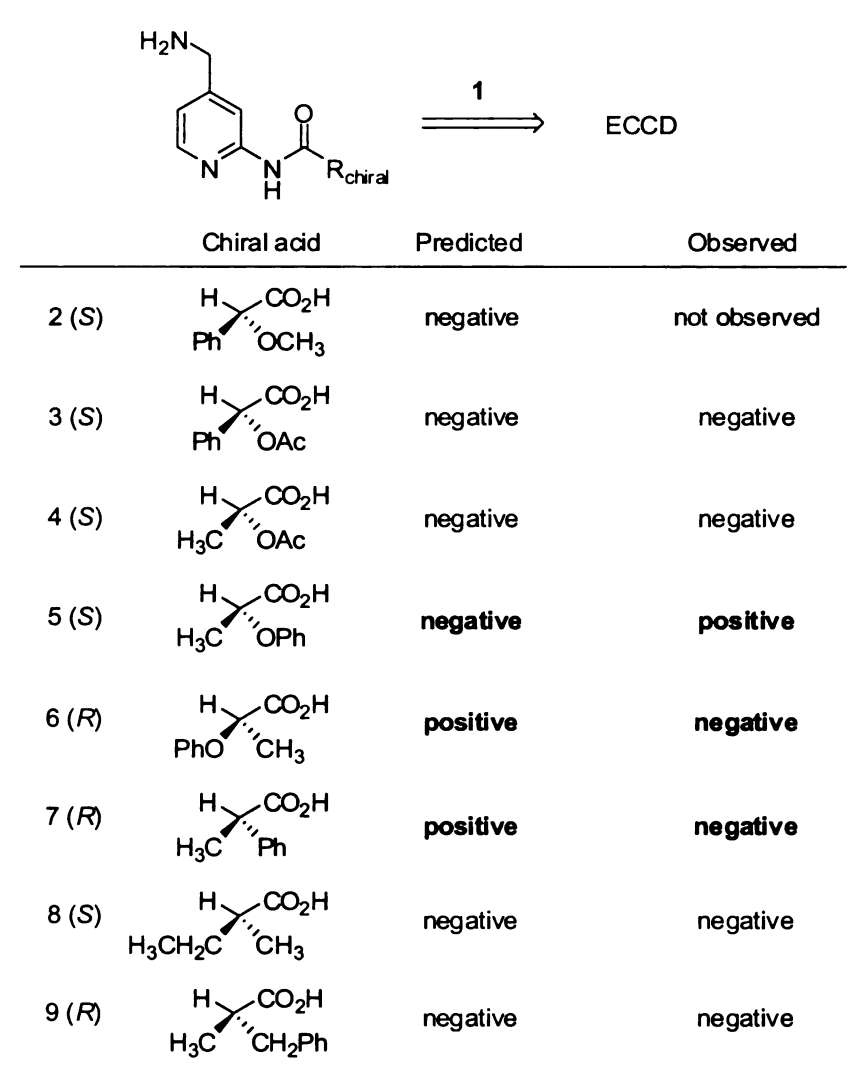


Table 2-1. Predicted and observed ECCD signs for chiral acids derivatized as amides and complexed with tweezer 1.

expensive (in terms of computer time) for medium to large molecules (i.e., over ~30 atoms). Monte Carlo conformational searches can obtain several low-energy conformations of a chiral molecule with or without chromophores, which we expected to help predict and understand our CD spectra. From these structures, the position of the chromophores and their electric transition dipole moments can be determined and then used to predict or explain ECCD spectra. This works well provided that the lowest energy conformations are CD active. If the CD-active conformations of our substrates

are not the lowest energy conformations, we would be limited in our use of molecular modeling.

2-1.1 Modeling of Derivatized Carboxylic Acids Complexed to Zinc Tetraphenylporphyrin

Our initial research was focused on the use of a carrier molecule with two sites of attachment for the porphyrin tweezer. This derivatization was necessary to use the

Figure 2-3. Carriers A and B used to derivatize chiral molecules with one site of attachment for use with ECCD (site of derivatization shown in blue).

ECCD method for stereochemical determination on molecules with only one site of attachment. Our first carrier molecule, carrier A (Figure 2-3), was used to derivatize chiral carboxylic acids as amides. Table 2-1 shows the carboxylic acids used for these studies. Initially, we developed a simplistic model of each molecule's conformation

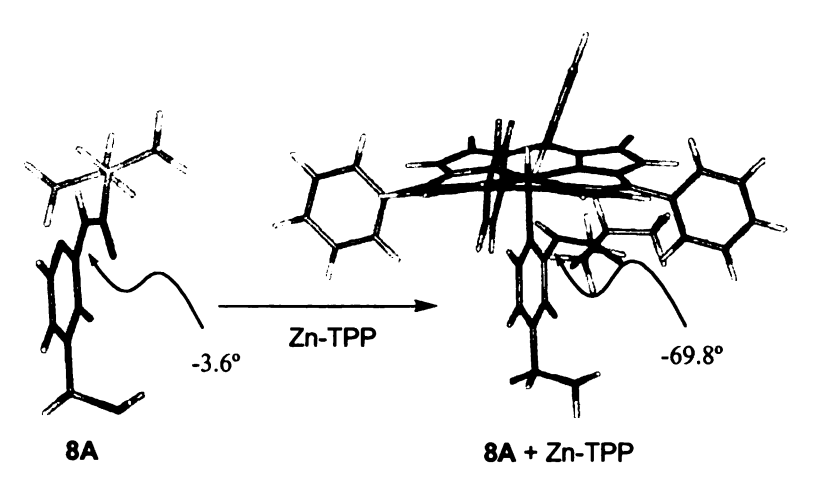


Figure 2-4. Binding of zinc porphyrin to the derivatized carboxylic acid forces rotation of the C(aryl)-N(amide) bond, causing the near coplanar amide to become staggered with respect to the aromatic ring.

based on a Monte Carlo conformational search of the derivatized carboxylic acid. Our expected ECCD signs were dictated by placing the medium group syn to the amide hydrogen, which in turn would lead to a preferred helicity of the bound porphyrin tweezer as a result of avoiding the steric interactions with the large group. This led to a number of predictions of ECCD which were not upheld by our experimental data. We believed this to be due to the lack of consideration of possible conformation changes in the derivatized carboxylic acid upon binding to the zinc porphyrin tweezer. Conformational analyses of various derivatized carboxylic acids coordinated to one zinc porphyrin suggested a flaw in the design of our carrier A. It became apparent that the coplanar amide-phenyl arrangement was not maintained due to steric crowding (Figure 2-4). Rotation of the Caryl-Namide bond upon binding of the derivatized carboxylic acid to the porphyrin tweezer led to many unpredictable conformers of conflicting ECCD sign. As can be seen from Table 2-2, Monte Carlo conformational searches of various carboxylic acids derivatized with carrier A yielded a large number of conformers within a small energy range. In many cases, the number of conformers with a predicted ECCD sign had an equal number of conformers with the opposite predicted sign. After evaluating the conformers, it became apparent that carrier A had too many freely rotating bonds, leading to a large number of low energy conformers. At this realization, we considered a more rigid carrier, carrier B (Figure 2-3). As opposed to carrier A, conformational searches of carrier B not only produced fewer low energy conformers, but all conformers for a given acid predicted the same ECCD sign (Table 2-3). From this information and the observed ECCD data, we were able to create a new mnemonic using carrier B (Figure 2-5). However, from the data obtained from the conformational

		No. of conformers	E range (kcal/mol)	Conformers w/in 1 kcal/mol	No. of conformers predicting (+) ECCD	No. of conformers predicting (-) ECCD
_	2A-TPP	37	8.2	5	5	0
	3A-TPP	73	9.2	7	4	3
	4A-TPP	34	7.4	6	3	3
	6A-TPP	63	9.2	9	6	3
	7A-TPP	59	9.5	14	9	5
	8A-TPP	24	9.5	6	1	5
	9A-TPP	71	9.9	14	7	7

Table 2-2. Conformational search results of various chiral carboxylic acids complexed to carrier A.

	No. of conformers	E range (kcal/mol)	Conformers w/in 1 kcal/mol	No. of conformers predicting (+) ECCD	No. of conformers predicting (-) ECCD
2B-TPP	64	9.9	7	0	7
3B- TPP	97	10	4	0	4
4B -TPP	61	9.8	4	0	4
6B -TPP	69	9.9	5	5	0
7B -TPP	21	9.8	2	0	2
8B -TPP	14	7.9	1	0	1
9B-TPP	22	9.8	3	0	3

Table 2-3. Conformational search results of various chiral carboxylic acids complexed to carrier B.

searches with carboxylic acids derivatized with carrier **B**, we observed that upon binding to the zinc porphyrin, an unexpected conformation of the amide moiety was predominating in which the large group is perpendicular to the amide carbonyl. We were interested in probing this conformation in order to better predict ECCD signs for novel compounds.

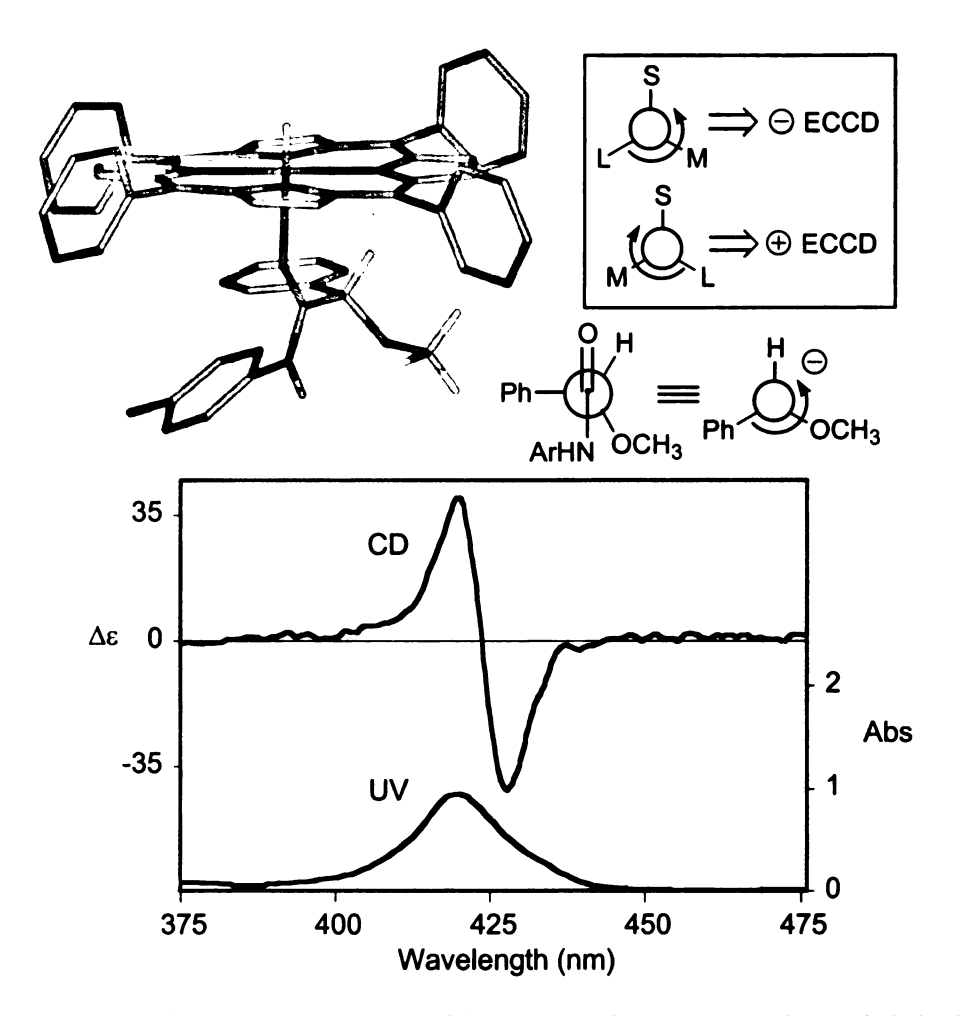


Figure 2-5. Mnemonic developed for determining the absolute stereochemistry of derivatized carboxylic acids using ECCD.

2-1.2. Modeling of Derivatized Carboxylic Acids with a Second-Generation Carrier

From initial modeling and geometry optimization of porphyrin tweezer 1 complexed with various derivatized carboxylic acids, the structures generated would be anticipated to show both the expected (from previous mnemonics) and unexpected ECCD couplet signs. As an initial hypothesis, we thought that perhaps sterics were playing a significant role in the interaction of the guest molecules with the tweezer. In considering the conformation of amides, hydrogens *alpha* to the carbonyl are often depicted as parallel to the carbonyl; in fact, semi-empirical calculations in our lab on carboxylic acids

derivatized as amides indicate that this is the most favored conformation. However, when bound to a porphyrin tweezer, it may not be favorable to have the medium and large groups both pointing towards the porphyrin face. Instead, it is possible for rotation to place the medium group nearly parallel to the carbonyl with the small and large groups facing the porphyrins which reverses the sign of the ECCD couplet (Figure 2-6). Geometry optimization and energy minimization using Spartan v.5.1.3 indicate that these amide conformers (with the medium group syn to the carbonyl) are close in energy to the previously expected conformer and may be preferred. Another possible hypothesis takes into consideration the change in the dipoles of this molecule as the pyridine nitrogen binds to the zinc. Normal dipole interactions would place the dipole of the carbonyl pointing opposite to that of the pyridine ring. However, once the nitrogen is bound, the dipole of the pyridine ring reverses, which may affect how the carbonyl is positioned in relationship to the pyridine ring (Figure 2-7). Semi-empirical studies were undertaken to explore this hypothesis. It appears that, regardless of basis set used, geometry

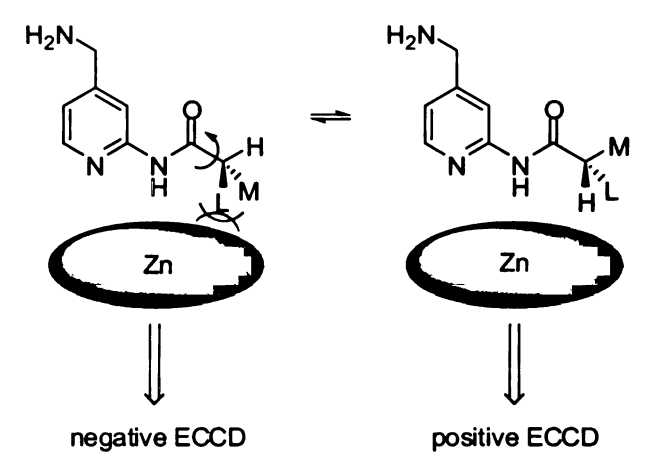


Figure 2-6. Rotation around the C(C=O)-C(chiral) bond leading to opposite ECCD predictions.

optimization which allows for a structure with the carbonyl dipole opposite to the

pyridine dipole generates structures lower in energy than structures with the carbonyl and pyridine dipoles aligned.

Figure 2-7. Possible conformational changes due to dipole interactions (shown in blue) between the carbonyl and the pyridine ring upon binding to the porphyrin tweezer.

2-1.3. Modeling of Chiral Carboxylic Acids Derivatized as Amides

Modeling the host-guest tweezer complexes provided us with many clues as to possible conformations that would lead to ECCD. However, it became of great interest to determine the actual conformations of the guest molecules alone. Information about the conformation of our derivatized carboxylic acids could lead to the development of better carrier molecules for derivatization, or even other tweezers that would take better advantage of conformational changes within our guest molecules. We chose to evaluate the conformation of the amide guests before they bind to the tweezer, and how these conformations are influenced upon binding with a single porphyrin in greater depth than we had previously explored with molecular mechanics.

An initial conformational search was undertaken to explore possible low-energy conformers for the derivatized carboxylic acids. Using Macromodel, a search was performed on (S)-phenylpropionic acid derivatized with 2-amino-4-(methylamino)pyridine. Of the 38 conformers within 8 kcal/mol of the global minimum, 17 occur with the methyl group syn to the carbonyl, 13 occur with the hydrogen syn to the

carbonyl, and three occur with the phenyl group syn to the carbonyl. The remaining conformers consist of conformations in which the carbonyl bisects the angle between two groups on the chiral center. Two conformers, one with the hydrogen syn to the carbonyl and one with the methyl group syn to the carbonyl (i.e., the two smallest substituents by A-values) were exported to be used in ab initio studies in Spartan. Calculated energies using the Hartree-Fock (HF) method with the 3-21G* basis set gave energies of -757.4280119 a.u. and -757.4313368 a.u., respectively, which translates to a difference in energy of 2.09 kcal/mol in favor of the conformer with the methyl group syn to the carbonyl (Figure 2-8). This was somewhat surprising since methyl is a larger group than hydrogen, but as we considered the molecules it became apparent that there were possible interactions between the hydrogen of the amide nitrogen and the substituents on the chiral center. Realizing that we needed to model these interactions more extensively, we turned to coordinate driving. However, we continued to use conformational searches in Macromodel to predict initial low energy conformers at which a minimum might be occurring.

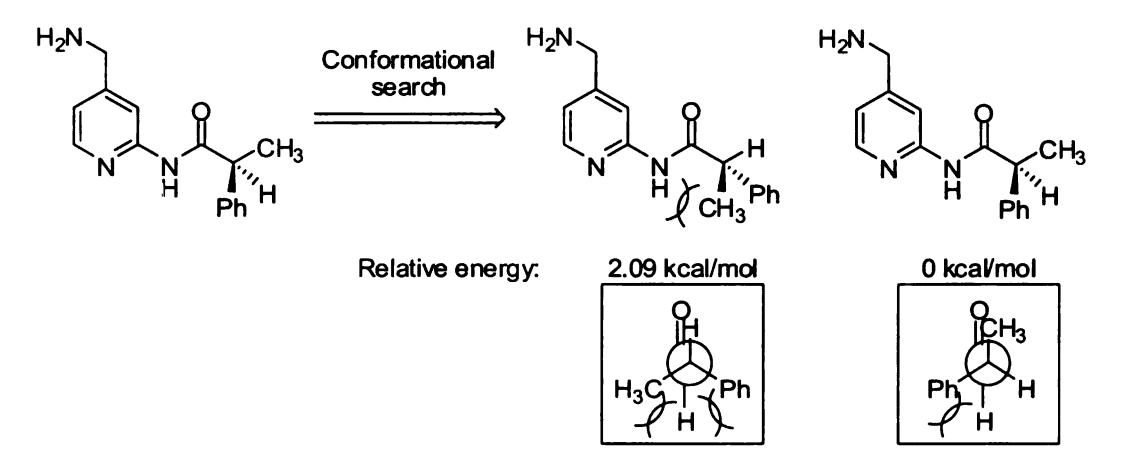


Figure 2-8. Relative energies of the lowest energy conformers generated from a conformational search of (S)-phenylpropionic acid derivatized with carrier A.

Initially, we believed that the production of the opposite CD spectrum than predicted could be due to rotation about the C-C bond between the carbonyl and the chiral center. This could occur due to steric interactions between the large and medium groups of the chiral center and the porphyrin binding to the pyridine nitrogen. Rotation could occur such that the small group is pointing toward the porphyrin face instead of *syn* to the carbonyl, as normally portrayed. This would slide the large and medium groups towards the carbonyl such that the carbonyl would more or less split the angle between the two groups (Figure 2-6). This would occur if the steric interactions of the large (and potentially medium) group were greater with the porphyrin face than the barrier of



Figure 2-9. The plane of the carbonyl and the plane of one group on the chiral center used for coordinate driving.

rotation past the carbonyl. To explore this possibility, coordinate driving studies were started using Spartan v. 5.0. Coordinate driving "drives" the molecule in question under the constraints that are set by the user. Molecules can be driven based on angles, reaction coordinates, etc. After each "drive," the molecule is reminimized with the driven coordinates constrained and the energy of the molecule is calculated at the level of theory chosen by the user. In this case, we were interested in driving the dihedral angle between the plane created by the carbonyl and the plane created by the chiral carbon and one of the groups on the chiral center (Figure 2-9).

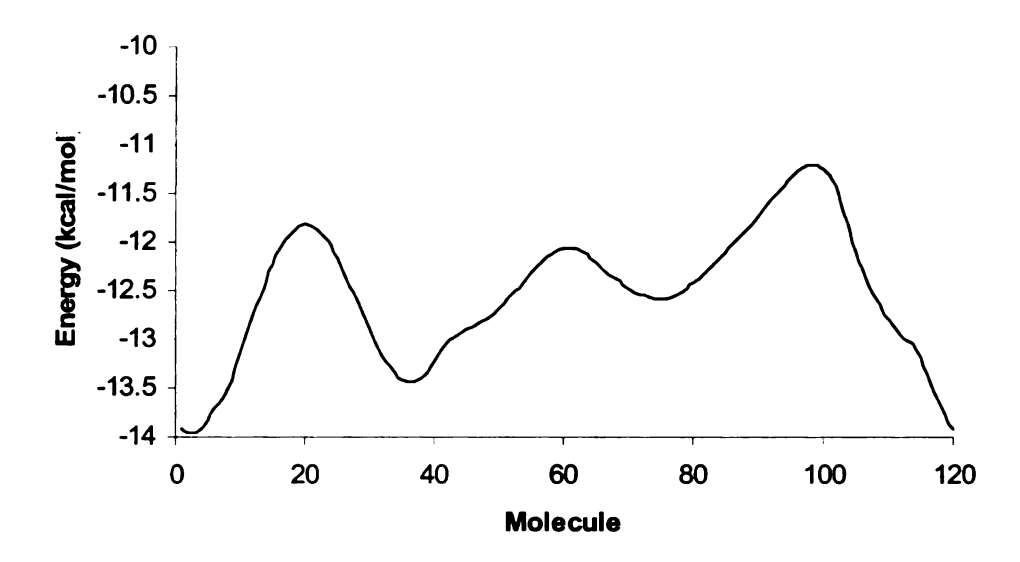


Figure 2-10. Graph of the energy values obtained from the coordinate driving of (2R)-2-bromopropionic acid derivatized with carrier **B**.

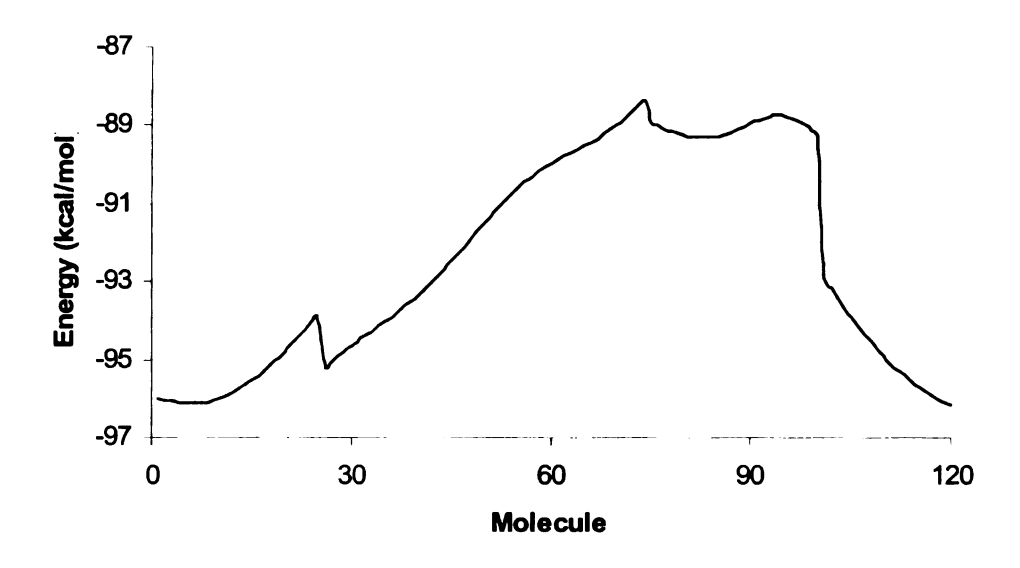


Figure 2-11. Graph of the energy values obtained from the coordinate driving of (2S)-2-acetoxypropionic acid derivatized with carrier **B**.

Initially, all calculations were performed using the plane created by the chiral carbon and the small group as the second plane. Calculations were done at the semi-empirical level with the PM3 basis set. This allowed for a relatively high level of calculation with a minimal use of computer resources and time. Initial calculations were done over 360° with 180 steps, creating drive angles of 2°. This produced extremely

large data files, as an individual file with complete energy information is created and saved for each drive step. After discovering this, the drive angle was changed to 3° (120 steps) to decrease the amount of computational time and resources needed. The results were plotted as a graph of energy (kcal/mol) versus molecule, where molecule is the degrees in units of 2° each from the starting dihedral angle between the two planes. Some of the graphs display expected energy diagrams with three minima that correlate to the various groups on the chiral carbon being syn to the carbonyl (e.g., the graph from the coordinate driving of (2R)-2-bromopropionic acid, Figure 2-10). However, as the groups on the chiral carbon change, the energy diagrams become more complex and less easily explained (e.g., the graph from the coordinate driving of (2S)-2-acetoxypropionic acid, Figure 2-11). These graphs often show only one minimum, with unusual peaks and plateaus in the energy plot which cannot be explained through conventional steric interactions.

To try to determine if these results are accurate and significant, a second study was initiated in which each molecule from the coordinate driving was subjected to a molecular mechanics geometry optimization. The idea is that normal geometry optimization will optimize a molecule to the nearest local minimum. In this case, separate geometry optimization of each step of the coordinate driving should tell us how many minima we have and the conformation of each of those minima, since each molecule should minimize to a local minimum. As can be seen from Figure 2-12, this was performed on the derivatized (2S)-2-acetoxypropionic acid. Indeed, five distinct minima are observed through coordinate driving of the $C_{C=0}$ - C_{α} bond. The minima correspond to the carbonyl syn to the hydrogen on the chiral carbon, the carbonyl

splitting the methyl and hydrogen, the carbonyl syn to the methyl, the carbonyl splitting the methyl and acetate, and the carbonyl splitting the hydrogen and the acetate, in order from left to right along the x-axis (the last apparent minimum is due to the carbonyl splitting the methyl and hydrogen with the hydrogen on the nitrogen pointing in the opposite direction as the other minimum of the same designation due to the nitrogen not being completely planar).

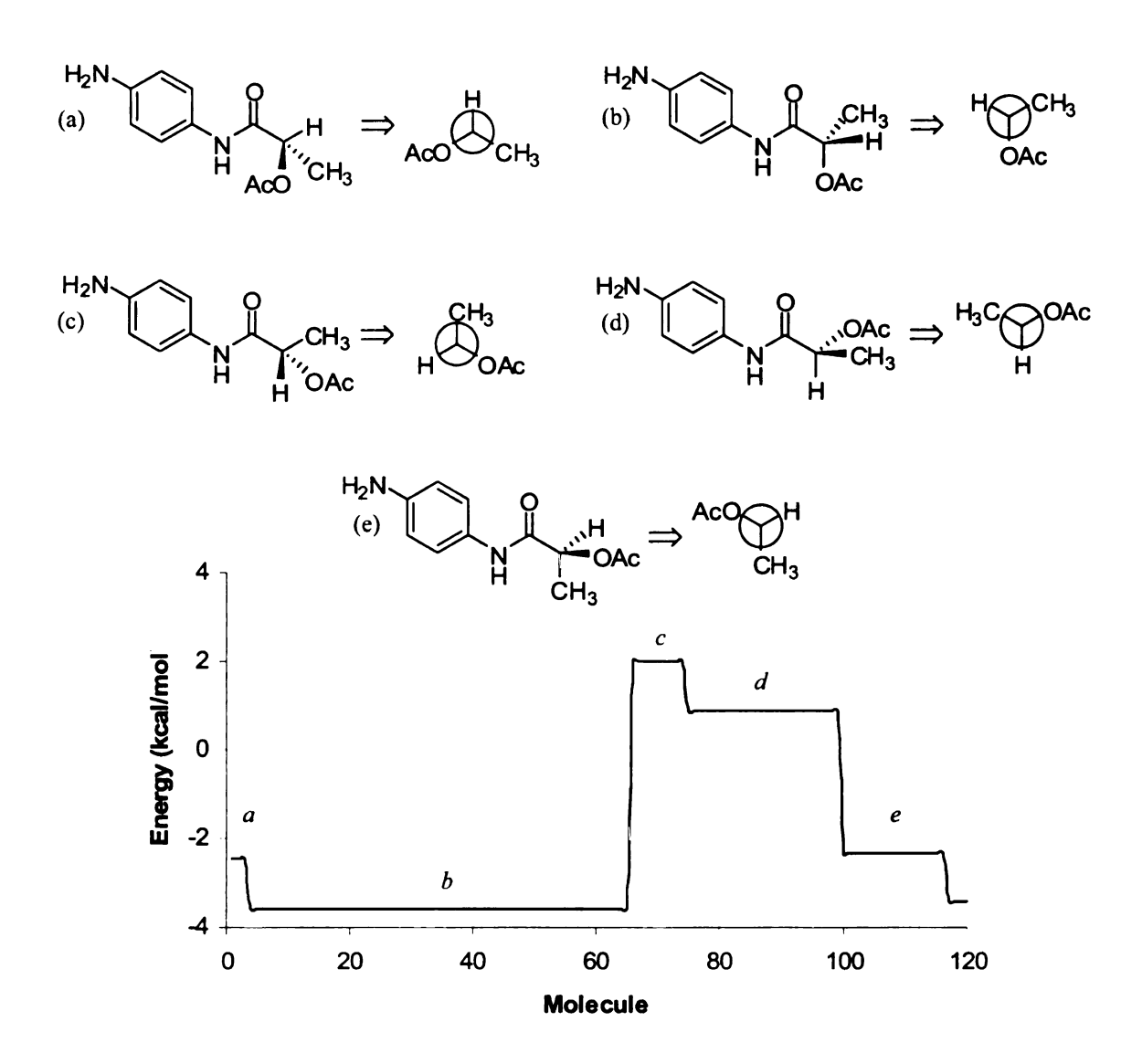


Figure 2-12. Graph of the energy values obtained from a molecular mechanics geometry optimization of each molecule from the coordinate driving of (2S)-2-acetoxypropionic acid derivatized with carrier **B** (Newman projections represent the view from α -carbon to carbonyl carbon).

To explore these minima and determine if these are actually the lowest energy minima, each minimum conformation from the coordinate driving calculation (at a molecular mechanics level) was subjected to a semi-empirical geometry optimization at the PM3 level of calculation (Figure 2-13). Interestingly enough, the results of this calculation do not entirely match those from the mechanics calculation. There are five distinct minima evident here, corresponding to the carbonyl splitting the hydrogen and

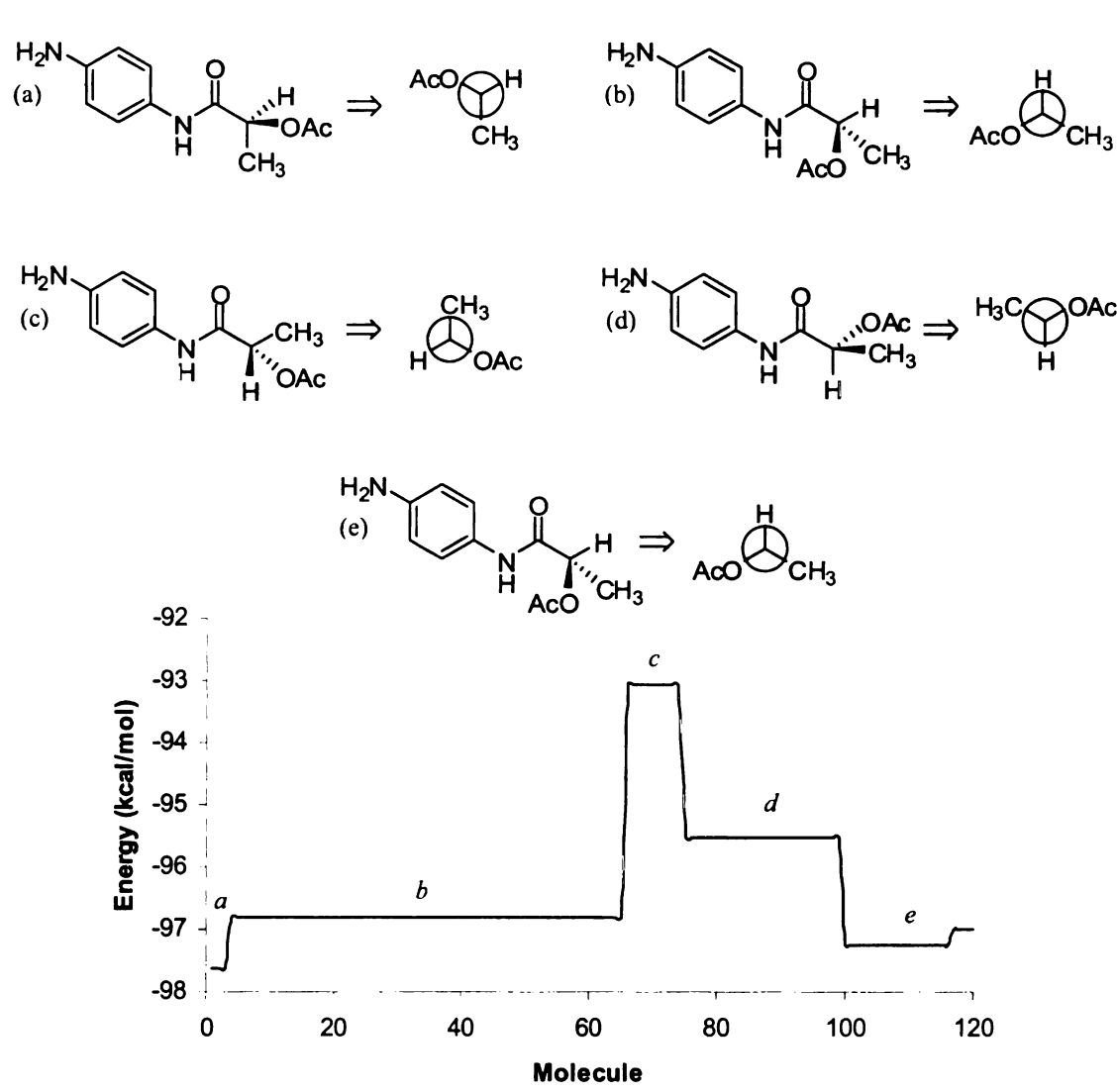


Figure 2-13. Graph of the energy values obtained from a PM3 geometry optimization of each molecule from the coordinate driving of (2S)-2-acetoxypropionic acid derivatized with carrier $\bf B$ (Newman projections represent the view from α -carbon to carbonyl carbon).

the acetate, the carbonyl syn to the hydrogen, the carbonyl syn to the methyl, the carbonyl splitting the acetate and the carbonyl, and the carbonyl syn to the hydrogen, from left to right across the x-axis. Differences in the energy of the two minima where the carbonyl is syn to the hydrogen are due to changes in the position of the hydrogen on the nitrogen (as described previously), which slightly changes the steric interaction of that hydrogen with other groups in the molecule.

It is known based on the calculations described above that the difference in energy between minima is much higher for 1,2-carriers (i.e., carboxylic acids derivatized as amides) than for 1,3-carriers (i.e., amines derivatized as amides) (Figure 2-14), with the carrier numbers referring to the distance between the aromatic ring and the carbonyl. This would indicate that it does appear feasible for conformation changes to be occurring for the 1,3-carriers which have not been observed in the 1,2-carriers, in which the lowest energy conformer is not actually the best conformation when bound to the tweezer. This would be expected to occur where the energy difference between conformations is low enough to allow for rotation about the $C_{C=O}$ - C_{α} bond, when the energy required for this conformational change is offset. A rotation to relieve steric strain between the groups on the chiral carbon and the porphyrin ring as the guest molecule approaches and binds to the host tweezer would possibly release more energy than is required to move past the rotational energy barriers. As a result, there are more conformational possibilities available to the derivatized carboxylic acids than we had previously thought. These

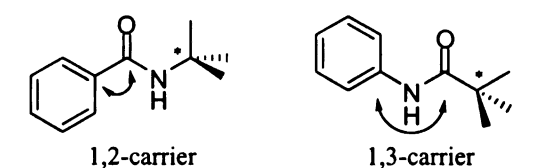


Figure 2-14. Examples of 1,2- and 1,3-carriers, from chiral amines and carboxylic acids, respectively.

additional conformations need to be evaluated to determine which conformation is most likely for an individual molecule, which conformations occur when complexed to a porphyrin, and which conformations would be expected to lead to an ECCD spectrum when complexed.

2-2. Exploration of Possible Binding Modes for Derivatized Carboxylic Acids with Zinc Tetraphenylporphyrin 1,5-Pentanediol Tweezer

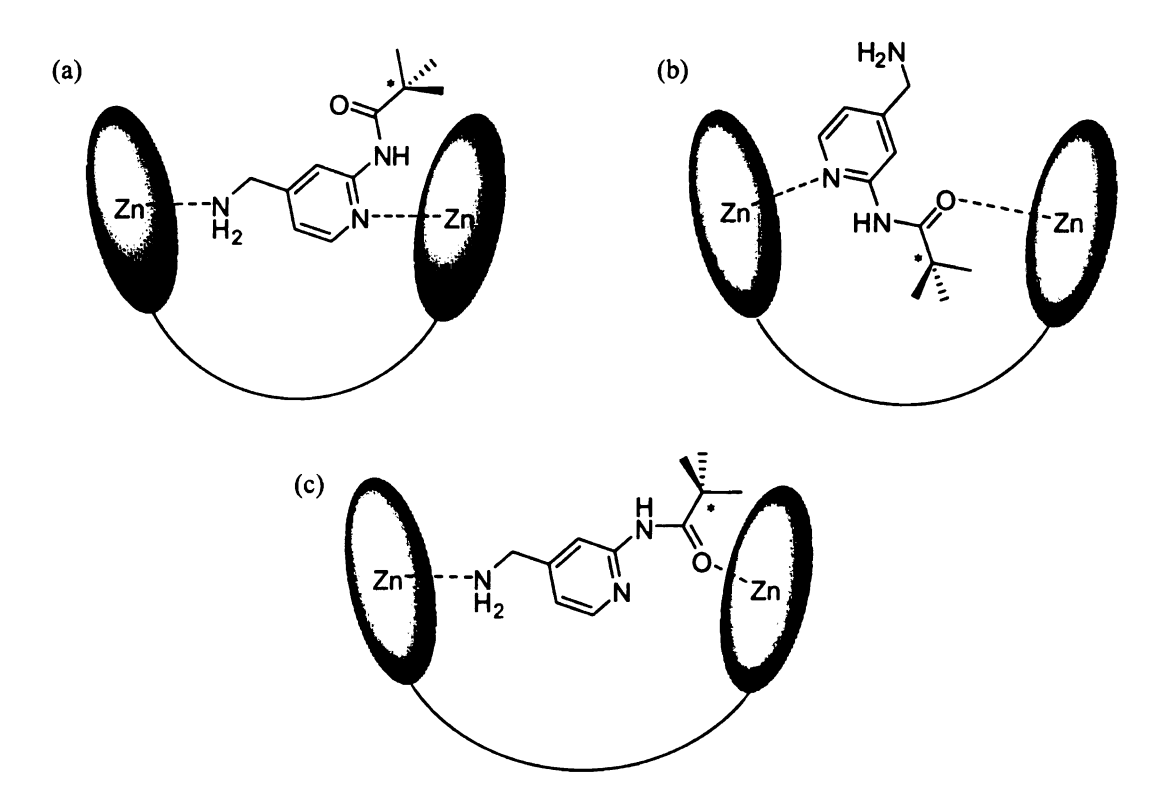


Figure 2-15. Possible binding modes for carboxylic acids derivatized with carrier A.

In trying to determine why we cannot predict with any certainty the CD results of carboxylic acids derivatized with 2-amino-4-(methylamino)pyridine, we have explored a number of conformational options but no one conformational explanation correlates with all compounds. With this in mind, we thought to explore differences in binding options between the guest and host molecules. There are three binding options for the derivatized guest to the porphyrin tweezer (Figure 2-15): (a) The carrier is binding at the pyridine

nitrogen and the primary amine. (b) The carrier is binding at the pyridine nitrogen and the carbonyl of the amide. (c) The carrier is binding at the primary amine and the carbonyl of the amide (the pyridine ring is flipping so that the pyridine nitrogen is syn to the carbonyl). Option (b) we see as least likely, as we would expect the free primary amine to bind more readily to the zinc than the carbonyl oxygen. Allowing for various binding possibilities, we need to determine what is happening conformationally at the chiral α-carbon of the amide. According to studies done by Wiberg and Rush.^{4,5} amides in the Z-conformation (i.e., where the carbonyl oxygen and the amide hydrogen are anti) prefer the substituents on the α -carbon to be staggered. Amides in the E-conformation (the carbonyl oxygen and the amide hydrogen are syn) prefer the substituents on the α carbon to be eclipsed with the carbonyl. Their studies, however, were only carried out with a methyl group as the α-carbon, so it is unclear how groups other than hydrogen would behave in terms of orientation with respect to the carbonyl.⁶⁻⁹ A recent study by Allinger, et al., 10 calculated structure, rotational barriers, vibrational spectra, and dipole moments for ketones using a molecular mechanics (MM4) force field (for reference see also the study of aldehydes by the same authors¹¹). Their findings indicate that for all ketones studied, the lowest energy conformer is not the one with an α-hydrogen eclipsed with the carbonyl. Instead, a significantly lower conformer is found where either a methyl group eclipses the carbonyl (for methyl ketones) or the carbonyl bisects the methyl groups (in isopropyl ketones). If this is true for ketones, it may be even more so in amides, where the substituents on the α -carbon could be in psuedo-A-1,3 interactions with the amide hydrogen (for the Z amide). It could be possible that the pseudo-A-1,2 interactions between the carbonyl and the α -substituents are less important sterically than the A-1,3 interactions between the amide hydrogen and the α -substituents (Figure 2-16).

Figure 2-16. Pseudo-A-1,2- and A-1,3-interactions of the amide nitrogen and carbonyl with the substituents on the chiral center.

To explore some of these issues and determine low energy conformations for our system, we have done several different types of calculations. To begin with, single-point energy calculations using density functional theory were done on all of the molecules that we have explored experimentally. Density functional theory (DFT) allows for electron correlation—taking into account the theory that electrons will react to and move away from each other in a molecule—without expensive (in terms of computer resources) calculations. 12 Ab initio and semi-empirical methods do not use electron correlation except in an averaged sense, and this approximation can introduce error. Using the B3LYP force field with different basis sets gave mixed results. The molecules surveyed included derivatives of (R/S)-2-bromopropionic acid, (R/S)-2-phenylpropionic acid, and (R/S)-2-phenoxypropionic acid. Calculations were done on each molecule in three different conformations: one with the small group syn to the carbonyl, one with the medium group syn to the carbonyl, and one with the large group syn to the carbonyl (size of the groups was based on reported A values¹³). Each conformation was subjected to geometry optimization with the 3-21G* basis set, and then the resulting conformer was optimized again with the 6-31G* basis set. To represent possible binding through the pyridine nitrogen, the N-methyl version of each molecule was also optimized with the 321G* basis set to observe possible changes in conformation due to the reversed dipole of the pyridine group. Each molecule gave distinctly different results, although in all cases the energy difference between the different conformations was no more than 6 kcal/mol. However, it still was not possible to correlate the calculations with experimental ECCD results. Although some of the molecules optimized to a single conformation, some did not, and even the ones that optimized to a single conformation were not consistent in the orientation of the α-carbon substituents relative to the carbonyl. Although potentially useful in evaluating and comparing conformers, none of the information from this study alone allowed for an explanation of the ECCD data. Thus, more computational studies were undertaken.

Previous coordinate driving studies on Spartan indicated that some of the molecules might not have well defined energy maxima and minima, perhaps suggesting more free rotation around the $C_{C=O}$ - C_{α} bond than expected. If there is more free rotation than expected around this bond, the conformation leading to ECCD results may not be the lowest energy conformer, but may instead be locked into a specific conformation when the carrier binds to the porphyrin tweezer, making it difficult to predict which conformation for each molecule is actually leading to the ECCD results observed. Depending on how the guest molecule is binding to the porphyrin tweezer, there could be multiple conformations that would lead to the observed ECCD. It came to our attention that perhaps calculations should be done on the derivatized chiral carboxylic acids taking into consideration other binding possibilities.

All of the previous calculations focused on the theory that the carboxylic acids derivatized with carrier A were binding through the primary amine and the pyridine

nitrogen (Figure 2-15a). However, it is a possibility that binding is occurring through the carbonyl present in the amide functionality. It has been suggested that the amide group does not actually exist as the traditional resonance forms normally used to explain amide behavior.^{4,5} In computational studies on the amide group, Wiberg, et al., have found a significant difference in how the electron density is distributed, where the majority of the electron density is located on the carbonyl oxygen as expected in one of the normal amide resonance forms. They propose, however, that this may be more characteristic of the ground state than previously believed. If this is true and a nearly negative charge is present on the oxygen, it would provide some basis for why we might see binding occurring through the amide carbonyl instead of the pyridine nitrogen (Figure 2-15c).¹⁴

Another possibility is hydrogen bonding of one of the chiral substituents to the amide N-H (Figure 2-17). Although this is a possibility, it does not account for all of the

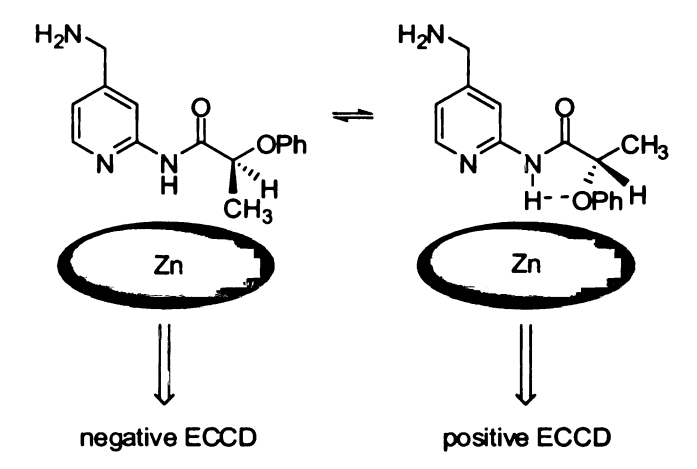


Figure 2-17. Possible conformational changes due to hydrogen bonding leading to a switch in the expected ECCD sign.

experimental data (i.e., conformations expected by hydrogen bonding do not always predict the correct ECCD sign). It appears that multiple effects of the substituents on the chiral carbon may be influencing the outcome of the ECCD, and those effects may include sterics and electronic effects, as well as hydrogen bonding. We continued our

modeling studies using Maestro, an improved graphical user interface (GUI) for Macromodel. We performed a number of conformational searches using chiral carboxylic acids derivatized with carrier B. To minimize the amount of data to only what is useful we analyzed each conformation. We only recorded data for the lowest energy conformer and then any others which would be expected to show ECCD when placed in the host system. This allowed us to evaluate which conformers would show ECCD and how they compare energetically to the lowest energy conformer (which may or may not be expected to show ECCD). In all molecules studied, the lowest energy conformer would not be expected to show ECCD based on our binding models. None of the conformers that would be expected to show CD have the medium group anti to the carbonyl, which was one of the proposed binding models. We also performed two studies in Spartan to look for the feasibility of hydrogen bonding between the hydrogen of the amide group and one of the groups on the chiral carbon. Using density functional, which takes electron effects into account, we were able to obtain conformations in which the phenoxy group has a weak hydrogen bond to the amide hydrogen. This was done through constraining the distance of the phenoxy oxygen to the amide hydrogen. However, we still would not expect this conformation to show much if any ECCD, because there is a group syn to the N-H where we expect the porphyrin face to approach. Another possibility that was proposed is $H-\pi$ stacking between the amide hydrogen and the phenyl ring of the phenyl or benzyl groups. This is very difficult to model with our software and this type of hydrogen binding does not seem to be supported within the methods we are using. NMR studies by another member of our group did not lead to conclusive evidence for H- π stacking.¹⁵

2-3. Exploration of a Novel Binding Model Involving Coordination of an α -Halogen and an Amide Carbonyl Oxygen to Zinc

As we have progressed in our understanding of the conformations of α -chiral carboxylic acids derivatized as amides, we have continued to pursue the use of ECCD to determine the absolute stereochemistry of α -chiral carboxylic acids with a variety of functional groups on the *alpha* carbon. We have been able to develop mnemonics which work for many compounds. However, carboxylic acids with halogens on the chiral center have completely thwarted our efforts to explain the observed ECCD. Based on our initial mnemonic (Figure 2-5), we would expect the exact opposite ECCD for every α -halocarboxylic acid we have tested (Table 2-4). A-values do not predict the observed ECCD. We were most intrigued by the possibility of cooperative binding to zinc by the carbonyl and halogen of α -haloamides when they are acting as bound guests in our zinc porphyrin tweezer system. This would place the halogen *syn* to the carbonyl (Figure 2-18). It is very difficult to model this type of cooperative bonding since most molecular

_	Mnemonic	Expected ECCD	Actual
R	H ₃ C H	positive	negative
S	H Br	negative	positive
S	H Br	negative	positive
S	Br Ph	negative	positive

Table 2-4. Representative α -halocarboxylic acids derivatized with carrier **B** showing unexpected ECCD signs.

modeling programs do not account for non-covalent, non-hydrogen bond interactions. It is possible to model these systems by placing restraints on the bond lengths, etc., between

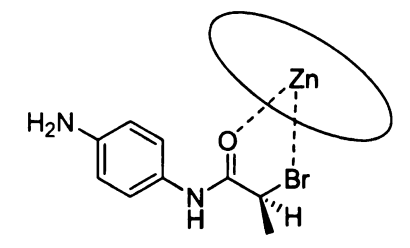


Figure 2-18. Possible cooperative binding between the carbonyl oxygen and the α -halogen with the metal core of the porphyrin.

the ligating atoms and the zinc, but this imparts false information into the calculations making them less than reliable. Due to the difficulties in modeling these systems, we looked into spectroscopic methods aided by molecular modeling for determining whether or not zinc is cooperatively binding to the halogen of the haloamides.

Another member of our group derivatized some of the chiral carboxylic acids to compounds similar to Mosher's amides, where the derivatizing amine contained a chiral center with an aromatic group that would be expected to produce different NMR

Figure 2-19. (2R)-2-bromopropionic acid as both diastereomers of a Mosher amide.

shielding patterns on the substituents of the carbonyl α -carbon (Figure 2-19).¹⁵ This method would allow us to determine the average conformation for free α -haloamides in solution, which we hoped to be able to relate to the bound systems. To determine expected shielding for the substituents, these compounds were first submitted for conformational searches in order to determine the most favored low energy conformers. By comparing the angle of the aromatic plane with the position of the substituents on the

 α -carbon, we had hoped to be able to predict which substituent would be shielded in each diastereomer.

The derivatized enantiomers were submitted for a Monte Carlo molecular mechanics conformational search in Spartan. The conformers were evaluated by relative energy and conformation of the substituents on the chiral centers. Each compound studied showed all three conformers (hydrogen, bromine and methyl syn to the carbonyl) within 1 kcal/mol of the lowest energy conformer. For all conformers under 1 kcal/mol from the lowest energy conformer, the medium group of the other chiral center (of the derivatizing group) was syn to the N-H bond. The problem occurs with the aromatic group that is expected to change the shielding for the chiral center of the derivatized carboxylic acid. The angle of the aromatic plane makes it difficult to predict if the substituents would be shielded or deshielded. This, along with the similar energy of different conformations on the C_{α} chiral center, makes it difficult to predict which groups should be shielded and deshielded, a necessary determination to interpret the NMR data appropriately. We also modeled different derivatizing amines to try to determine if larger aromatic or other substituents would assist in locking the conformation of the aryl ring into a favorable position. It does not appear that an increase in the size of the other substituents increases the likelihood of being able to determine the average conformation. The normal Mosher amide-type NMR studies thus did not appear to be useful to us in determining the conformation of the α-haloamides, since we had no way of interpreting the chemical shifts that we observed.

To probe expected conformations for the α -haloamides, we were interested in determining the typical conformation for α -haloamides as reported in the Cambridge

Crystallographic Database (CCD). Using Conquest, we searched for α -haloamides in which the carbonyl was bonded to a metal. We did not restrict the search through the type of oxygen-metal bond or type of metal. This search produced 274 positive hits; however, the majority of these compounds were groups with a CF₃ group *alpha* to the carbonyl. Only three compounds returned by the search were α -monohalogenated carbonyls. It cannot be determined from this small amount of data if variations in the O=C-C-X dihedral angles are due to the different types of halogens, different metals, or if there is simply not much preference for a specific dihedral angle or range of angles. We then simplified the search and looked for α -haloamides without metal to determine typical O=C-C-X dihedrals. This search returned 252 hits, but we discarded lactams (due

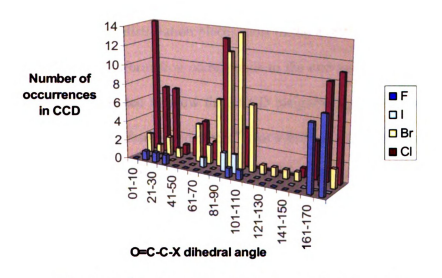


Figure 2-20. CCD data depicting dihedral angles of α-halocarbonyls.

to their locked conformation) and compounds with multiple α -halogens. Figure 2-20 shows the results from this study in the form of a bar graph. Here it is clear to see that the different halogens do have preferences (at least in crystalline form) for the O=C-C-X dihedral. Fluorine is shown to have the majority of its conformations with the halogen

anti to the carbonyl. Bromine and iodine favor conformations in which the halogen is perpendicular to the carbonyl, while chlorine favors conformations in which the halogen is either syn or anti to the carbonyl, with several exceptions. However, there is still enough diversity of conformations that it is not clear what we could expect with our systems merely based on reported crystal structures.¹⁶

It seemed that an in-depth study of a simple α -haloamide might be useful to check effects of dipole and charge distribution. We began a series of DFT single point energy calculations on bromoacetamide to calculate the energy, dipole moment, atomic charges, and charge density at specific O=C-C-Br dihedrals. Based on these results, the most favorable conformation still seems to be that in which the bromine is nearly *anti* (O=C-C-Br dihedral = 150°) to the carbonyl (Figure 2-21). With this conformation, the energy is minimized and the charge distribution places most of the negative charge on the bromine and the oxygen. This conformation corresponds to the one we had originally expected, which would not be expected to show the ECCD bisignate signs we have observed. It seems to be clear from our results and others¹⁶ that a free α -haloamide would be expected to exhibit an average conformation where the bromine is *anti* to the carbonyl and the plane of the carbonyl bisects the other two substituents. However, it appears that this is not the conformation that is present when the α -haloamides are guests in our zinc porphyrin tweezers, as the ECCD bisignates observed cannot be correlated with the predicted conformation of the free amides.

Figure 2-21. Lowest energy conformation for bromoacetamide based on DFT calculations.

We became aware of a series of papers published by Taniguchi, et al., 17-19 in which they observed an apparent hydrogen bonding chain between a carbonyl and an αhalogen in α-haloacetones. In their system, they believe a 2- to 3-molecule water chain forms a network between the carbonyl and the halogen, with both acting as hydrogen bond acceptors. They were able to observe this through Raman spectroscopy in which the position of the C-Br stretching band shifts upon addition of water. This led us to consider the possibility that bonding of the porphyrin zinc is occurring with both the carbonyl oxygen and the α-halogen of the amides—a sort of cooperative bonding which reverses the normal conformation of the α -haloamides and positions the halogen syn to the carbonyl as opposed to the expected anti conformation (Figure 2-18). It was unclear whether binding could be occurring solely through the bromine (i.e., no binding between the carbonyl oxygen and the zinc) or as a cooperative system involving the halogen, the metal, and the oxygen. However, based on previous NMR studies of the complexes, 15 it is relatively clear that the oxygen of the carbonyl is probably involved in some type of binding. It then became necessary to demonstrate cooperative binding in which the halogen is also in some way coordinated to the metal. We began by trying to reproduce Taniguchi's work in silico by modeling α-haloamides with water molecules in Spartan. Only semi-empirical solvation models are available in Spartan for calculating solvation without explicitly including water molecules. Initially we performed a DFT geometry optimization with the AM1aq solvation model on N-methyl-2(R)-bromopropionamide. The starting geometry had the α -hydrogen syn to the carbonyl. The final structure placed the bromine anti to the carbonyl with a solvated energy nearly 10 kcal/mol lower than the gas phase (Figure 2-22). This is not improbable since the polar solvent would be

Figure 2-22. DFT geometry optimization of N-methyl-2(R)-bromoacetamide using implicit solvation leading to a conformation with the bromine *anti* to the carbonyl.

expected to stabilize the dipoles associated with the carbonyl and the carbon-halogen bond. We tried a few more calculations with variations in the solvation model and/or level of calculation with similar results for all calculations. Unfortunately, solvation studies alone were not assisting in determining if water molecules could be linked between the halogen and the carbonyl oxygen due to the implicit nature of the models.

We decided to try modeling the water molecules explicitly, hoping hydrogen bonding in the calculations would account for the possibility of hydrogen bonding with a halogen. We began the calculation in Spartan as a DFT geometry optimization on N-

Figure 2-23. Geometry optimization of water molecules hydrogen bonded to N-phenyl-2-bromopropionamide.

methyl-2(R)-bromopropionamide, placing a single water molecule between the carbonyl oxygen and the bromine with no constraints or partial bonds. After the end of the first optimization, the water molecule had moved to the side of the carbonyl at an $O_{C=O}$ - H_{H2O} distance of 2.079Å, far enough away from the bromine that no hydrogen bonding would be possible. For the second optimization, we inserted a second water molecule in

between the oxygen and the bromine as before, with the initial water molecule in the same position it had at the end of the first minimization. At the end of the second optimization, the second water remained in position between the oxygen and the bromine with an O_{C-O} - H_{H2O} distance of 1.961Å and a Br- H_{H2O} distance of 3.26Å (Figure 2-23). This distance is a bit too long to be considered reasonable for a hydrogen bond between water and bromine. To determine if the calculation could even consider bromine as a hydrogen bond acceptor, we did a third calculation which left the first two water molecules in the same position they had at the end of the second calculation. We then placed a third water molecule \sim 1Å away from the bromine and resubmitted the molecule for geometry optimization. Here, the water molecule moved away from the bromine to a distance of 2.78Å, still rather far to be considered a hydrogen bond for most systems given the van der Waals radii of bromine and hydrogen as 1.85Å and 1.2Å, respectively. However, with the large electronic size of bromine, this may not be an unreasonable distance for hydrogen bonding.

We thought we might be able to use the same methods as Taniguchi and use Raman spectroscopy to see a change in the C-Br stretch upon binding of the zinc. We initially tried a solid sample of N-phenyl-2(R)-bromopropionamide in an available Raman instrument. The acquired spectrum was reasonable although the peaks were of very low intensity. A peak was apparent around 550 cm⁻¹, which we thought could be either a phenyl C-H out-of-plane bending or a C-Br stretch. This was a little low for a C-Br stretch, which should come around 660-700 cm⁻¹.

Since we were not able to definitively identify the peaks in the Raman spectrum, we turned to NMR as a possible method of determining conformation. We continued

using the model compound of N-phenyl-2(R)-bromopropionamide. Initially, we had thought to take NOEs of the amide without and with zinc. We believed that we would be able to see a change in NOEs from the amide hydrogen to the substituents on the *alpha* carbon upon addition of zinc if the conformation was changing as we believed. However, upon initial NMR testing, we saw changes in the spectra upon addition of zinc without doing NOEs. This suggested that we might be able to probe the conformation changes upon addition of zinc through NMR.

A large number of changes are seen in the NMR spectrum for N-phenyl-2methylpropionamide at room temperature when zinc bromide is added. The amide N-H proton moves downfield approximately 2 ppm, possibly due to increased shielding as the amide N-C_{C=O} bond has greater double bond character with the carbonyl oxygen binding to the zinc. The aromatic proton para to the amide is shifted downfield by 0.03 ppm, also in agreement with changes due to the carbonyl binding. The methine hydrogen is shifted downfield by 0.2 ppm. This could be due to changes in the electronic nature of the carbonyl as a result of binding, or due to a conformational change in which the hydrogen is no longer shielded as it was before the addition of the zinc. We would expect that, with no other effects, the medium group on the alpha carbon should be pseudo-anti to the carbonyl. This would place one of the two methyl groups pseudo-syn to the carbonyl prior to addition of zinc. The zinc is expected to approach the carbonyl from the same face as the α -carbon, as that face is less sterically hindered than the opposite face with the bulky N-phenyl group. The α-methyl would be expected to slide away from the bulky zinc, leading to a conformation in which the carbonyl bisects the proton and one methyl group, with the other methyl group anti to the carbonyl (Figure 2-24). This can possibly

be verified through the changes in the proton shifts for the methyl groups upon addition of zinc.

Initially, there were two doublets at 1.22 and 1.14 ppm corresponding to the two methyl groups. After addition of zinc, these two doublets both shifted downfield 0.04 ppm and a new doublet appeared farther upfield at 1.1 ppm. The two doublets indicate the initial conformation being the one in which the methyl group is *syn* to the carbonyl and therefore shielded. Upon addition of the zinc, the methyl group moves out of the shielding cone of the carbonyl and shifts downfield. However, the methyl group which

$$\begin{array}{c|c} Zn & Zn \\ \hline \\ CH_3 & CH_3 \\ \hline \\ CH_3 & CH_3 \end{array}$$

Figure 2-24. Rotation around the C(C=O)-C(chiral) bond due to coordination of the carbonyl oxygen with zinc.

was previously in the deshielding cone of the carbonyl is moved *anti* to the carbonyl, thus reducing the influence it feels from the carbonyl and causing it to resume a chemical shift more expected for methyl hydrogens. The same reasoning can be applied to the methine hydrogen, which shifts downfield 0.2 ppm upon addition of zinc. The hydrogen, which was outside of the influence of the carbonyl deshielding cone, is now brought within the deshielding region and shifted downfield.

Based on the modeling and NMR information, it does seem possible that there is cooperative binding occurring between the carbonyl oxygen, the α-halogen and the zinc core of the porphyrin tweezer. This conformation would be expected to lead to the observed ECCD spectra. However, it is unclear at this time if coordination can occur with other functional groups besides halogens, such as methoxy, phenoxy, or acetoxy.

Work is continuing on the synthesis and testing of cyclic α -haloamides and α -chiral amides with other functional groups to probe possible cooperative binding. These molecules do not allow for rotation around the $C_{C=O}$ - C_{chiral} bond, thus eliminating multiple conformations.

References:

- 1. Yang, Q.; Olmsted, C.; Borhan, B. Org. Lett. 2002, 4, 3423.
- 2. Schrodinger, Inc. Macromodel, 7.0; 1999.
- 3. Pillardy, J. C., C.; Wedemeyer, W.; Scheraga, H. Helv. Chim. Acta 2000, 83, 2214.
- 4. Wiberg, K. B.; Rush, D. J. J. Org. Chem. 2002, 67, 826.
- 5. Wiberg, K. B.; Rush, D. J. J. Amer. Chem. Soc. 2001, 123, 2038.
- 6. Deng, S. T., J. J. Amer. Chem. Soc. 2002, 2002.
- 7. Radom, L. R., N. V. Australian J. Chem. 1982, 35, 1071.
- 8. Schnur, D. M. Y., Y. H.; Dalton, D. R. J. Org. Chem. 1989, 54, 3779.
- 9. Avalos, M. B., R.; Barneto, J. L.; Bravo, J. L.; Cintas, P.; Jimenez, J. L.; Palacios, J. C. J. Org. Chem. 2001, 66, 7275.
- 10. Langley, C. H.; Lii, J.-H.; Allinger, N. J. Computational Chem. 2001, 22, 1426.
- 11. Langley, C. H.; Lii, J.-H.; Allinger, N. J. Computational Chem. 2001, 22.
- 12. Foreman, J. B. F., A., Exploring Chemistry with Electronic Structure Methods. 2nd ed.; Gaussian, Inc.: Pittsburgh, 1996.
- 13. Eliel, E. L.; Wilen, S. H., Stereochemistry of Organic Compounds. John Wiley and Sons, Inc.: New York, 1994.
- 14. Wiberg, K. B.; Rablen, P. R.; Rush, D. J.; Keith, T. A. J. Amer. Chem. Soc. 1995, 117, 4261.
- 15. Yang, Q. The Use of Exciton Coupled Circular Dichroism for the Absolute Stereochemical Determination of Chiral Carboxylic Acids. Ph. D. Dissertation, Michigan State University, East Lansing, 2004.
- 16. Structures were taken from the Cambridge Crystallographic Database. Structures used include: HALTOG, HALVOF, HALWOG, HAMDOO, HAMGOR, HAMLAI, HAMLUC, HAMMEN, HAMMIR, JIRSIM, NOCWAD, ZITMIY, and ZITWOE (CCD six-letter codes).
- 17. Kato, M.; Nanba, Y.; Taniguchi, Y. Chem. Phys. Lett. 1998, 289, 30.
- 18. Shiratori, Y.; Kato, M.; Taniguchi, Y. Spectrochimica Acta Part A 1999, 55, 2659.

19. Shiratori, Y.; Kato, M.; Taniguchi, Y. Spectrochimica Acta Part A 2000, 56, 1693.

Chapter 3

Development of Alternate Tweezers for Use With ECCD in the Absolute Stereochemical Determination of Small Molecules

In the process of derivatizing various carriers with chiral substrates and monitoring ECCD as discussed in the previous chapter, we observed various ECCD signs, often conflicting. Depending on the carrier used, the sign of the ECCD curve would reverse for the same chiral substrate of the same stereochemistry. In other words, (R)-2-bromopropionic acid would show a positive ECCD sign when derivatized with one carrier and a negative ECCD sign when derivatized with a different carrier. This suggests that there are either different modes of binding between the porphyrin tweezer and different carriers, dependent on the structure of the carriers, or different conformations of the derivatized carriers as discussed previously (q.v., Chapter 2). Determining the mode of binding for each carrier can be problematic, and potentially impossible without a crystal structure. Part of this difficulty lies in the large amount of rotational freedom present in the 1,5-diester linker joining the porphyrin chromophores studied. Because there is so much flexibility in the linker, the porphyrins can wrap

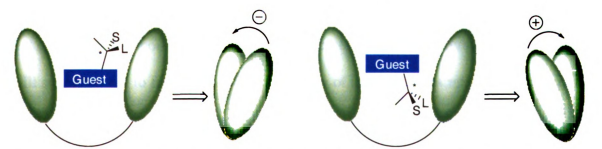


Figure 3-1. Representation of possible differences in binding between porphyrin tweezers and guest molecules, leading to opposite ECCD signs.

around the guest molecules in various ways, as shown in Figure 3-1.

Molecular modeling indicates there are numerous possible low energy conformations which differ in how the tweezer wraps around the guest (q.v., Chapter 2). In light of this, we were interested in designing a tweezer with a more rigid linkage. This would assist us in a number of ways, including making the prediction of the ECCD sign easier, rigidifying the host molecule to allow us to predict conformation with more confidence and easing molecular modeling costs in terms of number of conformations found and time for calculations.

3-1. Porphyrin Tweezer with a Diacetylene Linkage

The simplest linker that would afford rotation about an axis perpendicular to the porphyrins would consist of a diacetylene linker.² Rotational freedom would be afforded through the single bond connecting the triple bonds. If the acetylenes were connected to the *para* position of the porphyrins, as with the diester linkage, the porphyrins would be aligned at 180°, thereby showing no ECCD, and in fact unable to bind to diamines due to the lack of flexibility in the linker. However, if the acetylenes are connected through the *meta* positions of the phenyl substituents on the porphyrins, the porphyrins will have a fixed angle of approximately 120° relative to the acetylene as shown in Figure 3-2. Although the porphyrins are not necessarily face-to-face when joined by a bisacetylene linker, when a compound binds to the two zinc cores of the porphyrins, the porphyrins will swing around to face one another. Chirality of the guest substrate will influence the host porphyrin tweezer to adopt either a clockwise or counterclockwise orientation of the chromophores as viewed from front to back, leading to an ECCD bisignate curve. With this goal in mind, we began the synthesis of porphyrin tweezer 1 (Figure 3-3).

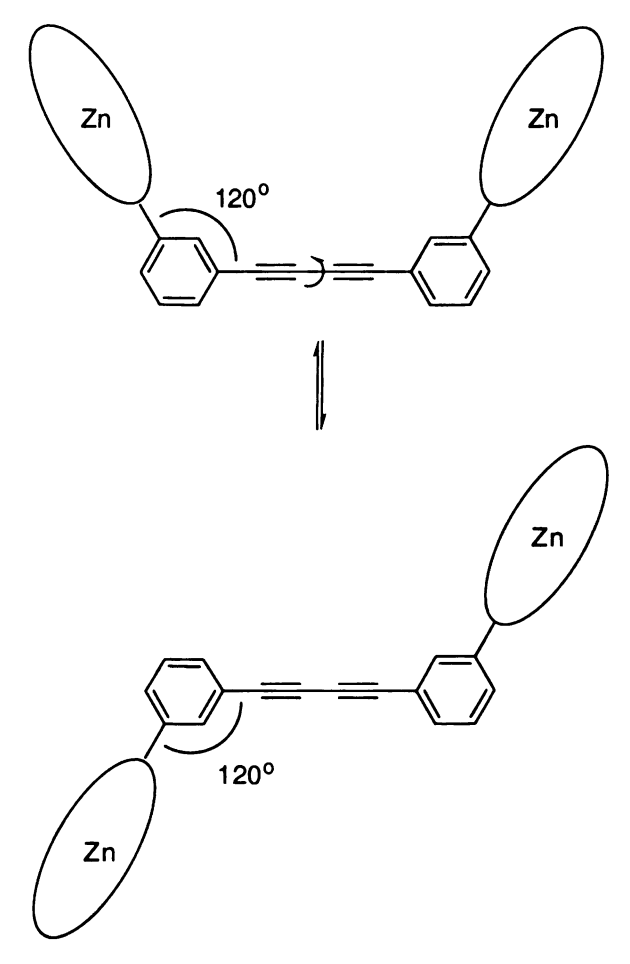


Figure 3-2. Indication of bite angle in proposed *meta*-substituted bisphenylacetylene linker.

A simple retrosynthetic analysis reveals that the most logical way to construct the desired tweezer is by homocoupling of an acetylenic porphyrin. In light of this, 3[(trimethylsilanyl)ethynyl]benzaldehyde 3 was synthesized from 3-bromobenzaldehyde and (trimethylsilyl)ethyne 2 through a palladium-catalyzed coupling.³ This was then used as the building block with benzaldehyde and pyrrole for the synthesis of the monosubstituted porphyrin to give 5,10,15-triphenyl-20-(3trimethylsilanylethynylphenyl)porphyrin 4 (Scheme 3-1).

Removal of the TMS group by TBAF yielded the deprotected acetylene porphyrin

5. Initial homocoupling reactions of 5 using standard Glaser-Hay coupling conditions did

		1
		,
		á

Figure 3-3. Proposed rigid porphyrin tweezer 1 utilizing a bisacetylene linker.

not proceed to give the desired product 1.⁴ The first reaction attempted was performed on a non-metallated (free base) porphyrin system, which bound to the copper used in the reaction, preventing the coupling reaction from occurring.⁵ To prevent this, the porphyrin was zincated with Zn(OAc)₂ to give zinc porphyrin 6. The coupling was then performed under an atmosphere of oxygen using Cu(OAc)₂•H₂O in pyridine, and after

Scheme 3-1. Synthesis of (trimethylsilyl)acetylene derivatized porphyrin 4.

Scheme 3-2. Synthesis of bisacetylene tweezer 1.

preparatory thin layer chromatography the homocoupled tweezer 1 was isolated in 88% yield (Scheme 3-2).^{3, 5} UV studies show an absorbance at 414nm (n-hexane; 416 nm in

methylcyclohexane), within the region expected for this type of metalloporphyrin tweezer.

To explore binding of this system, diamines of different lengths were used including 1,2-diaminopropane; 1,3-diaminopropane; 1,5-diaminopentane; L-ornithine; and L-lysine methyl ester. Initial titrations of achiral diamines were only somewhat successful with the diacetylene tweezer. 1,2-Diaminopropane and 1,3-diaminopropane showed no binding. 1,5-Diaminopentane showed a 7 nm red shift with addition of one equivalent of the diamine. The shift occurred from 416 nm to 423 nm (Figure 3-4). Nearly complete conversion to bound tweezer is seen at one equivalent, with a small

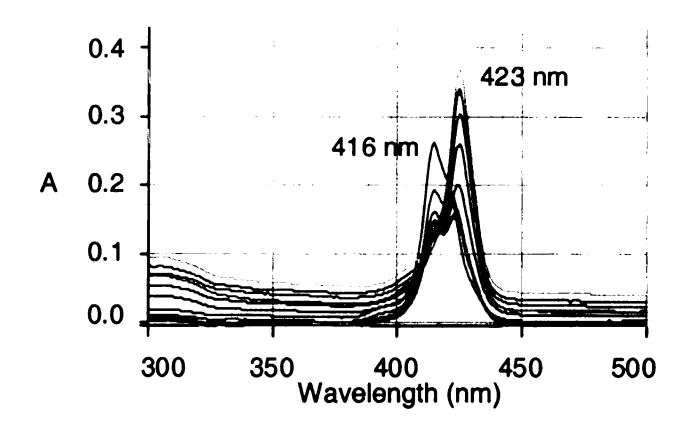


Figure 3-4. Red shift in UV-vis absorption of tweezer 1 with 1,5-diaminopentane.

shoulder still present at 416 nm. Attempts were made at inserting a chiral diamine as the guest in the tweezer host. Both L-lysine methyl ester (a 1,5-diamine) and L-ornithine (a 1,4-diamine) were used in UV studies. Most titrations with L-ornithine did not show any binding, even with 100 equivalents of the diamine. However, in two titrations a shift was observed with the addition of 100 equivalents. At 100 equivalents, two peaks of equal intensity are observed, one at 416 nm and one at 424 nm. With the addition of another 100 equivalents (total 200 equivalents) nearly complete conversion to the second peak at

424 nm is observed, with a small shoulder still present at 416 nm. There are a couple of possibilities for a shift occurring with such large equivalents of diamine. The shift could be due to residual ethanol still present from the deprotonation of the diamine, or it could be due to coordination of amine to the zinc outside of the tweezer pocket, i.e., not bidentate diamine binding. A titration of the tweezer with ethanol was undertaken to determine if residual ethanol could create the same shift as that seen with L-ornithine. Upon titration with ethanol, a shift is seen from 416 nm to 423 nm, leading us to believe that it is possible that residual ethanol is binding to the tweezer instead of L-ornithine. The L-ornithine may still be binding in some capacity to the tweezer, but it was unclear at this point exactly what type of binding, if any, was occurring. Another possibility is that the lack of binding and unusual binding pattern might be due to the carboxylic acid present in the amino acid. Synthesis of the methyl ester was undertaken but was unsuccessful using trimethylsilyldiazomethane.⁶

In testing other chiral diamines, L-lysine methyl ester did show binding with the bisacetylene tweezer with a 8 nm shift from 416 nm to 424 nm through addition of 15 equivalents, however, as discussed above no other size of diamines were found to show any binding to the bisacetylene tweezer 1. Unfortunately, we were unable to observe any ECCD curves when L-lysine methyl ester was coordinated to the host porphyrin tweezer. This could be due to the rigidity of the system, which may prevent optimum 1:1 binding of the guest diamine to the host tweezer. After viewing molecular models of this compound with various size diamines, it appears that the structure of the tweezer is too rigid to permit binding to diamines of various sizes. Although the tweezer can be modeled with different size diamines, a large amount of strain is seen in the linkage

between the porphyrins when large diamines are used (1,5-diamines and larger). Similar strain is observed with smaller diamines, as the porphyrins cannot flex enough through the linker to facilitate binding.

To possibly help alleviate binding problems due to the rigidity of the system, another synthesis was attempted to create porphyrin tweezer 7 (Figure 3-5). This tweezer would maintain the diacetylene linker but give more flexibility to the system through two methylene groups that attach to the linker in the *para* position of the porphyrin phenyl group. Two synthetic schemes were proposed such that convenient and inexpensive

Figure 3-5. Alternative bisacetylene porphyrin tweezer 7.

starting materials could be used. One route involved building the zinc porphyrin around the bromobenzaldehyde first. Grignard transformation followed by reaction with 1-bromo-3-trimethylsilylpropyne would lead to the trimethylsilylpropargylporphyrin. After addition of zinc and deprotection of the trimethylsilyl group, a Glaser-Hay coupling would lead to the desired porphyrin tweezer (Scheme 3-3). A second route would create a protected bromobenzaldehyde that would then be transformed into a Grignard reagent to react with 1-bromo-3-trimethylsilylpropyne (Scheme 3-4). The porphyrin would then

Scheme 3-3. Proposed synthesis of alternate tweezer 8.

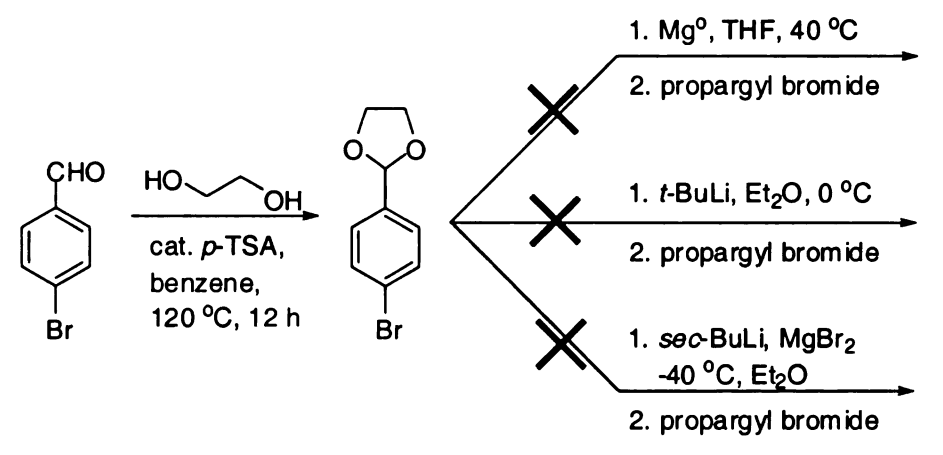
be built off of the deprotected aldehyde, the trimethylsilyl group deprotected, and a coupling reaction performed.

Following the first method described (Scheme 3-3), bromoporphyrin **9** was synthesized using *p*-bromobenzaldehyde, benzaldehyde, and pyrrole with BF₃•Et₂O and *p*-chloranil. Separation was effected using 20% CH₂Cl₂/hexanes. The first band from the column was collected and dried to give bromoporphyrin **9** in 98% yield. Reconsidering that this synthesis had the potential for loss of a large amount of starting material during the addition of the propargyl group, we decided to build the porphyrin onto the aldehyde with the propargyl group functionality already present on the aldehyde and did not pursue this route any further.

Following the second method described above (Scheme 3-4), formation of the protected bromobenzaldehyde 10 through the use of p-toluenesulfonic acid and ethylene glycol proceeded smoothly in 74% yield. The first attempt at attaching the trimethylsilylpropargyl group was by transforming the protected bromobenzaldehyde into a Grignard reagent through the use of activated magnesium. The reaction was heated to 40 °C and then refluxed for 12 h after addition of all reagents. Although some starting material was still present, a large mixture of products was seen, none of which was the desired product by NMR. The second attempt involved using t-butyl lithium with the protected bromobenzaldehyde to effect a lithium-halogen exchange. The reaction occurred with violent sputtering, and after work-up no starting material or desired product was evident. The third reaction followed literature precedent for alkylation of obromobenzaldehyde⁷ and started by forming the lithiated compound of the protected pbromobenzaldehyde. Reaction with magnesium bromide was expected to give the

Scheme 3-4. Proposed synthesis of tweezer 8 using a functionalized aldehyde.

Grignard, to then react with the trimethylsilylpropargyl bromide. Once again no starting material or desired product was evident (Scheme 3-5) with a large number of peaks evident by ¹H NMR and several spots by TLC chromatography. At the same time, synthesis was attempted for 3-bromo-1-(trimethylsilyl)propyne starting from



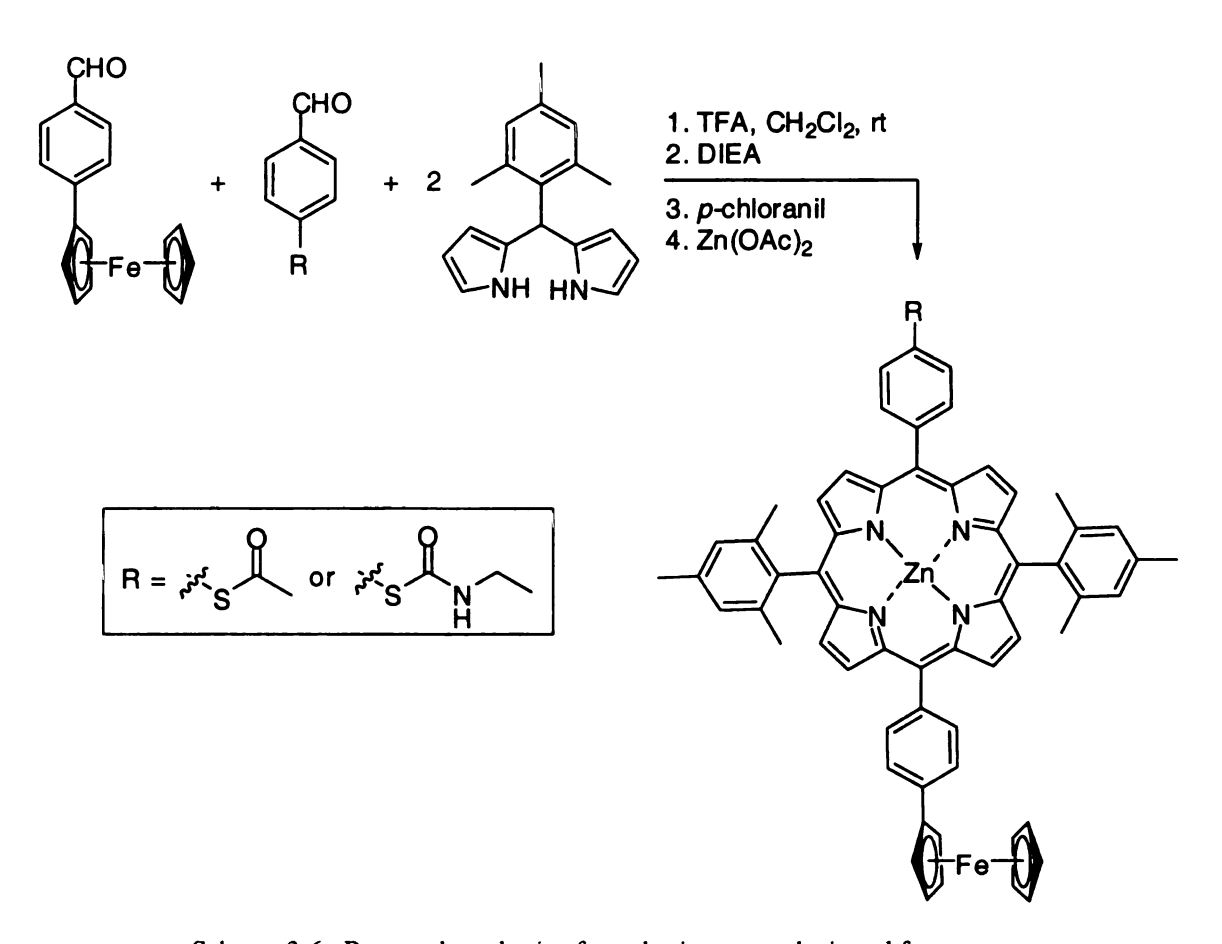
Scheme 3-5. Attempted synthetic routes for p-(1-trimethylsilylpropargyl)benzaldehyde.

(trimethylsilyl)acetylene and methylene bromide.⁸ NMR spectra indicated no reaction after a number of attempts. After the difficulties encountered in synthesizing the bispropargyl porphyrin tweezer 8, this route was abandoned in favor of other promising linkers.

3-2. Porphyrin Tweezer with a Ferrocene Linkage

In pursuit of a more rigid tweezer with greater bite angle flexibility than the bisacetylene tweezer, we decided to synthesize tweezers with a ferrocene-based linker (Figure 3-6). Although the rigidity of the linker again could pose issues for the ability of the tweezer to bind diamines of various sizes, the nature of the ferrocene linker permits more flexibility than covalently bound linkers, as the bond from the pentadienyls to the iron core can expand and contract slightly. A bisporphyrin ferrocene has not previously been reported, although the monosubstituted compounds have been synthesized. The synthesis of the monoporphyrin ferrocene is accomplished through the use of a ferrocene monoaldehyde which is then reacted with a dipyrrole and benzaldehyde to form the desired porphyrin on one of the ferrocene rings (Scheme 3-6). However, use of this method for a bisaldehyde ferrocene could be problematic, since it will be very difficult to

Figure 3-6. Structure of the proposed bisporphyrin ferrocene tweezer 11.



Scheme 3-6. Reported synthesis of porphyrin monosubstituted ferrocenes.

control the reactions with multiple reactive aldehydes in solution. In light of this, we attempted the synthesis of a bisporphyrin ferrocene through coupling of a ferrocene derivative to a porphyrin derivative.

Our first attempt at synthesis of 11 involved palladium coupling of bis(tributyltin)ferrocene and monobromoporphyrin. Monobromoporphyrin 9 was synthesized using p-bromobenzaldehyde, benzaldehyde, and pyrrole as shown in Scheme 3-7. However, we realized that the integrations for the proton NMR were not calculating correctly even though it appeared we only had one product by thin layer and column chromatography. We submitted the product from one reaction for mass spectrometry (MS) analysis. MS indicated a mixture of tetraphenylporphyrin; 5-(p-bromophenyl)-

Scheme 3-7. Synthesis of 5-(p-bromophenyl)-10,15,20-triphenylporphyrin 9.

10,15,20-triphenylporphyrin; 5,10-di(p-bromophenyl)-15,20-diphenylporphyrin; and 5,10,15-tri(p-bromophenyl)-20-phenylporphyrin products. Unfortunately, thin layer chromatography under several solvent systems only shows one spot (not unexpected since there should not be much difference in polarity between porphyrins with different number of bromines attached). We tried to separate the compounds by slow column

chromatography, extractions, and recrystallizations, but no separation was apparent by NMR. Since additional brominated compounds will complicate the coupling of 9 and 13, we needed to find a way to make only monobrominated porphyrin. We decided to try synthesizing the 5-(p-bromophenyl)-10,15,20-triphenylporphyrin 9 using an excess of benzaldehyde, which should increase the production of tetraphenylporphyrin (TPP) and decrease the production of all of the brominated compounds, hopefully leading to production of only monobrominated product 9 plus TPP. TPP will not react in the coupling, so we do not need to separate it from the desired product. We ran the same brominated porphyrin synthesis reaction with nearly 7 equivalents of benzaldehyde (as compared to 3 for a typical synthesis of monosubstituted porphyrin), with the normal ratio of 4:1 for pyrrole:4-bromobenzaldehyde. After column chromatography, benzaldehyde was still present in the product so the desired product was recrystallized from CHCl₃/hexanes. NMR of the recrystallized product showed no benzaldehyde and matched the expected integrations for the desired monosubstituted product 9, possibly contaminated with a small amount of tetraphenylporphyrin. Since TPP will not react in the coupling reaction, we have used the 5-(p-bromophenyl)-10,15,20-triphenylporphyrin **9** produced in this reaction without further purification.

Bis(tributyltin)ferrocene 12 was synthesized through a reported procedure (Scheme 3-8).^{10, 11} While the syntheses of 9 and 12 proceeded in good yield, the coupling was more problematic. We started by trying to couple the bromoporphyrin 9 and bis(tributyl)tin ferrocene 12 using PdCl₂(PPh₃)₂ in dry DMF (Scheme 3-9).^{12, 13} The bis(tributyltin)ferrocene did not dissolve in DMF when added but the bromoporphyrin 9 was added to the suspension to yield a purple solution. After workup, we obtained only

Scheme 3-8. Reported synthesis of bis(tributyltin)ferrocene 12.

Scheme 3-9. Attempted coupling of 5-(p-bromophenyl)-10,15,20-triphenylporphyrin 9 with bis(tributyltin)ferrocene 12 using PdCl₂(PPh₃)₂.

starting material, most likely due to lack of solubility of the bis(tributyltin)ferrocene 12 in the reaction mixture.

We next tried a coupling using Pd₂(dba)₃ and AsPh₃ (Scheme 3-10).¹⁴ This reaction was run per literature precedent. After workup, the residue was chromatographed on silica gel with a 1:1 mixture of CH₂Cl₂ and hexane. The first band was yellow, the second orange, and the third purple. The third band was dried and recrystallized with CHCl₃/hexanes to give only starting material. Since after repeated trials the palladium couplings were not working, we decided to switch coupling reactions. Due to the difficulties in installing multiple functionalities on the porphyrin, it seemed ideal to keep the monobromoporphyrin 9 as a starting material and change the ferrocene functionality.

Scheme 3-10. Attempted coupling of 5-(p-bromophenyl)-10,15,20-triphenylporphyrin 9 with bis(tributyltin)ferrocene 12 using Pd₂(dba)₃.

We decided to synthesize the ferrocene tweezer using bis(boronic acid) ferrocene 13 and 5-(p-bromophenyl)-10,15,20-triphenylporphyrin 9 (Scheme 3-12). Arylation of ferrocene derivatives through the boronic acids has been reported. However, formation of the bis(boronic acid) ferrocene 13 using TMEDA, n-butyl lithium, and tributoxyborate was initially problematic. The reported procedure was done on a 10 g scale, but the first time we did the reaction (on a 1 g scale), we did not obtain any product. We were concerned that perhaps the reaction had not been dry enough, so the ferrocene was dried in the oven for 3 h prior to attempting the reaction again. After reaction completion, we obtained an orange solid, but this decomposed upon evaporation of the solvent under vacuum (possibly due to high temperature) and turned dark brown while H NMR showed no product.

On the third attempt we dried the ferrocene in the oven overnight, during which time it sublimed and formed crystals. This reaction proceeded as before but using triisopropyl borate instead of the reported tributyl borate, and upon addition of the ferrocene dianion to the boronic ester the solution turned orange. The solution precipitated yellow solid upon acidification, and this was filtered and washed with ether to give a brown solid of very low yield (2.2%) which was paramagnetic. The ¹H NMR peaks from this compound match those reported, ¹⁵ but there is no mention in any of the references about the desired compound being paramagnetic.

After some discussion, the TMEDA was distilled directly before using it in the synthesis of the ferrocene bis(boronic acid) 13. Following the same procedure as before but using tributyl borate, the synthesis worked and we obtained 13 in 36% yield (Scheme 3-11). Although the yield was low, the reaction was done on a large scale and no optimization was pursued since over 6 g of material was obtained.

Scheme 3-11. Synthesis of bis(boronic acid)ferrocene 13.

We next proceeded to couple the monobrominated porphyrin 9 with the bis(boronic acid) ferrocene 13 (Scheme 3-12). Following a literature procedure, ¹⁵ coupling of 13 and 9 yielded the bis(tetraphenylporphyrin) ferrocene 14 in 95% yield. It was a little surprising that the coupling worked in such good yield, so we submitted the product for MALDI (necessary due to the high molecular weight). Major peaks were found at 1545, 1466, 1387, 1307 with a matrix of N-bromoacetamide (138 g/mol). The product compound is expected to have a molecular weight of 1411.47. Based on the peak at 1545, subtracting out the matrix gives a molecular ion peak of 1407, which would be the expected ion peak if the product lost four N-H protons. This could occur due to the

Scheme 3-12. Coupling of zinc 5-(p-bromophenyl)-10,15,20-triphenylporphyrin with bis(boronic acid) ferrocene.

basic workup. This led us to believe we had formed the desired compound. Zincation of this compound followed the coupling to give bis(zinc tetraphenylporphyrin) ferrocene 11. We then took 11 and subjected it to UV-Vis testing. All compounds tested (n-butylamine, 1,3-diaminopropane, 1,4-diaminobutane, and 1,10-diaminodecane, L-lysine, and L-ornithine) show binding and approximately 10 nm shifts from 416.5 nm to 427 nm using from 1 to 5 equivalents of diamine. However, ECCD of the ferrocene porphyrin

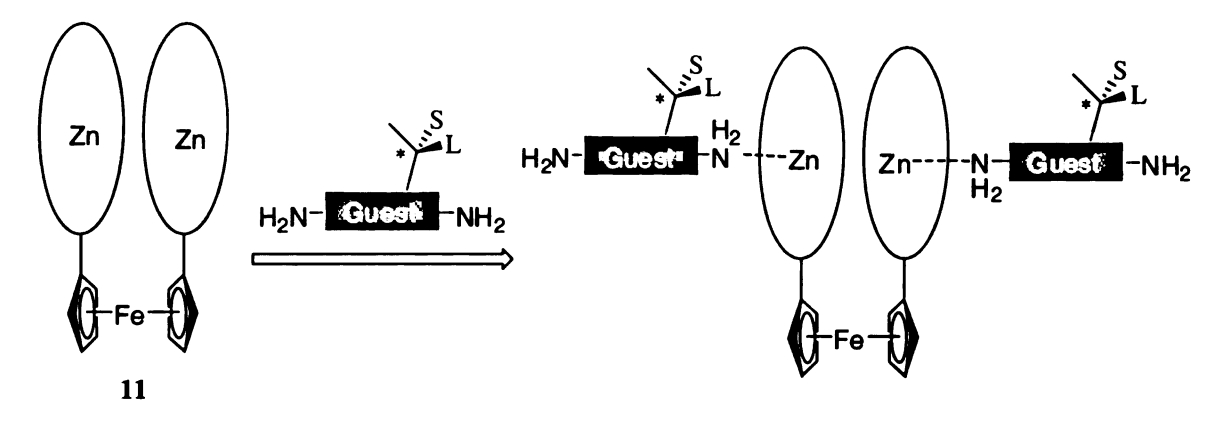


Figure 3-7. Representation of possible binding outside of tweezer core for bis(zinc porphyrin) ferrocene 11.

tweezer with chiral substrates has not been obtained using L-lysine or L-ornithine. It is possible that this tweezer suffers from a similar problem as the diacetylene in that the binding pocket of the tweezer is too small to permit guests into the pocket, thus preventing observance of ECCD. Binding may occur on the outside of the tweezer pocket as shown in Figure 3-7. The iron core of the ferrocene may also be interfering with the substrate binding leading to unexpected or unpredictable conformations that are not ECCD active.

3-3. Porphyrin Tweezer with a Urea Linkage

It has recently been reported in literature that porphyrins with a urea linker can be made to maintain a face-to-face orientation. Takagishi, et al., showed that they were able to make a porphyrin tweezer where both porphyrins are held face-to-face through the use of bulky methyl groups which interact with the tweezer linker (i.e., steric interactions between the methyl groups on the phenyl ring and the urea carbonyl prevent rotation around the urea bond, Figure 3-8). We thought this might be useful to allow us to form porphyrin oligomers or polymers with urea linkages. Steric interactions between the phenyl substituents on the porphyrins prevent them from stacking directly on top of one

Figure 3-8. Representation of Takagishi's dimer showing steric interaction between the urea carbonyl and the methyl substituents on the phenyl rings.

another, leading to a helical structure. The addition of a chiral guest could then be used to influence the direction of the helix (P or M), which in turn could be monitored through ECCD (Figure 3-9). The electric dipole interaction between a series of porphyrins should lead to an amplified ECCD signal with very small amounts of material. It could be possible then to control the number of porphyrins (or polymeric units) to change solubility, ECCD amplitude, etc. Based on molecular modeling, these systems form beautiful helices as expected (Figure 3-10). The synthesis of these systems appeared to be very simple and straightforward with a minimum of steps.

Synthesis of the diamine porphyrin necessary for formation of the amide linkage can be obtained through known literature procedures. Most syntheses begin with a nitroaldehyde to form aminoporphyrins, ¹⁷⁻¹⁹ so it was necessary to obtain 4-methyl-3,5-dinitrobenzaldehyde 16 which would allow us to make the desired monosubstituted porphyrin. This aldehyde is not commercially available, so there were two routes that we looked at using to get this compound. One was nitration of the methylaldehyde, but this

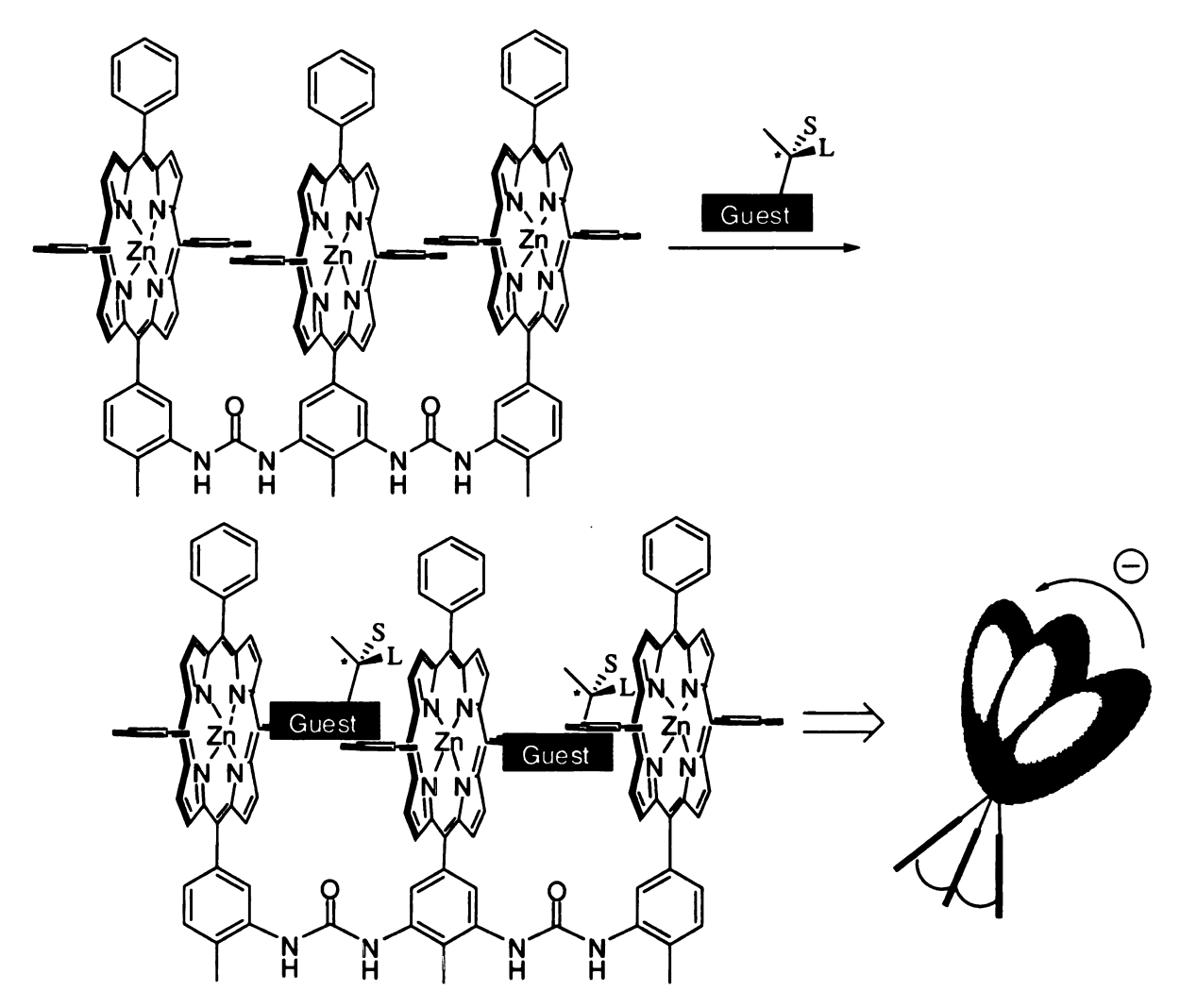


Figure 3-9. Schematic showing control of helix direction upon addition of a chiral guest to a porphyrin trimer connected by urea linkages, leading to ECCD.

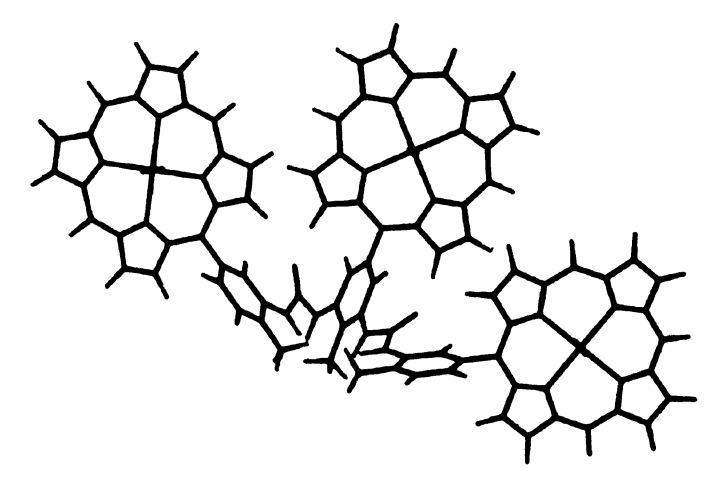


Figure 3-10. Spartan molecular model of helix formed from urea-linked porphyrins (phenyl rings not shown for clarity).

led to concerns of overnitration and potential generation of explosive products. We opted for a second route starting from 4-methyl-3,5-dinitrobenzoic acid, which is inexpensive and readily available. Reduction of the acid to the alcohol 15 proceeded smoothly with BH₃•THF solution, which is reported to be a mild reduction technique that does not

Scheme 3-13. Synthesis of alcohol 15 and benzaldehyde 16 from 4-methyl-3,5-dinitrobenzoic acid.

reduce nitro groups, even at room temperature and extended reaction times.²⁰ Yields of this reaction were good for both small and large scale with average yields around 80%. Oxidation of the alcohol to the aldehyde was accomplished with pyridinium chlorochromate (PCC) (Scheme 3-13). Column chromatography and recrystallization gave pure 4-methyl-3,5-dinitrobenzaldehyde 16 in yields of 50% from first-crop recrystallization.

Once the aldehyde 16 was in hand, attempts were made to synthesize the 5-(4-methyl-3,5-dinitro)-10,15,20-triphenylporphyrin 17 (Scheme 3-14). Use of the standard monosubstituted porphyrin synthesis (1:3:4, nitroaldehyde:benzaldehyde:pyrrole) gave porphyrin products with some 4-methyl-3,5-dinitrophenyl substituents. Integration of the proton NMR peaks indicated that we had formed at least some of the disubstituted product, so the compound was submitted for mass spectroscopy. Analysis of the mass spectra indicated that the product was a mixture of compounds comprised mainly of disubstituted and trisubstituted porphyrin, with some monosubstituted also present.

Separation of these compounds appeared straightforward based on TLC, but column chromatography was run repeatedly with very little separation. Adjustment of the reactant ratios (0.5:3.5:4, nitroaldehyde:benzaldehyde:pyrrole) also produced mono-, di-, and trisubstituted porphyrins, although with less trisubstituted than previously. Separation by column chromatography was still unsuccessful.

Scheme 3-14. Synthesis of 5-(4-methyl03,5-dinitrophenyl)-10,15,20-triphenylporphyrin 17.

Pursuing other reported methods for nitroporphyrin synthesis, ¹⁷⁻¹⁹ we tried formation of the monosubstituted porphyrin using propionic acid. This reaction is reported to give very low yields of the monosubstituted product, but when we tried it

$$O_2N$$
 $+$ 3
 $+$ 4
 $+$ 4
 $+$ 4
 $+$ 4
 $+$ 4
 $+$ 4
 $+$ 60°C, 30 m

Scheme 3-15. Attempted synthesis of 5-(4-methyl-3,5-dinitro)-10,15,20-triphenylporphyrin using propionic acid.

(1:3:4, nitroaldehyde:benzaldehyde:pyrrole) no porphyrin was formed in the crude product mixture by NMR (Scheme 3-15). A second reaction (2:3:4,

nitroaldehyde:benzaldehyde:pyrrole) gave a very small amount of porphyrin, but the product mixture was mostly insoluble black solid.

Other monosubstituted porphyrin syntheses in our lab have been successful using dipyrroles to generate disubstituted porphyrins, ^{21, 22} so we thought perhaps this would be a way to also obtain the monosubstituted compound we desired. We began by reacting

Scheme 3-16. Synthesis of (4-methyl-3,5-dinitrophenyl)dipyrrole 18 and phenyldipyrrole 19.

the dinitroaldehyde with excess pyrrole in the presence of trifluoroacetic acid to give (4-methyl-3,5-dinitrophenyl)dipyrrole 18 in 90% yield (Scheme 3-16). We thought that using two dipyrrole units might give a better yield than using one dinitrodipyrrole plus pyrrole and benzaldehyde, thus phenyldipyrrole 19 was also formed by reacting excess pyrrole with benzaldehyde. This reaction was less successful (probably due to the decreased reactivity of benzaldehyde as compared to 4-methyl-3,5-dinitrobenzaldehyde) but gave 49% yield of the desired product after purification (Scheme 3-16).

While searching for references on the use of dipyrroles, we came across a paper in which the authors had used various salts to increase the yield of porphyrin reactions.²³ An addition of 0.1 equivalents of sodium chloride is reported to give the best results, so

we attempted the use of sodium chloride in the synthesis of (4-methyl-3,5-dinitrophenyl)dipyrrole 18. Using freshly distilled pyrrole, this reaction yielded >99% of the desired product after purification.

Coupling of the two dipyrroles 18 and 19 was attempted using benzaldehyde and TFA. However, when *p*-chloranil was added, the solution turned purple immediately and then brown. Workup of the products gave only insoluble compounds and a very small amount of soluble product, which was not enough for NMR. The same reaction conditions were tried again with dinitrodipyrrole 18, pyrrole, and benzaldehyde (1:2:3). Once again no porphyrin products were present in any of the bands separated by column chromatography. Reactions catalyzed with trifluoroacetic acid (TFA) seem to be much faster than those catalyzed by BF₃•OEt₂, and the additional reactivity of the dinitrodipyrrole may be causing the formation of unwanted side products in the TFA reactions. The reaction of dinitrodipyrrole 18, pyrrole, and benzaldehyde (1:3:2) was attempted again but with BF₃•OEt₂ instead of TFA. After oxidation and column chromatography, the desired 5-(4-methyl-3,5-dinitrophenyl)-10,15,20-triphenylporphyrin

Scheme 3-17. Synthesis of 5-(4-methyl-3,5-dinitrophenyl)-10,15,20-triphenylporphyrin 17 from (4-methyl-3,5-dinitrophenyl)dipyrrole 18.

17 was obtained in 17% yield (Scheme 3-17). Reported yields in literature range from 4-9% using various other methods (such as the ones initially used here, i.e., propionic acid, etc.), 17-19 so this method is a significant improvement.

In reviewing these procedures, it seemed to be superfluous to workup the dipyrrole reaction before formation of the porphyrin. Avoiding the workup would eliminate the need to remove excess pyrrole after the dipyrrole reaction before adding more pyrrole for the porphyrin formation. These two reactions were then attempted consecutively, with no intermediate workup. Following similar procedures as before, dinitrobenzaldehyde 18, sodium chloride, and 15 equivalents of pyrrole were combined in a small flask. After stirring for 5 minutes, TFA was added and the solution was stirred for another 5 minutes. This solution was then diluted, and benzaldehyde and additional solvent added. This solution was stirred under nitrogen for 30 minutes, then shielded from light upon addition of BF₃•OEt₂. After stirring at room temperature overnight and successive column chromatographic separations, the desired product 17 was isolated in 3% yield. While this was a very low yield, it did indicate that the reaction could be done without an intermediate workup and the yield was not significantly worse than those previously reported in literature using other conditions.²¹ As we had obtained a significant amount of tetraphenylporphyrin (TPP) from the reaction, we thought changing the reactant ratios might lead to increased product and we initially tried increasing the benzaldehyde. The same reaction as above was performed but with 6 equivalents of benzaldehyde, giving the product in 10% yield, but with an increased amount of TPP formed, as well as formation of phenyldipyrrole 19. The same reaction again with 1 equivalent of benzaldehyde led to isolation of the product in 14% yield with almost no

Scheme 3-18. Synthesis of 5-(4-methyl-3,5-dinitrophenyl)-10,15,20-triphenylporphyrin 17 using a pseudo "one pot" procedure.

TPP formed (Scheme 3-18). This brings us close to the same yield obtained after doing the reaction in two separate steps, indicating this is a simpler way for forming 5-(4-methyl-3,5-dinitrophenyl)-10,15,20-triphenylporphyrin 17 as it decreases the time needed for intermediate workup and reduces the use of excess pyrrole and chromatography solvents.

Scheme 3-19. Reduction of the nitro groups of 17 to give 5-(3,5-diamino-4-methylphenyl)-10,15,20-triphenylporphyrin 20.

The next step in the synthesis of the urea-linked tweezer is reduction of the nitro groups to amines. Initial attempts at reducing the nitro groups of 17 with H₂ and palladium on carbon²⁴ led to reduction of only one nitro group. Reduction using various other literature methods was also attempted.²⁵ Reported methods such as SnCl₂•H₂O and HCl²⁶ did not work as either no reduction occurred or only one of the nitro groups was reduced. Reduction using a protocol developed in our lab for reduction of aryl nitro groups was also attempted. This method uses zinc dust and CaCl₂ in ethanol and water to reduce nitro groups.²⁷ However, the starting porphyrin 17 is not soluble in ethanol, and attempts to use other solvent systems (such as tetrahydrofuran) did not succeed, as only starting material was recovered in all cases. Modification of the SnCl₂ procedure with a basic 5-(3,5-diamino-4-methylphenyl)-10,15,20workup finally yielded triphenylporphyrin 20, although in low yield (7% yield, Scheme 3-19). Coupling of the diamine with one equivalent of triphosgene produced multiple products (Scheme 3-20).²⁸ Separation of the products by column chromatography led to the isolation of three bands. ¹H NMR of each band revealed an interesting phenomenon. The first band obtained from

Scheme 3-20. Formation of porphyrin polymer 21 from 5-(3,5-diamino-4-methylphenyl)-10,15,20-triphenylporphyrin 20 and triphosgene.

column chromatography showed broader peaks than normally observed for substituted porphyrins but in the expected region for porphyrin protons, with a peak at 8.81, 8.17, and 7.73 ppm. The second compound obtained showed only broad singlets, still at 8.81, 8.18, and 7.73 ppm. The third compound also showed very broad peaks at 8.81, 8.18, and 7.74 ppm, but with a contamination showing distinct splitting with a doublet at 8.056 (J=7.2Hz), and two triplets at 7.561 (J=7.5Hz) and 7.422 ppm (J=7.2Hz). The first band obtained was thought to be the desired dimer, but this was difficult to determine by NMR, so each band was submitted for MALDI mass spectrometry. MALDI revealed that the three bands were higher order polymers, instead of the dimer, trimer, and tetramer we had anticipated. While waiting for MALDI results, the suspected dimer was submitted for zincation with an excess of zinc acetate, which proceeded in good yield (Scheme 3-21). UV-Vis of the zincated compound showed a peak at 428 nm. Binding with chiral substrates did not lead to any observed ECCD; however, this compound should be investigated further for use in stereochemical determination as well as a possible useful molecule for other applications such as electron transport and energy transfer.²⁹

Although we have not yet found the "ideal" porphyrin tweezer, the work that has been done to date has provided insight into the types of tweezers necessary for ECCD-active host-guest complexes. Too many degrees of freedom in the tweezer linker will generate complexes with many possible conformations leading to ambiguous ECCD spectra. However, tweezers that are too rigid do not permit incorporation of a wide enough range of guests to be practically useful. Of course, all of these conclusions should be accepted cautiously as the structures of compounds 1, 4, 5, 6, 11, 14, 19, 21,

$$\begin{array}{c|c} & & & \\ & & \\ NH & N \\ NH & NH \\ NH & N \\ NH & NH \\ NH &$$

Scheme 3-21. Synthesis of zinc porphyrin polymer 22 from porphyrin polymer 21.

and 22 are based solely on ¹H NMR data. An ideal tweezer therefore is one that has minimal degrees of freedom in the linker but can accommodate guests of varying size. Further work with metal complex tweezers (similar to the ferrocene-based tweezer) or tweezers with linkers that can act as rigid or flexible (such as conjugated dienyl linkers) may hold the key to an ideal host bisporphyrin tweezer.

Experimental materials and general procedures:

Anhydrous CH_2Cl_2 was dried over CaH_2 and distilled. The solvents used for CD and UV-Vis measurements were purchased from Aldrich and were spectroscopy grade. All reactions were performed in dried glassware under nitrogen unless otherwise noted. Column chromatography was performed using SiliCycle silica gel (230-400 mesh). 1H_1 -NMR spectra were obtained on Varian Inova 300 MHz or 500 MHz instruments and are reported in parts per million (ppm) relative to the solvent resonances (δ), with coupling constants (J) in Hertz (Hz). IR studies were performed on a Galaxy series FTIR 3000 instrument (Matteson). UV-Vis spectra were recorded on a Perkin-Elmer Lambda 40 spectrophotometer, and are reported as λ_{max} [nm]. CD spectra were recorded on a JASCO J-810 spectropolarimeter, equipped with a temperature controller (Neslab 111), and are reported as λ [nm] ($\Delta\varepsilon_{max}$ [1 mol $^{-1}$ cm $^{-1}$]).

=−TMS

(Trimethylsilyl)ethyne³⁰ (2). Ethynyl magnesium bromide (0.5 M solution in THF, 30.0 mL, 0.015 mol, 1.07 equiv) was cooled to 0 °C and trimethylsilyl chloride (1.78 mL, 0.014 mol, 1 equiv) was added dropwise. The solution was allowed to warm to room temperature and sit for 48 h without stirring. The reaction mixture was extracted with cold saturated aqueous NH₄Cl and the organic layer dried over Na₂SO₄. The solution was filtered to yield (trimethylsilyl)ethyne solution in THF (36.74 g, 73%). ¹H NMR (300 MHz, CDCl₃, ppm): δ 1.84 (s, 1H), 0.08 (s, 9H).

3-(Trimethylsilanylethynyl)benzaldehyde³ (3). (Trimethylsilyl)ethyne 2 (3.8 g, 0.0387 mol, 1.8 equiv), 3-bromobenzaldehyde (4 g, 0.0216 mol, 1 equiv), Pd(OAc)₂ (56 mg, 0.25 mmol, 0.01 equiv), triphenylphosphine (112 mg, 0.43 mmol, 0.02 equiv), and dry, deaerated triethylamine (21 mL) were combined in a flask and brought to quick reflux under argon by placing the flask in an oil bath preheated to 100 °C. The solution was refluxed for 10 h then cooled to room temperature. The reaction mixture was filtered and the filtrate extracted with saturated NaHCO₃ and CH₂Cl₂. The organic layers were combined and the solvent removed to give a brown oil. This oil was purified by column chromatography (5% EtOAc/hexanes) to give 3-(1-trimethylsilylethyne)benzaldehyde (3.342 g, 77%). ¹H NMR (300MHz, CDCl₃, ppm): δ 9.87 (s, 1H), 7.97 (s, 1H), 7.81 (d, 1H, 7.2 Hz), 7.72 (d, 1H, 7.8 Hz), 7.59 (m, 1H), 0.08 (s, 9H).

5-(3-Trimethylsilanylethynylphenyl)-10,15,20-triphenylporphyrin (4).

(Trimethylsilanylethynyl)benzaldehyde **3** (20.2 mg, 0.1 mmol, 1 equiv), pyrrole (26.8 mg, 0.4 mmol, 4 equiv), and benzaldehyde (31.8 mg, 0.3 mmol, 3 equiv) were combined in a flask with CH₂Cl₂ (15 mL) and the solution purged with N₂ for 15 minutes. BF₃•OEt₂ (5.07 μL, 0.04 mmol, 0.1 equiv) was added, the reaction vessel shielded from light, and stirred at room temperature overnight. *p*-Chloranil (98 mg, 0.4 mmol, 4 equiv) was added and the flask placed in a preheated oil bath at 45 °C. The solution was refluxed for 2 h, then cooled to room temperature and the solvent volume reduced under vacuum. The reaction mixture was purified by column chromatography (1:2, CH₂Cl₂:hexanes) to give 5-(3-trimethylsilanylethynylphenyl)-10,15,20-triphenylporphyrin (30.9 mg, 44%). ¹H NMR (300 MHz, CDCl₃, ppm) δ 8.9 (m, 8H), 8.4 (s, 1H), 8.2 (m, 7H), 7.9 (m, 2H), 7.8 (m, 9H), 0.92 (s, 9H), -2.7 (s, 2H).

5-(3-Ethynylphenyl)-10,15,20-triphenylporphyrin (5). 5-(3-

Trimethylsilanylethynylphenyl)-10,15,20-triphenylporphyrin 4 (88.5 mg, 0.1355 mmol, 1 equiv) was dissolved in THF (5 mL) with stirring. Tetrabutylammonium fluoride (1 M solution in THF, 0.4 mL, 0.4 mmol, 3 equiv) was added and the solution stirred at room temperature for 24 h. The reaction mixture was extracted with H_2O and CH_2Cl_2 , the organic layer dried with Na_2SO_4 , and the solvent removed under vacuum to give 5-(3-ethynylphenyl)-10,15,20-triphenylporphyrin (77 mg, 98%). ¹H NMR (300 MHz, CDCl₃, ppm) δ 8.9 (m, 8H), 8.4 (s, 1H), 8.2 (m, 7H), 7.9 (m, 2H), 7.8 (m, 9H), 3.2 (s, 1H), -2.8 (s, 2H).

5-(3-Ethynylphenyl)-10,15,20-triphenylzincporphyrin (6). 5-(3-Ethynylphenyl)-10,15,20-triphenylporphyrin 5 (18 mg, 0.0282 mmol, 1 equiv) and Zn(OAc)₂•2H₂O (93 mg, 0.423 mmol, 15 equiv) were combined in CH₂Cl₂ and stirred at room temperature overnight. The color of the solution changed from dark purple to reddish purple during the course of the reaction. The reaction mixture was purified with column chromatography (CH₂Cl₂) and the purple band collected. The solvent was evaporated to yield 5-(3-ethynylphenyl)-10,15,20-triphenylzincporphyrin (16.6 mg, 76.8%). ¹H NMR (300 MHz, CDCl₃, ppm) δ 8.9 (m, 8H), 8.4 (s, 1H), 8.2 (m, 7H), 7.9 (m, 2H), 7.8 (m, 9H), 3.2 (s, 1H).

Bis[5-(3-ethynylphenyl)-10,15,20-triphenylzincporphyrin] (1). 5-(3-Ethynylphenyl)-10,15,20-triphenylzincporphyrin 6 (90 mg, 0.1397 mmol, 1 equiv) was combined with Cu(OAc)₂•H₂O (235 mg, 1.174 mmol, 8.4 equiv) and pyridine (12 mL). The solution was stirred at 40 °C under an atmosphere of O₂ for 24 h. The solution changed colors from purple to blue-green over the course of the reaction. The reaction mixture was extracted with H₂O and NaHCO₃ until the aqueous layer was clear. The organic layer was dried with Na₂SO₄, filtered and dried to solid under vacuum to yield bis[5-(3-ethynylphenyl)-10,15,20-triphenylzincporphyrin] (79 mg, 88%). ¹H NMR (300 MHz, CDCl₃, ppm) δ 8.9 (m, 8H), 8.4 (s, 1H), 8.2 (m, 7H), 7.95 (m, 2H), 7,7 (m, 12H).

5-(4-Bromophenyl)-10,15,20-triphenylporphyrin (9). 4-Bromobenzaldehyde (119 mg, 0.643 mmol, 1 equiv), benzaldehyde (469 mg, 4.42 mmol, 6.9 equiv), and pyrrole (145 mg, 2.16 mmol, 3.36 equiv) was dissolved in CH₂Cl₂ (150 mL) with stirring. The reaction mixture was stirred under N₂ for 30 minutes, then BF₃•OEt₂ (24 μL, 0.193 mmol, 0.3 equiv) was added. The reaction mixture was stirred for 7 h at room temperature while shielded from light. Excess *p*-chloranil added and the reaction stirred open to air at room temperature for 2 h. The solution was then evaporated on a rotary evaporator and washed with MeOH. The reaction mixture was purified with column chromatography (25% CHCl₃/hexanes) and the first band collected and dried under vacuum to give 5-(4-bromophenyl)-10,15,20-triphenylporphyrin (500mg, 98%). ¹H NMR (300 MHz, CDCl₃, ppm): δ 8.83-8.81 (m, 8H), 8.23-8.20 (m, 6H), 8.08 (dd, 2H, 8.9/8.1Hz), 7.88 (dd, 2H, 8.4/7.8Hz), 7.75-7.73 (m, 9H), -2.82 (s, 2H). ¹³C NMR (300MHz, CDCl₃, ppm): δ 141.8, 141.7, 135.5, 134.3, 134.2, 129.6, 127.5, 127.4, 126.4, 120.0.

2-(4-Bromophenyl)-1,3-dioxolane³¹ (10). 4-Bromobenzaldehyde (12 g, 0.065 mol, 1 equiv), ethylene glycol (4.3 g, 0.07 mol, 1.07 equiv), and p-toluenesulfonic acid (2 mg, 0.01 mmol, 0.0001 equiv) dissolved in benzene (15 mL) and refluxed at 120 °C with a Dean-Stark trap for 12 h. The reaction mixture extracted with brine and H₂O, the organic layer dried with Na₂SO₄, and the solvent removed under vacuum to give 2-(4-bromophenyl)-1,3-dioxolane (11.08 g, 74.5%). ¹H NMR (300 MHz, CDCl₃, ppm) δ 7.6-7.3 (dd, 4H), 5.75 (s, 1H), 4.1-3.9 (m, 4H).

Bis(tributyltin)ferrocene³² (12). Hexane (5 mL) was added to ferrocene (1.01 g, 5.43 mmol, 1 equiv) with stirring to give a reddish-orange suspension. The mixture was stirred under N₂ for 10 minutes to help break up the ferrocene clumps. *n*-Butyl lithium (1.7 M solution in hexane, 7.0 mL, 12 mmol, 2.2 equiv) was added quickly, then TMEDA (1.8 mL, 11.9 mmol, 2.2 equiv) was added to the mixture dropwise over 30 minutes via a syringe pump. The solution was stirred at room temperature overnight to give an orange solution. The reaction mixture was cooled to 0 °C and SnBu₃Cl (3.7 mL, 14 mmol, 2.5 equiv) was added dropwise over 1 h via a syringe pump. The solution was allowed to warm to room temperature, stirred for 1 h, and poured into ice water (100 mL). The reaction mixture was extracted with water and the aqueous layer extracted with

hexane until the organic washings were nearly clear. The organic layers were combined, dried with Na_2SO_4 , and the solvent removed under vacuum to give a dark amber oil. Ferrocene and (tributyltin)ferrocene were distilled off to yield pure bis(tributyltin)ferrocene (2.6 g, 62.7%). ¹H NMR (300 MHz, CDCl₃, ppm): δ 4.23 (m, 4H), 3.96 (m, 4H), 1.9-1.0 (m, 54H).

Ferrocene bis(boronic acid)¹⁵ (13). TMEDA was distilled prior to use. To a stirred suspension of ferrocene (10.1 g, 54.2 mmol, 1 equiv) in Et₂O (200 mL) at room temperature was added a mixture of *n*-butyl lithium (50.2 mL, 120 mmol, 2.22 equiv), TMEDA (18.2 mL, 120 mmol, 2.22 equiv), and Et₂O (100 mL). The solution turned light orange and was stirred at room temperature overnight. The reaction mixture was cooled to 0 °C and added dropwise over 1 h to a -78 °C solution of tributoxyborate (34.0 g, 131 mmol, 2.41 equiv) in Et₂O (200 mL). The resulting solution was stirred at -78 °C for 1 h then allowed to warm to room temperature. After 14 h, the reaction mixture was hydrolyzed with 10% aqueous KOH (150 mL) to give a light tan solution. The organic layer was extracted with more 10% aqueous KOH (400 mL) and the aqueous layers combined and cooled in an ice bath. The aqueous layers then acidified with 10% H₂SO₄ to pH 2 and filtered to give ferrocene bis(boronic acid) (6.050g, 36%). ¹H NMR (300 MHz, DMSO, ppm): δ 7.46 (s, 4H), 4.33 (s, 4H), 4.16 (s, 4H).

Ferrocene bis[tetraphenylporphyrin] (14). 5-(4-Bromophenyl)-10,15,20-triphenylporphyrin 9 (107 mg, 0.154 mmol, 2 equiv), ferrocene bisboronic acid 13 (21 mg, 0.077 mmol, 1 equiv), and Pd(PPh₃)₄ (0.8mg, 6.9x10⁻⁴ mmol, 0.009 equiv) were dissolved in freshly distilled toluene (2 mL). Na₂CO₃ (2 M aqueous solution, 2 mL) was added and the reaction was refluxed for 5 days. After cooling, toluene was added and the reaction mixture was extracted with water. The organic layers were combined, dried with Na₂SO₄, and the solvent removed under vacuum to give a purple solid. The residue was purified by column chromatography (15% CH₂Cl₂:hexane) and the fourth band collected (starting materials preceded the desired compound). The solvent was removed under vacuum to give ferrocene bis[tetraphenylporphyrin] (80 mg, 74%). ¹H NMR (300 MHz, CDCl₃, ppm): δ 8.88-8.84 (m, 16H), 8.22 (d, 12H, 5.5Hz), 8.07 (d, 4H, 5.4Hz), 7.87 (m, 4H), 7.76 (m, 20H), 7.37 (m, 8H), -2.8 (m, 4H).

Ferrocene zinc bis(tetraphenylporphyrin) (11). Ferrocene bis(tetraphenylporphyrin) (80 mg, 0.057 mmol, 1 eq) was dissolved in CH₂Cl₂ (10 mL) with stirring. Zn(OAc)₂ (208 mg, 1.13 mmol, 20 eq) was added and the solution was stirred at room temperature for 3 d. The reaction was filtered through celite and washed with CHCl₃ to give 52 mg (60% yield) of product. ¹H NMR (300 MHz, CDCl₃, ppm): δ 8.92-8.88 (m, 16H), 8.19 (m, 12H), 8.04 (m, 4H), 7.86 (d, 4H, 8.1Hz), 7.74 (d, 20H, 6.9Hz), 7.33 (s, 8H).

$$O_2N$$
 O_2
 O_2

4-Methyl-3,5-dinitrobenzylalcohol²⁰ (15). 4-Methyl-3,5-dinitrobenzoic acid (5 g, 22.1 mmol, 1 equiv) was dissolved in freshly distilled THF (11 mL) and BH₃•THF (1M solution in THF, 29 mL, 28.7 mmol) was added slowly under nitrogen with rapid

stirring., generating a large evolution of H_2 . The reaction mixture was stirred vigorously overnight then water was carefully added to destroy excess BH_3 . Saturated brine was added to the reaction mixture and the organic layer was separated. The aqueous layer was washed with Et_2O (3x25mL) and all organic fractions were combined, dried with Na_2SO_4 , and filtered. The solvent was removed under vacuum to give 4-methyl-3,5-dinitrobenzylalcohol (3.771 g, 80.4%). ¹H NMR (300 MHz, CDCl₃, ppm): δ 8.02 (s, 2H), 4.70 (s, 2H), 2.48 (s, 3H).

4-Methyl-3,5-dinitrobenzaldehyde³³ (16). 4-Methyl-3,5-dinitrobenzylalcohol (3.771 g, 17.8 mmol, 1 equiv) was dissolved in freshly distilled CH₂Cl₂ (100 mL) with stirring. Pyridinium chlorochromate (PCC) (5.76 g, 26.7 mmol, 1.5 equiv) was added and the solution was stirred overnight at room temperature. Diethyl ether was added and the solution filtered and the filtrate was evaporated to give a light brown solid. The residue was purified by column chromatography (CHCl₃) and the first band was collected and dried to give an off-white solid. This solid was recrystallized by dissolving it in CHCl₃ and gradually adding hexanes while the solution was stirred over a steam bath to give 4-methyl-3,5-dinitrobenzaldehyde (1.884 g, 50%). ¹H NMR (300 MHz, CDCl₃, ppm): δ 10.05 (s, 1H), 8.45 (s, 2H), 2.65 (s, 3H).

(4-Methyl-3,5-dinitrophenyl)dipyrrole (18). 4-Methyl-3,5-dinitrobenzaldehyde (256 mg, 1.22 mmol, 1 equiv) was dissolved in pyrrole (2.5 g, 37.3 mmol, 30 equiv) with stirring. The reaction mixture was stirred under nitrogen for 5 minutes then trifluoroacetic acid (9.2 μL, 0.119 mmol, 0.1 equiv) was added. The reaction mixture was stirred under nitrogen for another 5 minutes, then quenched with NaOH (0.2 M) and extracted with EtOAc and H₂O. The organic layers were combined, dried with Na₂SO₄, and the solvent was removed under vacuum to give a light brown oil. Bulb-to-bulb distillation at 200 °C at 0.5 torr gave (4-methyl-3,5-dinitrophenyl)dipyrrole (259 mg, 49.4%) as a yellow powder. ¹H NMR (300 MHz, CDCl₃, ppm): δ 8.05 (s, 2H), 7.79 (s, 2H), 6.74 (s, 2H), 6.17 (q, 2H), 5.86 (s, 2H), 5.56 (s, 1H), 2.52 (s, 3H); ¹³C NMR (300 MHz, CDCl₃, ppm): δ 151.8, 143.7, 129.8, 127.5, 125.8, 118.4, 109.0, 108.1, 42.9, 14.4.

2,2'-(Phenylmethylene)bispyrrole (Phenyldipyrrole, 19). Benzaldehyde (253 mg, 2.36 mmol) was dissolved in pyrrole (3.96 g, 58.9 mmol, 25 equiv) with stirring. The mixture was stirred under nitrogen for 5 minutes, then trifluoroacetic acid (18.2 μL, 0.236 mmol, 0.1 equiv) was added. The reaction mixture was stirred under nitrogen for another 5

minutes, then quenched with NaOH (0.2 M) and extracted with EtOAc and H_2O . The organic layers were combined, dried with Na_2SO_4 , and the solvent removed under vacuum to give a light brown oil. Bulb-to-bulb distillation at 230 °C at 0.5 torr gave phenyldipyrrole (259 mg, 49.4%). ¹H NMR (300 MHz, CDCl₃, ppm): δ 7.86 (s, 2H), 7.35 (m, 3H), 7.25 (d, 2H), 6.69 (s, 2H), 6.22 (m, 2H), 5.96 (s, 2H), 5.47 (s, 1H).

5-(4-Methyl-3,5-dinitrophenyl)-10,15,20-triphenylporphyrin (17). (4-Methyl-3,5-dinitrophenyl)dipyrrole (50 mg, 0.15 mmol, 1 equiv), benzaldehyde (48 mg, 0.45 mmol, 3 equiv) and pyrrole (20.2 mg, 0.3 mmol, 2 equiv) were dissolved in CH₂Cl₂ (60 mL) and stirred at room temperature under N₂ for 30 min. The reaction vessel was shielded from light and BF₃•OEt₂ (5.7 μL, 0.045 mmol, 0.3 equiv) was added. The reaction mixture was stirred at rt for 12 h, during which time the solution became dark red. *p*-Chloranil (75 mg, 0.30 mmol, 2 equiv) was added to the reaction mixture and the solution stirred for 15 min. The solvent was removed under vacuum and the residue was purified by column chromatography (50% CH₂Cl₂/hexanes) to give 5-(4-methyl-3,5-dinitrophenyl)-10,15,20-triphenylporphyrin (18.8 mg, 17%). ¹H NMR (300 MHz, CDCl₃, ppm): δ 8.95

(d, 2H, 5.1Hz), 8.86 (d, 6H, 6.6Hz), 8.76 (d, 2H, 4.8Hz), 8.21 (d, 6H, 7.2Hz), 7.78 (m, 9H), 2.93 (s, 3H), -2.8 (s, 2H). Mass (DCI): found 718.3, expected 718.7.

5-(4-Methyl-3,5-dinitrophenyl)-10,15,20-triphenylporphyrin (17)(one-pot procedure). 4-Methyl-3,5-dinitrobenzaldehyde (50 mg, 0.238 mmol 1 equiv) was dissolved in pyrrole (244 mg, 3.637 mmol, 15.3 equiv). After stirring the solution for 5 minutes under nitrogen, trifluoroacetic acid (1 µL, 0.013 mmol, 0.05 equiv) was added and the reaction mixture stirred a further 5 minutes under nitrogen. Then the solution was transferred to a 2 L flask and diluted with CH₂Cl₂ (1 L). Benzaldehyde (254 mg, 2.34 mmol, 10 equiv) was added and the solution stirred for 30 minutes under nitrogen. The reaction vessel was shielded from light and BF₃•OEt₂ (3 µL, 0.024 mmol, 0.1 equiv) was added. The solution was stirred at room temperature for 3.5 h. p-Chloranil (1.5 g, 6.1 mmol, 25.6 equiv) was added and then the solution stirred for 30 minutes. The solvent was removed under vacuum and the residue was purified by column chromatography (1:3 CHCl₃/hexanes). The second band was collected and the solvent removed under 5-(4-methyl-3,5-dinitrophenyl)-10,15,20vacuum to give triphenylporphyrin (27 mg, 15.8%). Analytical results matched that of the product from the multistep reaction.

5-(4-Methyl-3,5-diaminophenyl)-10,15,20-triphenylporphyrin (20). 5-(4-Methyl-3,5-dinitrophenyl)-10,15,20-triphenylporphyrin 17 (994 mg, 1.383 mmol, 1 equiv) was dissolved in CH₂Cl₂ (25 mL) with stirring. Concentrated HCl (25 mL) was added and the solution turned green. SnCl₂•2H₂O (1.997 g, 8.851 mmol, 6.4 equiv) was added and the closed solution was stirred at room temperature overnight. Water was added and the solution very slowly basified with aqueous NaHCO₃. The solution was extracted with CH₂Cl₂ and the organic layers collected and dried with Na₂SO₄. The solvent was removed under vacuum to give 5-(4-methyl-3,5-diaminophenyl)-10,15,20-triphenylporphyrin (67 mg, 7.4%) as a purple solid. ¹H NMR (300 MHz, CDCl₃, ppm): δ 8.95 ppm (d, 2H, 5.1Hz), 8.86 (d, 6H, 6.6Hz), 8.76 (d, 2H, 4.8Hz), 8.21 (d, 6H, 7.2Hz), 7.78 (m, 9H), 2.93 (s, 3H), -2.8 (s, 2H). Mass (DCI): found 658.3, expected 658.28.

Polymer (21). To a stirred solution of 5-(4-methyl-3,5-diaminophenyl)-10,15,20-triphenylporphyrin **20** (67 mg, 0.102 mmol, 1 equiv) and triethylamine (130 mL, 0.94 mmol, 9.2 equiv) in CH₂Cl₂ (20 mL) was added triphosgene (15 mg, 0.051 mmol, 0.5 equiv) in CH₂Cl₂ (5 mL). The reaction mixture was stirred under N₂ for 16 h. The solvent was removed under vacuum and the residue purified by column chromatography (25% CHCl₃/hexanes) to give porphyrin polymer (11 mg). ¹H NMR (300 MHz, CDCl₃, ppm): δ 8.81 ppm (b), 8.17 (b), 7.73 (b), 2.0 (s, 3H) -2.8 (s, 2H).

Zinc polymer (22). Polymer **21** (11mg, 0.008 mmol, 1 equiv) was dissolved in CH₂Cl₂ (2 mL) and Zn(OAc)₂ (15 mg, 0.082 mmol, 10 equiv) was added. The reaction mixture was stirred overnight at room temperature and then filtered through a celite plug and washed with CH₂Cl₂. The solvent from the filtrate was removed under vacuum to give zinc polymer (16 mg, 99%). ¹H NMR (300 MHz, CDCl₃, ppm): δ 8.9 (b), 8.2 (b), 7.7 (b), 2.0 (s, 3H).

References:

- 1. Yang, Q. The Use of Exciton Coupled Circular Dichroism for the Absolute Stereochemical Determination of Chiral Carboxylic Acids. Ph. D. Dissertation, Michigan State University, East Lansing, 2004.
- 2. Nakash, M.; Clyde-Watson, Z.; Feeder, N.; Teat, S. J.; Sanders, J. K. M., Chemistry: A European Journal 2000, 6, 2112.
- 3. Austin, W. B.; Bilow, N.; Kelleghan, W. J.; Lau, K. S. Y., J. Org. Chem. 1981, 46, 2280.
- 4. Twyman, L. J.; Sanders, J. K. M., Tetrahedron Lett. 1999, 40, 6681.
- 5. Lindsey, J. S.; Prathapan, S.; Johnson, T. E.; Wagner, R. W., *Tetrahedron* **1994**, *50*, 8941.
- 6. Itaya, T.; Mizutani, A.; Watanabe, N., Chem. Pharm. Bull. 1989, 37, 1221.
- 7. Knobloch, K.; Eberbach, W., Org. Lett. 2000, 2, 1117.
- 8. Lan, Y. F.; Hammond, G. B., J. Org. Chem. 2000, 65, 4217.
- 9. Gryko, D. T.; Zhao, F.; Yasseri, A. A.; Roth, K. M.; Bocian, D. F.; Kuhr, W. G.; Lindsey, J. S., J. Org. Chem. 2000, 65, 7356.
- 10. Cunningham, A. F., J. Amer. Chem. Soc. 1991, 113, 4864.
- 11. Guillaneux, D.; Kagan, H. B., J. Org. Chem. 1995, 60, 2502.
- 12. Liu, C. M.; Chen, B. H.; Liu, W. Y.; Wu, X. L.; Ma, Y. X., J. Organomet. Chem. 2000, 598, 348.
- 13. Liu, C. M.; Guo, Y. L.; Wu, X. L.; Liang, Y. M.; Ma, Y. X., J. Organomet. Chem. **2000**, 612, 172.
- 14. Shi, X. L.; Amin, S. R.; Liebeskind, L. S., J. Org. Chem. 2000, 65, 1650.
- 15. Knapp, R.; Rehahn, M., J. Organomet. Chem. 1993, 452, 235.
- 16. Yagi, S.; Yonekura, I.; Awakura, M.; Ezoe, M.; Takagishi, T., Chem. Comm. 2001, 557.
- 17. Collman, J. P.; Gagne, R. R.; Reed, C. A.; Halbert, T. R.; Lang, G.; Robinson, W. T., J. Amer. Chem. Soc. 1975, 97, 1427.
- 18. Rose, E.; Kossanyi, A.; Quelquejeu, M.; Soleilhavoup, M.; Duwavran, F.; Bernard, N.; Lecas, A., J. Amer. Chem. Soc. 1996, 118, 1567.

- 19. Landrum, J. T.; Grimmett, D.; Haller, K. J.; Scheidt, W. R.; Reed, C. A., J. Amer. Chem. Soc. 1981, 103, 2640.
- 20. Yoon, N. M.; Pak, C. S.; Brown, H. C.; Krishnamurthy, S.; Stocky, T. P., J. Org. Chem. 1973, 38, 2786.
- 21. Lee, C. H.; Lindsey, J. S., Tetrahedron 1994, 50, 11427.
- 22. Littler, B. J.; Miller, M. A.; Hung, C. H.; Wagner, R. W.; O'Shea, D. F.; Boyle, P. D.; Lindsey, J. S., J. Org. Chem. 1999, 64, 1391.
- 23. Li, F. R.; Yang, K. X.; Tyhonas, J. S.; MacCrum, K. A.; Lindsey, J. S., *Tetrahedron* 1997, 53, 12339.
- 24. Gowda, D. C.; Mahesh, B., Synth. Comm. 2000, 30, 3639.
- 25. Arai, T.; Inudo, M.; Ishimatsu, T.; Akamatsu, C.; Tokusaki, Y.; Sasaki, T.; Nishino, N., J. Org. Chem. 2003, 68, 5540.
- 26. Gosztola, D.; Yamada, H.; Wasielewski, M. R., J. Amer. Chem. Soc. 1995, 117, 2041.
- 27. Sivakumar, M., Michgan State University, unpublished results, 2002.
- 28. Collman, J. P.; Wang, Z.; Straumanis, A., J. Org. Chem. 1998, 63, 2424.
- 29. Girolami, G. S.; Hein, C. L.; Suslick, K. S., Angew. Chem. Intl. Ed. 1996, 35, 1223.
- 30. Penney, J. M.; Miller, J. A., Tetrahedron Letters 2004, 45, 4989.
- 31. Lee, Y.; Silverman, R. B., Org. Lett. 2000, 2, 303.
- 32. Cunningham, A. F., J. Amer. Chem. Soc. 1991, 113, 4864.
- 33. Remy, D. C.; King, S. W.; Cochran, D.; Springer, J. P.; Hirshfield, J., J. Org. Chem. 1985, 50, 4120.

Chapter 4

Use of Ru(bpy)₂Cl₂ for Determination of Absolute Stereochemistry of *Erythro* 1,2 Aminoalcohols and Diols

Erythro diols have long posed a problem in determination of their absolute stereochemistry. For their counterparts, threo diols, it is a simpler matter to determine the absolute stereochemistry, and there have been many methods developed to facilitate the process. Use of Mosher's ester derivatives or variations allows for the determination of stereochemistry through ¹H NMR. ¹ However, both enantiomers of the threo diol must be derivatized in order to ensure correct assignment of the absolute stereochemistry. Exciton-coupled circular dichroism has also been used over the past several decades to determine the absolute stereochemistry of threo diols. ²⁻⁴ Due to the arrangement of the alcohols in threo diols, it is evident from a Newman projection that there should be one favored low energy conformation. For example, consider threo-2,3-dihydroxypentane.

Figure 4-1. Newman projections of low energy conformers of (2R, 3R)-2,3-dihydroxypentane. When derivatized with chromophores (X), the expected lowest energy conformer would lead to a negative ECCD bisignate curve.

As can be seen in Figure 4-1, the (2R, 3R) isomer has two conformers with three gauche interactions (indicated by the blue arrows), and only one conformer where there are two gauche interactions, thus this conformer would be expected to be the predominant low-energy conformation. If the hydroxyl groups are derivatized with an appropriate chromophore, interaction between the chromophores would lead to an expected negative ECCD bisignate curve. Comparing the enantiomer of the previously analyzed molecule, the (2S, 3S) isomer also has only one conformer where there are two gauche interactions (Figure 4-2). However, since the hydroxyl groups have the opposite configurations as before, this conformation would be expected to lead to a positive ECCD bisignate curve

Figure 4-2. Newman projections of low energy conformers of (2S, 3S)-2,3-dihydroxypentane. When derivatized with chromophores (X), the expected lowest energy conformer would lead to a positive ECCD bisignate curve.

when derivatized with chromophores. As shown in these examples, *threo* 1,2-diols can be analyzed by ECCD to provide an absolute stereochemical determination.

However, similar analysis of *erythro* diols shows a fatal flaw. As before, a simple comparison of the Newman projections of *erythro*-2,3-dihydroxypentane gives three possible conformations. The (2R, 3S) isomer shown in Figure 4-3 has one conformation with two gauche interactions and two conformations with three gauche interactions.

However, the expected lowest energy conformation (the conformation with only two gauche interactions) would not be expected to show ECCD, since the chromophores

Figure 4-3. Newman projections of low energy conformers of (2R, 3S)-2,3-dihydroxypentane. When derivatized with chromophores, no ECCD is expected to be observed.

Figure 4-4. Newman projections of low energy conformers of (2S, 3R)-2,3-dihydroxypentane. When derivatized with chromophores, no ECCD is expected to be observed.

would be in an antiperiplanar position. The other two conformations, which would both be expected to show ECCD when derivatized, are expected to be similar in energy due to the same number of gauche interactions. Thus, the ECCD signals (one negative, one positive) expected from the two higher-energy conformations would cancel out leading to no observed ECCD. This can be demonstrated to be also true for the enantiomer, the (2S, 3R) isomer, as shown in Figure 4-4. As before, there is one conformation with only two gauche interactions, but it would not be expected to show ECCD due to the orientation of

the chromophores (antiperiplanar). The other two conformations should be similar in energy and the ECCD bisignate curves will cancel out leading to no observed ECCD.

In light of this, we hoped to design a system that would allow for the simple determination of absolute stereochemistry for *erythro* diols using ECCD. Initial consideration of the problems inherent with the *erythro* diols led us to believe that a system in which the diol was in a locked conformation provided the best opportunity for facile analysis of possible conformations and would allow us to predict with some certainty the position of the chromophores. Since it is logical that in order to determine the exact conformation it is beneficial to rigidify the system, we wanted to devise a system in which the diol becomes part of a six-membered ring, with two chromophores attached to the ring (Figure 4-5). If we know the most stable conformation of the system

$$R_1$$
 R X Q R X Q R

Figure 4-5. Transformation of erythro diols into six-membered rings functionalized with chromophores (X).

(presumably a lowest energy chair formation), we should be able to predict the ECCD for the possible *erythro* 1,2-diol stereochemistries. Hence, we would be able to derivatize a small amount of diol sample, subject it to ECCD, and from the observed sign determine the absolute stereochemistry of the diol. To this end, we initially considered converting the *erythro* diols into dioxanes.

4.1. Conversion of *erythro*-1,2-diols into dioxanes

To determine what stereochemistry was necessary for the six-membered ring system, we studied all of the Newman projections for the possible conformations. We started by looking at 2,3-pentanediol as the erythro diol and an (R,R) bis-chromophore

(Figure 4-6). Both possible stereochemistries [(2R, 3S)-2,3-pentanediol and (2S, 3R)-2,3-pentanediol] for the *erythro* diol were examined as Newman projections after

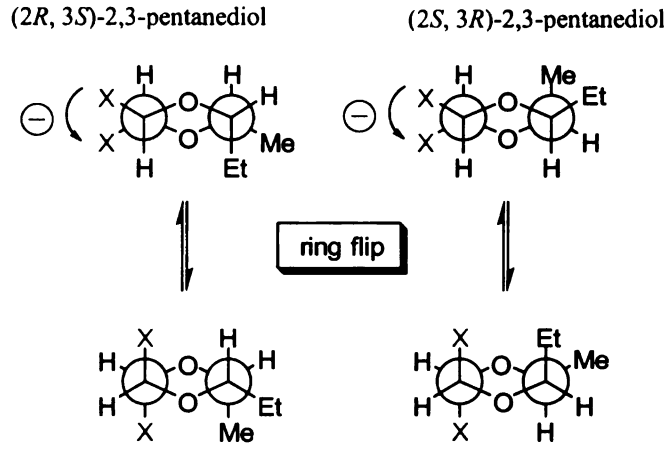


Figure 4-6. Newman projections of the product formed from (2R, 3S)-2,3-pentanediol or (2S, 3R)-2,3-pentanediol and an (R, R) bis-chromophore.

derivatizations with the bis-chromophore to form a dioxane (Figure 4-6). When these two are combined to give a six-membered ring, it becomes apparent that both systems would predict the same ECCD sign when the chromophores are in the equatorial position (when the two chromophores are both axial, there would be no ECCD sign expected since they are antiperiplanar). So a chiral bis-chromophore of this stereochemistry [either (R, R) or (S, S)] will not work.

We then looked at the conformations for a six-membered ring obtained from a meso chromophoric system. In this case, there are several possible conformations that need to be considered. Using the same diol as before—including both possible stereochemistries—we compared the various Newman projections using an (R, S) meso bis-chromophore, including the two different configurations depending on whether the diol reacts with the bis-chromophore from the top or the bottom. Here, the (2R, 3S) diol would give either a positive or negative ECCD sign depending on which conformation is

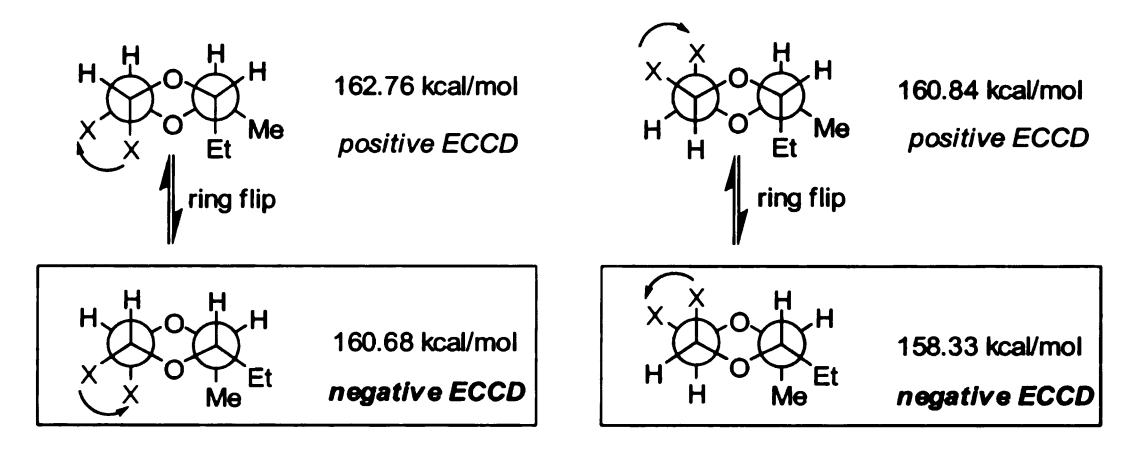


Figure 4-7. Newman projections of the product formed from (2R, 3S)-2,3-pentanediol and an (R, S) meso bis-chromophore (X) indicating an expected negative ECCD bisignate curve.

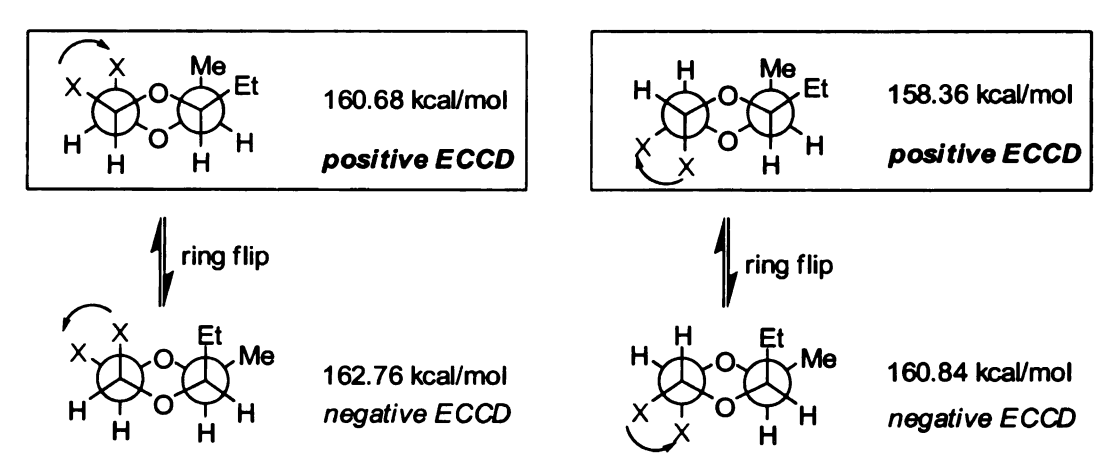


Figure 4-8. Newman projections of the product formed from (2S, 3R)-2,3-pentanediol and an (R, S) bischromophore (X) indicating an expected positive ECCD bisignate curve.

considered. Since it was unclear as to which conformation would be favored, analysis via molecular modeling was performed to see if there was enough difference in energy to favor one conformation over another (Figure 4-7).⁵ In both configurations, the lowest energy structure by approximately 2 kcal/mol is the one in which the chromophores are oriented counterclockwise from front to back. This can be explained due to the preference for the larger group of the diol (in this case, ethyl) to be equatorial, since in both cases the chromophores (presumably larger than the substituents of the diol) have one chromophore oriented axial and one equatorial. Thus, based on molecular mechanics calculations (Spartan v.5.0), the (2R,3S) diol would be expected to give a negative ECCD

sign. We then performed the same analysis on the (2S,3R) diol, again with an (R,S) bischromophore (Figure 4-8). Here the lowest energy conformers—again by approximately 2 kcal/mol—are oriented clockwise from front to back, leading to the expectation of a positive ECCD sign. As such it appears that converting *erythro* 1,2-diols into dioxanes substituted with *meso* chromophores could be a valid way of determining the absolute stereochemistry of *erythro* 1,2-diols.

At this point, it became necessary to make a starting chromophoric system which would be simple to use as a derivatizing agent for diols. Although porphyrins are excellent chromophores, they are not necessarily a good initial chromophore as it could be difficult to synthesize the needed compounds, so we chose to start with (R,S)-1,2-dibromo-1,2-diphenylethane, where the phenyl groups would act as the requisite chromophores for ECCD analysis. However, a substitution reaction of a diol displacing

Scheme 4-1. Synthesis of *meso*-1,2-dibromo-1,2-(4,4'-dinitrophenyl)ethane 2 from 4-nitrobenzyl chloride.

the bromines is more likely to go through an S_N1 reaction since the carbocation will be stabilized by resonance with the aromatic rings. To destabilize this reaction pathway, we opted to use *para* substituted phenyl rings where the substituents are strongly electron withdrawing nitro groups, as shown in 1 (Scheme 4-1). Synthesis of this molecule could be achieved through bromination of *trans*-4,4'-dinitrostilbene, which is easily synthesized from 4-nitrobenzyl chloride.⁶

Synthesis of trans-4,4'-dinitrostilbene proceeded as reported in literature with 66% yield on a 4g scale. Allylic bromination reactions are typically performed in the dark, 6-9 so the first time the reaction was run the reaction flask was shielded from light and the concentration of the reaction was controlled to favor the meso product. However, only 8% yield of the desired product was obtained, with the remaining material being decomposed starting material and small amounts of chiral bromination products. The reaction was then run in the darkroom to ensure absence of ambient light, but this reaction again gave chiral bromination products. We then found a literature procedure which described the bromination proceeding entirely to the meso product if the reaction was run under radical conditions; i.e., light. The reaction was run in ambient light and a 2:1 mixture of starting material and desired *meso* product was obtained. We attempted to crystallize the product out but were unsuccessful. The reaction was run again using a superbright light. The solution went from orange-yellow to pale yellow as the bromine was consumed over a period of five days. After workup, the product was recovered through filtration in 20% yield. The solvent from the filtrate was removed under reduced pressure and the solid obtained was washed with EtOAc and filtered to obtain an additional 10% pure meso-1,2-dibromo-1,2-(4,4'-dinitrophenyl)ethane.

After obtaining the desired bis-chromophore starting material, the next step was derivatization of a diol. The first substitution reaction performed was with racemic p-

Scheme 4-2. Synthesis of the unexpected product bis-(4-nitrophenyl)acetylene 3.

dioxane-2,3-diol (Scheme 4-2). After dissolving the diol in THF, sodium hydroxide was added dropwise and then the bis-chromophore was added. Although the bis-chromophore was not very soluble in THF, the reaction changed color gradually from colorless to pale yellow, at which point the reaction was stopped. No substitution product was obtained, and the major product by ¹H NMR was the double elimination product of the bis-chromophore, bis-(4-nitrophenyl)acetylene. We then decided to try a variety of reaction conditions using racemic *trans*-1,2-cyclohexanediol to try to determine optimal conditions for the substitution. Since S_N2 is favored with polar aprotic solvents, we set up three reactions using dimethylsulfoxide (DMSO), acetonitrile (ACN), and

Scheme 4-3. Attempted derivatizations of *trans*-1,2-cyclohexanediol in various solvents.

dimethylformamide (DMF). All of these reactions used no base; we added the diol and the bis-chromophore and stirred them together at room temperature (Scheme 4-3). Both compounds dissolved easily in DMSO and DMF, but there was considerable cloudiness in the ACN reaction mixture. The DMF reaction mixture showed no reaction by NMR after 2 hours of stirring and workup. DMSO was difficult to remove from the reaction mixture but the reaction contained only starting material from TLC. The ACN reaction mixture was rotavapped and ¹H NMR taken in DMSO. The reaction showed small shifts in ¹H NMR, but it was unclear if the peaks were from the individual starting materials or from the product as there should not be much difference in the chemical shifts. ¹³C NMR would be expected to be more conclusive, as there should be a significant shift in the

carbon that was attached to the bromine (normally appearing around ~53ppm) which becomes bonded to an oxygen as an ether (normally appearing around ~85ppm). A total of eight peaks were observed in the ¹³C NMR of the product in DMSO. The carbons in question in the product have peaks at 73.830 ppm (C-OH) and 51.930 ppm (C-Br), as compared to 73.875 ppm (C-OH) and 51.826 ppm (C-Br) in the starting materials. Thus it was apparent that none of the desired product had been formed and no reaction had occurred.

In a reference on sources of nucleophilic oxygen, Hutchins and Taffer report the use of HMPA or N-methyl-2-pyrrolidone (NMP) to increase the nucleophilicity of alcohols for use in substitution reactions to form ethers. However, in their chiral examples they do note considerable racemization (80% inversion for NMP, 70% inversion for HMPA), even with a strong base to neutralize the reaction. As our previous attempts to synthesize dioxanes using diols had failed, we decide to increase the nucleophilicity of the oxygens using HMPA (Scheme 4-4). Initially, we tried to run the

Scheme 4-4. Attempted derivatization of trans-1,2-cyclohexanediol using HMPA in ACN.

reaction in HMPA alone, but the bis-chromophore was not soluble so ACN was added to improve solubility. Workup and a pipet column to remove the HMPA revealed no reaction had taken place.

Although the dioxanes seemed like a promising solution to the problem of absolute stereochemical determination for *erythro* diols, the difficulties in synthesis led

us to believe there might be other methods that would be more amenable to diols without resorting to unusual or harsh synthetic conditions. Development of the dioxane method is still an option, but we would prefer to have a method that is facile and rapid for general use. We began exploring other possibilities, and one of the most captivating was the idea of using metal complexes as achiral hosts for our chiral diols.

4.2. Consideration of cis-Ru(bpy)₂Cl₂ as a chromophoric host

As the formation of dioxanes from *erythro* diols seemed unlikely to yield a viable method of creating the necessary chromophoric system, we considered the possibility of using a metal center to coordinate the *erythro* diols. A metal center with two or more chromophores could be forced to adopt a chiral configuration upon coordination to a chiral diol. It was necessary that the metal in question be well-characterized with a known ability to form chiral complexes. The cis-Ru(bpy)₂X₂ series fit these qualifications well, where X may be any other ligand. cis-Ru(bpy)₂X₂ is known to form two enantiomers, the Δ isomer and the Λ isomer (Figure 4-9).¹¹ At room temperature in a

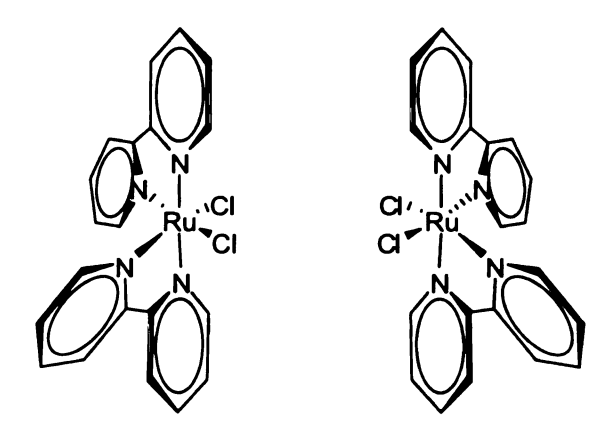


Figure 4-9. Λ and Δ forms of cis-Ru(bpy)₂Cl₂.

compound with no differentiation between the X_2 ligands (e.g., Cl_2), cis-Ru(bpy)₂ X_2 exists as a racemic mixture, and a single pure isomer (Δ or Λ) will racemize over time in solution.¹² Both forms are CD active and show opposite signals. However, it has been

shown that one isomer can be preferred with the addition of a ligand that can induce chirality, such as chiral sulfoxide ligands. With this precedent, we believed it might be possible to do a similar type of conformational preference with a chiral diol. If we could add a chiral *erythro* diol to the Rubpy₂Cl₂, displacing the chlorines, we could potentially force the Rubpy₂X₂ to exist in one form, or if not, perhaps increase the enantiomeric excess of one form versus the other. There are two ways we envisioned this occurring: 1. The incoming chiral guest binds preferentially to one form or the other (Δ and Λ). As the guest binds to, for example, Λ -Rubpy₂Cl₂, that ruthenium is locked into the Λ conformation. All of the remaining mixture of *cis*-Ru(bpy)₂Cl₂ ($\Delta > \Lambda$) racemizes. As this process continues, a large excess of ruthenium with the chiral guest (in this example as the Λ form) accumulates and this will be evident in the ECCD (Figure 4-10). 2. The incoming chiral guest changes the stereochemistry at the ruthenium center to fit with

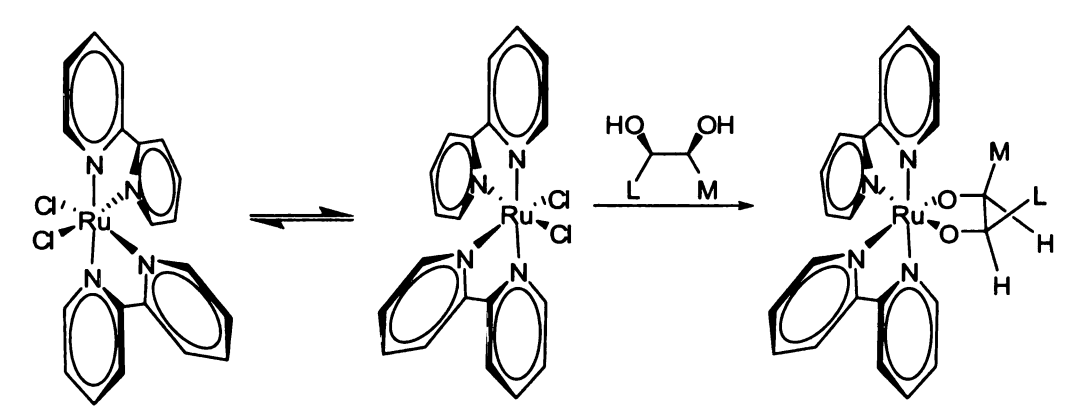


Figure 4-10. Possible method of stereodifferentiation where the chiral erythro diol binds preferentially to Λ -cis-Ru(bpy)₂Cl₂.

itself. For example, if the lowest energy conformation the ruthenium plus guest would adopt would be Λ (dependent on the conformation of the chiral diol), the incoming guest can bind to any ruthenium molecule, but when it binds the conformation of the bipyridine groups around the ruthenium will change to, or maintain, the Λ conformation (Figure 4-

11). With these possibilities in mind, we began trying to form complexes of chiral diols and cis-Ru(bpy)₂Cl₂.

Molecular modeling in Spartan⁵ indicates that there would be significant strain in one conformation versus the other upon binding to a chiral guest. As seen in Figure 4-12, $Ru(bpy)_2Y$ [where Y is (2R,3S)-pentanediol] shows different levels of strain depending on which conformation of $Ru(bpy)_2Cl_2$ it complexes with. Notice in particular the strain

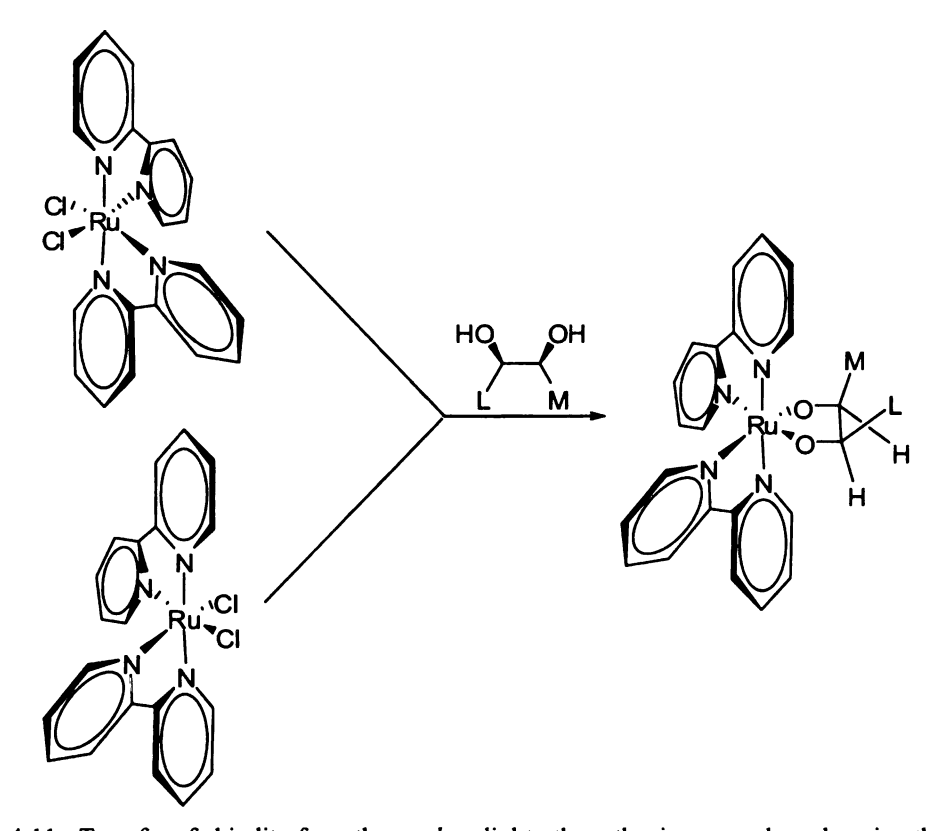


Figure 4-11. Transfer of chirality from the *erythro* diol to the ruthenium complex, changing the initial stereochemistry of the ruthenium to match the diol.

in the bipyridines in the structure on the right. In this conformation, the ethyl and methyl groups are pointing towards the bipyridine rings, causing them to buckle to try to avoid steric interactions. In the conformation on the left, both groups are pointing away from the bipyridine rings, leading to a less strained system. However, strain energy values for

these two conformations are very close in energy (within 1 kcal/mol) which makes it difficult to accurately determine which conformation is preferred.

We were unsure how well Spartan could model metal centers, specifically ruthenium, and when we were running conformational searches we required the program to look at the conformation of cyclic systems involving a metal (the metal to the diol

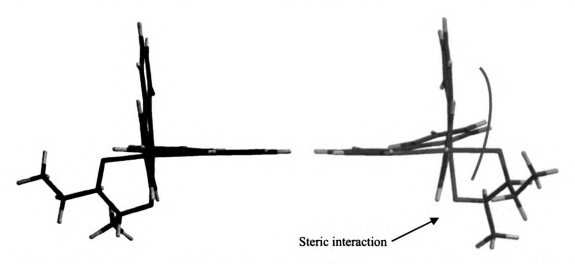


Figure 4-12. Spartan models of Ru(bpy)₂Y where Y is (2R,3S)-pentanediol. Note the curve of the bipyridine in the structure on the right (emphasized with a blue curved line).

forming a 5-membered ring). It was unclear whether Spartan was correctly modeling the changes that can occur in a cyclic system (where one atom is a metal) that would relieve or create strain. Modeling with a molecular model kit seemed to indicate that there would be a difference in preferred conformation for each enantiomer due to steric interactions, so we continued to pursue this method.

4.3. Studies of cis-Ru(biq)2Cl2 and cis-Ru(bpy)2Cl2

Initially, we pursued the synthesis of cis-Ru(biq)₂Cl₂ (where biq refers to biquinoline) since it was expected to have a larger electric transition dipole moment and thus would show stronger ECCD spectra. Most literature references make cis-Ru(biq)₂Cl₂ using similar methods as those for bipyridine. We chose to follow the most

Scheme 4-5. Attempted synthesis of cis-Ru(biq)₂Cl₂.

Scheme 4-6. Synthesis of chirally enhanced cis-Ru(bpy)₂Cl₂.

recent literature reference and attempted formation of *cis*-Ru(biq)₂Cl₂ from RuCl₃, 2,2'-biquinoline, LiCl and ascorbic acid (Scheme 4-5).¹⁴ However, multiple attempts at this reaction generated only starting material. With more circular dichroism and other spectral information readily available on *cis*-Ru(bpy)₂Cl₂ compounds, we began synthesis of this compound instead. Using the same method as described for formation of *cis*-Ru(biq)₂Cl₂, formation of *cis*-Ru(bpy)₂Cl₂ proceeded without difficulty through reaction of RuCl₃ with 2,2'-bipyridine in the presence of LiCl and ascorbic acid (Scheme 4-6). Literature reports were conflicting in the recommended workup, with some references filtering the reaction mixture and using the crude solid without further purification, while one reference submitted the solid to a Soxhlet extraction for three days. We chose to attempt both workups to determine if there was a difference in purity of the final compound. We filtered the crude reaction mixture and washed the solid obtained with water. The aqueous filtrate from this step was then extracted with CH₂Cl₂ to give *trans*-

Ru(bpy)₂Cl₂ in a 4:1 mixture *trans:cis* by ¹H NMR. The solid from the filtration was submitted to a modified Soxhlet extraction for 24 hours, reserving a small sample of the crude solid. After 24 hours, ¹H NMR was taken of the initial crude solid, the solid from the Soxhlet extraction, and the filtrate from the extraction. The product was determined to be racemic *cis*-Ru(bpy)₂Cl₂ with no difference, including impurities, evident by ¹H NMR between the crude solid and the solid and filtrate from the Soxhlet extraction, and the product showed no CD spectrum. Since there appeared to be no benefit in extracting the crude solid and using the filtrate, all further reactions were done with the crude solid obtained from simple filtration of the reaction mixture. However, after a couple of weeks of storing the crude compound in a closed vial protected from light at room temperature, a very weak ECCD spectrum was observed. Since any inherent chirality could prevent use of this method for *erythro* diols, it was imperative that the *cis*-Ru(bpy)₂Cl₂ start and

Scheme 4-7. Synthesis of racemic cis-Ru(bpy)₂Cl₂.

remain racemic. We remade the cis-Ru(bpy)₂Cl₂ and once again weak ECCD was observed for the crude product. This indicates that either the Δ or Λ form of the cis-Ru(bpy)₂Cl₂ is enantio-enhanced, probably due to the use of ascorbic acid. Synthesis of cis-Ru(bpy)₂Cl₂ was performed again without ascorbic acid (Scheme 4-7), leading to a

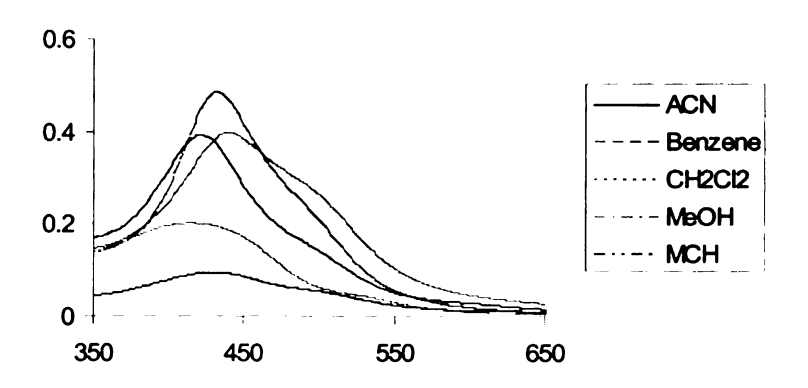


Figure 4-13. UV-Vis studies on RuCl₃ in acetonitrile (solid line), benzene (large dashes), CH₂Cl₂ (small dashes), MeOH(dash-dot-dash), and methylcyclohexane (dash-dot-dot-dash).

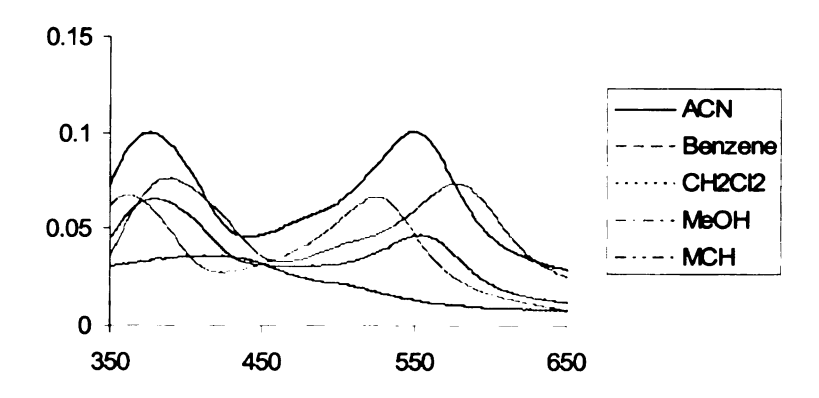


Figure 4-14. UV-Vis studies on cis-Ru(bpy)₂Cl₂ in acetonitrile (solid line), benzene (large dashes), CH₂Cl₂ (small dashes), MeOH(dash-dot-dash), and methylcyclohexane (dash-dot-dot-dash).

pure product with no ECCD spectrum. To our knowledge, enhancement of one conformation of cis-Ru(bpy)₂Cl₂ using ascorbic acid has not been previously reported.

To determine the optimal solvent for use in ECCD studies of *cis*-Ru(bpy)₂Cl₂ and related compounds, we carried out a series of UV studies to observe differences in the UV spectra with varying solvents. As a reference, we first did UV studies on RuCl₃, using acetonitrile (ACN), benzene, dichloromethane (CH₂Cl₂), methanol (MeOH), and methylcyclohexane (MCH). Since RuCl₃ is not soluble in many solvents, we first made a stock solution of RuCl₃ in ACN at 1x10⁻² M. One μL of stock solution was diluted to 1 mL in the desired solvent to give a 1x10⁻⁵ M solution which was used for obtaining UV

spectra. As can be seen in Figure 4-13, the observed UV absorption for RuCl₃ is very solvent dependent. UV studies of cis-Ru(bpy)₂Cl₂ in the same solvents as RuCl₃ show the same solvent dependency (Figure 4-14). In all solvents except methylcyclohexane (MCH), Ru(bpy)₂Cl₂ shows two absorption peaks, one near 375 nm and one near 550-575 nm, corresponding to the ligand π - π * transition and the metal-ligand charge transfer band (MLCT). As acetonitrile and methanol are common solvents for UV studies of ruthenium bipyridine complexes, we chose these solvents to continue our studies.

4.3.1. Complexation and studies of Ru(bpy)₂Cl₂ with erythro-1,2-diols, -diamines, and -aminoalcohols

To test the possibility of diol coordination to the cis-Ru(bpy)₂Cl₂, we first attempted to coordinate the ruthenium with an inexpensive and readily available *threo* diol, (S,S)-(-)-hydrobenzoin (Scheme 4-8). After refluxing cis-Ru(bpy)₂Cl₂ overnight

Scheme 4-8. Attempted complexation of (S, S)-(-)-hydrobenzoin with cis-Ru(bpy)₂Cl₂.

with an excess of diol in EtOH:H₂O (2:1), the solution was filtered, but NMR and UV of the solid and the filtrate showed only unreacted *cis*-Ru(bpy)₂Cl₂ and diol. Unsure if the problem was complexation with the diol or the procedure, we attempted to add base to deprotonate the diol and force complexation. Use of *n*-BuLi generated trace amounts of benzaldehyde and starting materials, but no evidence of unreactive complexation

Scheme 4-9. Attempted complexation of (S, S)-(-)-hydrobenzoin with cis-Ru(bpy)₂Cl₂ using n-BuLi.

Scheme 4-10. Control reaction of (S, S)-(-)-hydrobenzoin with n-BuLi.

(Scheme 4-9). A control reaction run with (S,S)-(-)-hydrobenzoin and n-BuLi showed no reaction (Scheme 4-10), indicating the ruthenium was oxidizing the diol to benzaldehyde. Since the complexation was not proving as facile as we had hoped, we searched for a similar complexation in literature and found an example of complexation between cis-Ru(bpy)₂Cl₂ and 3,5-di-tert-butylcatechol.¹⁵ This literature protocol involves refluxing cis-Ru(bpy)₂Cl₂ for an hour in methanol before adding a substrate to coordinate.

Coordination of a terminal chiral 1,2-diol to *cis*-Ru(bpy)₂Cl₂ was attempted by refluxing *cis*-Ru(bpy)₂Cl₂ in methanol for one hour, then adding (1*S*)-1-phenylethane-1,2-diol to the reaction mixture. After filtration, the crude solid of the reaction mixture was dissolved in acetonitrile and diluted with spectroscopy grade methanol and the ECCD spectrum was measured. The spectrum showed a few small peaks in the MLCT band region and one strong peak at 398 nm. While slightly asymmetric, the ECCD bisignate curve centers at 297 nm, with a positive peak appearing first at 309 nm and a

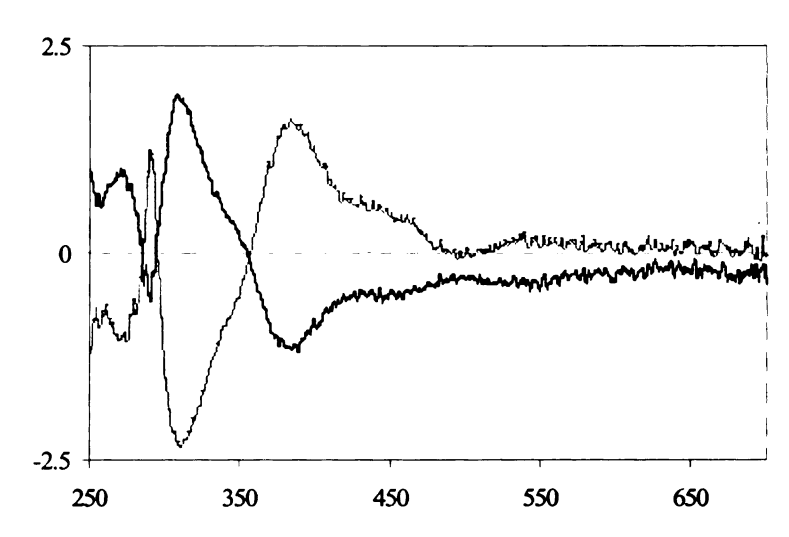


Figure 4-15. ECCD spectra of cis-Ru(bpy)₂Cl₂ complexed with (1S)-1-phenylethane-1,2-diol (solid blue line) and (1R)-1-phenylethane-1,2-diol (dashed pink line) in spectroscopy grade MeOH.

negative peak following at 291 nm for the R diol, and the reverse is observed for the S diol (Figure 4-15). This indicates that the chiral diol is influencing the racemic ruthenium molecule and causing the formation of a new chiral ruthenium species. The chirality of the diol influences the arrangement of the bipyridine groups around the ruthenium core in such a way that a specific chiral conformation is preferred. However, it is not possible at this point to determine the nature of the influence of the chiral molecule on the ruthenium, as no definitive data has been obtained which supports the formation of a complex other than the ECCD data. As was anticipated, using diols of opposite stereochemistry leads to ECCD spectra of opposite sign. Although initially we had hoped to create a system that would allow for the stereochemical determination of chiral terminal diols.

To try to extend our new method, we chose to test coordination of aminoalcohols.

Accordingly, (-)-norephedrine, a readily available *erythro-*1,2-aminoalcohol, was added

to cis-Ru(bpy)₂Cl₂ previously refluxed in methanol. The solution was refluxed overnight, then cooled and filtered. While cis-Ru(bpy)₂Cl₂ shows only 8 proton peaks in the NMR due to the symmetry of the molecule, the solid obtained from the reaction of norephedrine and cis-Ru(bpy)₂Cl₂ showed multiple peaks in the ¹H NMR, indicating potential coordination of the (-)-norephedrine. A CD scan of the compound from 700-200nm in spectroscopy grade MeOH showed an unusual series of peaks. There were four peaks at 646 nm (positive), 553 nm (negative), 489 nm (positive), and 417 nm (negative), ascribed to the ligand charge transfer bands of the metal complex. These peaks are rather weak and difficult to characterize as ECCD bisignate curves. However, a bisignate curve was observed centered at 297 nm, with a positive peak appearing first at 301 nm and the

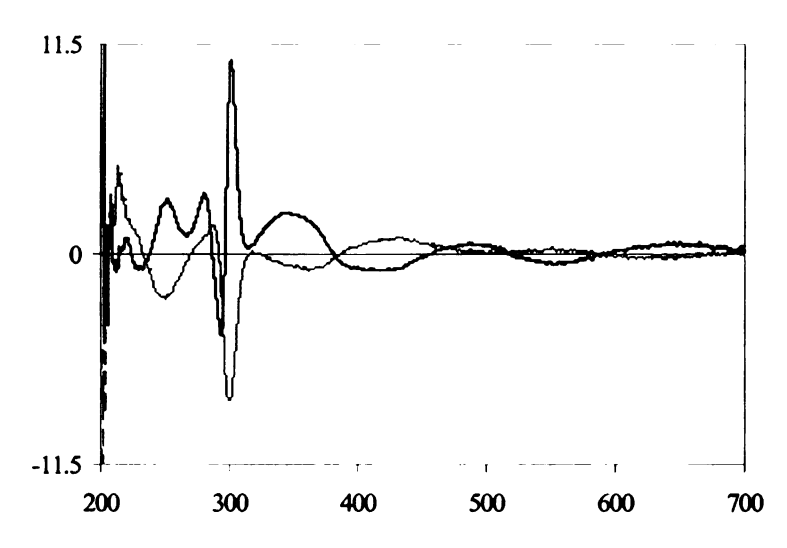


Figure 4-16. ECCD spectra of *cis*-Ru(bpy)₂Cl₂ complexed with (-)-norephedrine (solid blue line) and (+)-norephedrine (dashed pink line) in spectroscopy grade MeOH.

negative peak following directly after at 293 nm due to the interaction of the electric transition dipole moments of the bipyridine ligands. Testing of the product formed in the same manner from (-)-norephedrine's enantiomer, (+)-norephedrine, was rapidly performed to show a nearly exact opposite CD curve (Figure 4-16).

Testing of another available compound, D-allo-threonine, was performed after converting the carboxylic acid to an ester and complexing the product with cis-Ru(bpy)₂Cl₂. A CD scan of the compound from 700-200nm, also in spectroscopy grade MeOH, showed a similar spectrum as that for norephedrine. Again weak peaks were observed at 500 nm (positive) and 375 nm (negative), as well as a bisignate curve

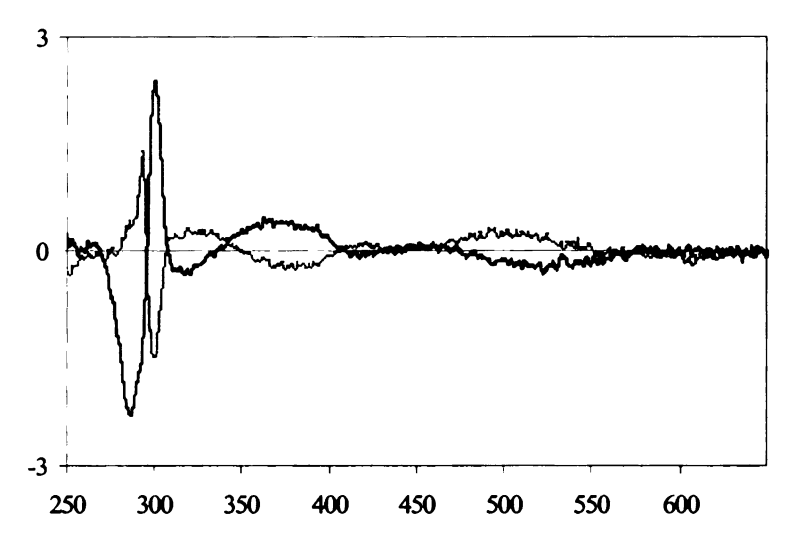


Figure 4-17. ECCD spectra of *cis*-Ru(bpy)₂Cl₂ complexed with L-allo-threonine methyl ester (solid blue line) and D-allo-threonine methyl ester (dashed pink line) in spectroscopy grade MeOH.

centered at 297 nm, with a negative peak appearing first at 300 nm and a positive peak appearing at 293 nm (Figure 4-17). ECCD analysis of the enantiomer, L-allo-threonine methyl ester, reacted with Ru(bpy)₂Cl₂ again revealed a nearly perfectly opposite ECCD spectrum. These two examples indicate that this method might be a viable way for distinguishing between enantiomers of 1,2-erythro-aminoalcohols.

Analysis of the potential complexes that may be forming has been performed using Spartan v.7.0. All calculations were done using molecular mechanics. Interestingly enough, the strain energy values make no sense when comparing enantiomers, and do not predict the observed ECCD sign. The differences in energy are

so large as to be ridiculous. However, when the models are viewed from the perspective of A-values, new light is shed on a possible conformational preference. If the possible complex conformations are evaluated in terms of which side of the *erythro* diol or aminoalcohol is larger (by A-values), then it is a simple matter of determining which conformation allows for the large group to sit equatorial or pseudo-equatorial. Although the ring formed by the anticipated coordination of the aminoalcohol to the ruthenium is

Figure 4-18. Representation of pseudo-axial and -equatorial positions for the possible complexes forming between cis-Ru(bpy)₂Cl₂ and erythro compounds (bipyridine rings not shown for clarity).

not a 6-membered ring, the Ru-O and Ru-N bonds are long enough to allow more conformational freedom with respect to the two carbons in the ring than would normally be observed in a purely organic 5-membered ring. This allows the two groups attached to the aminoalcohol to take up positions pseudo-axial or pseudo-equatorial, where the large group prefers to be in the pseudo-equatorial position to avoid steric interactions with the bipyridines also attached to the ruthenium (Figure 4-18).

However, even considering the large group to be pseudo-equatorial, there are still two possibilities for binding to the ruthenium, similar to a top and bottom face approach. Here, too, sterics play a large role, in that the conformation is favored in which the large group is pseudo-equatorial and pointing away from the bipyridine rings. This presents the large group as pointing into an empty quadrant.

This work is still in progress in our lab and other compounds are currently undergoing testing. More data is being obtained to support the proposed complexes as described above. At this point, it does seem that reaction of cis-Ru(bpy)₂Cl₂ with erythro 1,2-diols, -diamines, -aminoalcohols, and perhaps even other functional groups such as thiols might make ECCD a viable tool for absolute stereochemical determination of these types of compounds. Only a small amount of sample is needed for the reaction, and the reaction conditions are mild. Once a mnemonic has been sufficiently tested, only one enantiomer will need to be reacted to be certain of the stereochemistry. Further development of this method will include screening of other ruthenium ligands, particularly ligands with stronger electric dipole transitions and bulkier ligands which may increase preference for one conformer.

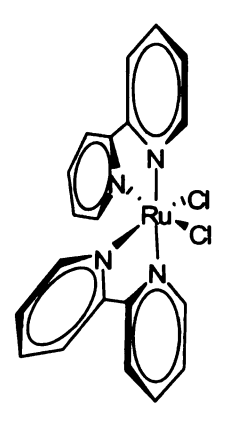
Experimental materials and general procedures:

Anhydrous CH_2Cl_2 was dried over CaH_2 and distilled. The solvents used for CD and UV-Vis measurements were purchased from Aldrich and were spectroscopy grade. All reactions were performed in dried glassware under nitrogen unless otherwise noted. Column chromatography was performed using SiliCycle silica gel (230-400 mesh). ¹H-NMR spectra were obtained on Varian Inova 300 MHz or 500 MHz instruments and are reported in parts per million (ppm) relative to the solvent resonances (δ), with coupling constants (J) in Hertz (Hz). IR studies were performed on a Galaxy series FTIR 3000 instrument (Matteson). UV-Vis spectra were recorded on a Perkin-Elmer Lambda 40 spectrophotometer, and are reported as λ_{max} [nm]. CD spectra were recorded on a JASCO J-810 spectropolarimeter, equipped with a temperature controller (Neslab 111) for low temperature studies, and are reported as λ [nm] ($\Delta \varepsilon_{max}$ [1 mol⁻¹ cm⁻¹]).

Trans-4,4'-dinitrostilbene⁶ (1). 4-Nitrobenzylchloride (4 g, 23.34 mmol, 1 equiv) was heated to 55 °C in EtOH (12 mL). KOH (1.4 g, 25.06 mmol, 1.07 equiv) was dissolved in a mixture of water (1.2 mL) and EtOH (4.8 mL) and the solution was added dropwise to the 4-nitrobenzylchloride solution. Upon beginning the addition, the resultant solution immediately turned brilliant green then red. As the remaining KOH solution was added a precipitate appeared and the solution turned brown with yellow precipitate. Vigorous stirring was required as there was a significant amount of precipitate. The temperature of

the sand bath was raised to 70 °C. The solution was stirred for 1 h then cooled overnight and filtered. The residue was washed with ethanol to give *trans*-4,4'-dinitrostilbene (4.1405 g, 65.7%) as a bright yellow solid. ¹H NMR (300 MHz, CDCl₃, ppm): δ 8.25 (d, 4H, 8.7Hz), 7.68 (d, 4H, 8.4Hz), 7.29 (s, 2H).

Meso-1,2-dibromo-1,2-(4,4'-dinitrophenyl)ethane⁹ (2). Dinitrostilbene (1 g, 4 mmol, 1 equiv) was dissolved in nitromethane (100 mL) with stirring. Bromine (840 mg, 5.26 mmol, 1.4 equiv) was added to additional nitromethane (100 mL) and this solution added to the dinitrostilbene solution. The resultant dark yellow-brown solution was stirred at room temperature under a superbright light for 5 d. The solution became pale red then very pale yellow. The reaction mixture was quenched with aqueous NaHSO₃ and filtered to give the product (323.5 mg) as an off-white solid. The filtrate evaporated and the yellow solid remaining was washed with EtOAc and filtered to recover additional product (169.1 mg). These products were combined to yield meso-1,2-dibromo-1,2-(4,4'-dinitrophenyl)ethane (492.6 mg, 31%) as an off-white solid. ¹H NMR (300 MHz, DMSO, ppm): δ 8.31 (d, 4H, 9.3Hz), 7.98 (d, 4H, 8.7Hz), 6.38 (s, 2H). ¹³C NMR (300 MHz, DMSO, ppm): δ 147.4, 147.2, 129.5, 124.0, 51.9.



cis-Ruthenium(bipyridine)dichloride (chirally enhanced, 4). RuCl₃ (1.0 g, 4.821 mmol), LiCl (1.310 g, 30.90 mmol, 6.4 equiv), 2,2'-dipyridine (1.523 g, 9.751 mmol, 2 equiv), and L-ascorbic acid (1.046 g, 5.939 mmol, 1.1 equiv) were dissolved in dry DMF (12 mL). The solution was refluxed for 1 hour then cooled to room temperature. Acetone (30 mL) was added and the solution stored in the freezer overnight. The next morning, the solution was filtered to give a black solid, which was washed with cold water (5 mL x 2), then diethyl ether (5 mL x 2). The solid was dried under vacuum to give cis-ruthenium(bipyridine)dichloride (1.70 g, 73% yield). Used without further purification. ¹H NMR (300 MHz, DMSO, ppm) δ 9.96 (d, 2H, 5.7Hz), 8.63 (d, 2H, 8.1Hz), 8.47 (d, 2H, 8.1Hz), 8.05 (t, 2H, 7.8Hz), 7.76 (t, 2H, 6.0Hz), 7.67 (t, 2H, 7.5Hz), 7.50 (d, 2H, 5.4Hz), 7.09 (t, 2H, 6.3Hz).

cis-Ruthenium(bipyridine)dichloride (racemic, 5). RuCl₃ (1.0 g, 4.821 mmol), LiCl (1.310 g, 30.90 mmol, 6.4 equiv), and 2,2'-dipyridine (1.523 g, 9.751 mmol, 2 equiv) were dissolved in dry DMF (12 mL). The solution was refluxed for 1 hour then cooled to room temperature. Acetone (30 mL) was added and the solution stored in the freezer overnight. The next morning, the solution was filtered to give a black solid, which was

washed with cold water (5 mL x 2) then diethyl ether (5 mL x 2). The solid was dried under vacuum to give racemic *cis*-ruthenium(bipyridine)dichloride (1.70 g, 73% yield) of product. Used without further purification. ¹H NMR (300 MHz, DMSO, ppm) δ 9.96 (d, 2H, 5.7Hz), 8.63 (d, 2H, 8.1Hz), 8.47 (d, 2H, 8.1Hz), 8.05 (t, 2H, 7.8Hz), 7.76 (t, 2H, 6.0Hz), 7.67 (t, 2H, 7.5Hz), 7.50 (d, 2H, 5.4Hz), 7.09 (t, 2H, 6.3Hz).

Representative procedure for reacting Ru(bpy)₂Cl₂ with chiral diols and aminoalcohols. cis-Ru(bpy)₂Cl₂ (100 mg, 0.21 mmol) was dissolved in MeOH (3 mL) and refluxed for 1 hour. D-allo-threonine methyl ester (28 mg, 0.21 mmol, 1 equiv) in MeOH (2 mL) and NaOH (16.8 mg, 0.42 mmol, 2 equiv) in MeOH (4 mL) were added and the solution refluxed overnight to give a colored solution. The solution was cooled to room temperature and filtered. The precipitate was washed with MeOH (2 mL x 2) to give a dark colored solid. The solid was subjected to UV and ECCD studies without further purification.

(1S)-1-Phenylethane-1,2-diol product. Ru(bpy)₂Cl₂ (100 mg, 0.21 mmol) was dissolved in MeOH (3 mL) and refluxed for 1 hour. (1S)-1-phenylethane-1,2-diol (29 mg, 0.21 mmol, 1 equiv) in MeOH (2 mL) and NaOH (16.8 mg, 0.42 mmol, 2 equiv) in MeOH (4 mL) were added and the solution was refluxed overnight to give a colored solution. The solution was cooled to room temperature and filtered. The precipitate was washed with MeOH (2 mL x 2) to give a purple solid. ECCD (nm): 308.2 (1.9), 290.9 (-0.6).

(1R)-1-phenylethane-1,2-diol product. Ru(bpy)₂Cl₂ (100 mg, 0.21 mmol) was dissolved in MeOH (3 mL) and refluxed for 1 hour. (1R)-1-phenylethane-1,2-diol (29 mg 0.21 mmol, 1 equiv) in MeOH (2 mL) and NaOH (16.8 mg, 0.42 mmol, 2 equiv) in MeOH (4 mL) were added and the solution was refluxed overnight to give a colored solution. The solution was cooled to room temperature and filtered. The precipitate was washed with MeOH (2 mL x 2) to give a purple solid. ECCD (nm): 310.8 (-2.4), 289.9 (1.25).

(-)-Norephedrine product. Ru(bpy)₂Cl₂ (100 mg, 0.21 mmol) was dissolved in MeOH (3 mL) and refluxed for 1 hour. (-)-Norephedrine (32 mg, 0.21 mmol, 1 equiv) in MeOH (2 mL) and NaOH (16.8 mg, 0.42 mmol, 2 equiv) in MeOH (4 mL) were added and the solution was refluxed overnight to give a colored solution. The solution was cooled to room temperature and filtered. The precipitate was washed with MeOH (2 mL x 2) to give a black solid. ECCD (nm): 302.2 (7.7), 294.7 (-3.4).

(+)-Norephedrine product. Ru(bpy)₂Cl₂ (100 mg, 0.21 mmol) was dissolved in MeOH (3 mL) and refluxed for 1 hour. (-)-Norephedrine (32 mg, 0.21 mmol, 1 equiv) in MeOH (2 mL) and NaOH (16.8 mg, 0.42 mmol, 2 equiv) in MeOH (4 mL) were added and the solution was refluxed overnight to give a colored solution. The solution was cooled to room temperature and filtered. The precipitate was washed with MeOH (2 mL x 2) to give a black solid. ECCD (nm): 300.1 (-6.9), 288.0 (1.4).

D-allo-Threonine methyl ester product. Ru(bpy)₂Cl₂ (100 mg, 0.21 mmol) was dissolved in MeOH (3 mL) and refluxed for 1 hour. D-allo-threonine methyl ester (28 mg, 0.21 mmol, 1 equiv) in MeOH (2 mL) and NaOH (16.8 mg, 0.42 mmol, 2 equiv) in MeOH (4 mL) were added and the solution was refluxed overnight to give a colored solution. The solution was cooled to room temperature and filtered. The precipitate was washed with MeOH (2 mL x 2) to give a purple solid. ECCD (nm): 299.8 (-1.5), 292.1 (1.4).

L-allo-Threonine methyl ester product. Ru(bpy)₂Cl₂ (100 mg, 0.21 mmol) was dissolved in MeOH (3 mL) and refluxed for 1 hour. L-allo-Threonine methyl ester (28 mg, 0.21 mmol, 1 equiv) in MeOH (2 mL) and NaOH (16.8 mg, 0.42 mmol, 2 equiv) in MeOH (4 mL) were added and the solution was refluxed overnight to give a colored solution. The solution was cooled to room temperature and filtered. The precipitate was washed with MeOH (2 mL x 2) to give a purple solid. ECCD (nm): 300.1 (2.2), 290.4 (-2.3).

References:

- 1. Dale, J. A.; Mosher, H. S. J. Am. Chem. Soc. 1973, 95, 512.
- 2. Adam, W.; Diaz, M. T.; Saha-Moller, C. Tetrahedron: Asymmetry 1998, 9, 589.
- 3. Hoch, U.; Humpf, H.-U.; Schreier, P.; Saha-Moller, C.; Adam, W. Chirality 1997, 9, 69.
- 4. Nakanishi, K.; Schooley, D. A.; Koreeda, M.; Miura, I. J. Am. Chem. Soc. 1972, 94, 2865.
- 5. Wavefunction, Inc. Spartan SGI, 7.0.1; 1998.
- 6. Harder, T.; Wessig, P.; Bendig, J.; Stosser, R. J. Am. Chem. Soc. 1999, 121, 6580.
- 7. Bellucci, G.; Bianchini, R.; Chiappe, C.; Marioni, F. J. Org. Chem. 1990, 55, 4094.
- 8. Butcher, T. S.; Zhou, F.; Detty, M. R. J. Org. Chem. 1998, 63, 169.
- 9. Hartshorn, M. P.; Opie, M. C. A.; Vaughan, J. Australian J. Chem. 1973, 26, 917.
- 10. Hutchins, R. O.; Taffer, I. M. J. Org. Chem. 1983, 48, 1360.
- 11. Hua, X.; von Zelewsky, A. Inorganic Chem. 1995, 34, 5791.
- 12. Knof, U.; von Zelewsky, A. Angew. Chem. Inter. Ed. 1999, 38, 302.
- 13. Hesek, D.; Inoue, Y.; Everitt, S. R. L.; Kunieda, M.; Ishida, H.; Drew, M. G. B. Tetrahedron: Asymmetry 1998, 9, 4089.
- 14. Keyes, T. E.; Vos, J. G.; Kolnaar, J. A.; Haasnoot, J. G.; Reedijk, J.; Hage, R. *Inorg. Chim. Acta* **1996**, *245*, 237.
- 15. Haga, M.-a.; Dodsworth, E. S.; Lever, A. B. P. Inorg. Chem. 1986, 25, 447.

